MODE II INTERLAMINAR FRACTURE TOUGHNESS OF INTERLEAVED COMPOSITE MATERIALS

ADNAN AKSOY

MODE II INTERLAMINAR FRACTURE TOUGHNESS OF INTERLEAVED COMPOSITE MATERIALS

by

Adnan Aksoy

A Thesis Submitted to the Faculty of the
College of Engineering
in Partial Fulfillment of the Requirements for the Degree
of Master of Science in Engineering

Florida Atlantic University
Boca Raton, Florida
April, 1990

MODE II INTERLAMINAR FRACTURE TOUGHNESS OF INTERLEAVED COMPOSITE MATERIALS

by

Adnan Aksoy

This thesis was prepared under the direction of the canditate's thesis advisor, Dr. Leif A. Carlsson, Department of Mechanical Engineering. It was submitted to the faculty of the College of Engineering and was accepted in partial fulfillment of the requirements for the degree of Master of Science.

SUPERVISORY COMMITTEE

Leif A. Carlsson
Thesis Advisor

Gary C. Salivar

Karl N. Shivakumar

Chairman, Department of Mechanical Engineering

Roger Messenger for SED
Dean, College of Engineering

K. D. Bradshaw
Dean of Graduate Studies

2/7/89
Date

ACKNOWLEDGEMENTS

The author wishes to express his gratitude to his thesis advisor, Dr. Leif A. Carlsson. His support, excellent guidance and good humor made it a pleasure to complete this work. Special thanks are due Dr. G. C. Salivar and Dr. K. K. Stevens while serving on his committee. The author is also grateful to Dr. J. E. Masters of American Cyanamid Company for the generous donation of materials and expertise and Dr. J. M. Cuschieri and Chris Dentos of The Department of Ocean Engineering at Florida Atlantic University for the use of their facilities.

The author also gives his deepest appreciation to his family, Turkish Education Foundation and Hulusi Damgacıoglu of Alarko/Turkey for their support and encouragements.

ABSTRACT

Author: Adnan Aksoy

Title: Mode II Interlaminar Fracture Toughness of Interleaved Composite Materials

Institution: Florida Atlantic University

Degree: Master of Science

Year: 1989

Interlaminar mode II fracture toughness, G_{IIC}, of thermoset and thermoplastic interleaved (TSI and TPI) composites were investigated over a wide range of interleaf thickness. TPI specimens had four to about seven times larger G_{IIC} than those without an interleaf. Poor adhesion observed for some TPI specimens were likely to be due to contaminated film materials. Thermoset interleaves were less effective in enhancing the mode II fracture toughness. However, even 0.043 mm thermoset interleaves gave three times larger G_{IIC} than those without an interleaf. Estimates of the volume of the yielded material around the crack tip based on a quasi-elastic finite element approach and Irwin's model showed that the yield zone height reaches a peak value for increasing interleaf thickness for both TSI and TPI specimens. Furthermore, fracture toughness data correlates well with yield zone heights.

Table of Contents

List of Figures

List of Tables

Nomenclature

K	Stress intensity factor
P	Load
a	Crack (delamination) length
G	Total strain energy release rate
C	Compliance
b, W	Beam width
CSB	Cracked sandwich beam
E_1	Axial modulus of lamina in fiber direction
E_2	Transverse modulus of lamina
G_{12}	Inplane shear modulus of a unidirectional lamina
G_{13}	Out-of-plane shear modulus of a unidirectional lamina
ν	Poisson's ratio
ν_{12}	Poisson's ratio of a unidirectional lamina
C_{SH}^*	Compliance calculated from the beam theory including shear deformation
δ	Center point out-of-plane displacement
L	Beam half-span
h	Beam half-thickness
W_c, W_d	Displacements in the z direction (out-of-plane)
U_c, U_d	Displacements in the x direction

G_I, G_{II}	Mode I and mode II strain energy release rates
T_C, F_C	Nodal forces in the x (horizontal) and z (out-of-plane) directions, respectively
τ	Shear stress
V	Shear force
A	Beam area
k	Shear correction factor
D_{11}'	Element of inverse bending stiffness matrix
A_{55}^*	Element of inverse extensional stiffness matrix
P_C	Critical load at unstable crack growth
P_{SC}	Load at onset of subcritical crack growth
P_{NL}	Load at onset of nonlinearity
G_{IIC}	Mode II fracture toughness
G_{IISC}	Subcritical fracture toughness in mode II
G_{IINL}	Mode II fracture toughness calculated using P_{NL}
G_I	Mode I fracture toughness
σ_y	Tensile yield strength of interleaf material
τ_y	Shear yield strength of interleaf material
t_i	Interleaf thickness
TSI	Thermoset (FM 300 I) interleaved
TPI	Thermoplastic (film E) interleaved
r_p	Yield zone height

Chapter 1 Introduction to Fiber Reinforced Composites

1.1 Introduction

A unique aspect of composites is that the material can be engineered to meet the demands of a specific application. The type of resin, fiber and laminate stacking sequence are design parameters enabling the engineer to meet the structural requirements.

Composite laminates made from continuous fibers and polymer resins (e.g. graphite/epoxy) are very attractive for a variety of aerospace applications owing to their high strength and stiffness-to-weight ratios and low coefficients of thermal expansion. The weight advantage of these materials, however, is significantly reduced because of the relatively low interlaminar damage resistance. In particular, low velocity hard object impact loading is likely to cause delamination (interlaminar cracking). In the assessment of damage resistance, defined as the ability of a material/structure to undergo an "impact event" without damage [1], delamination initiated by interlaminar normal and shear stresses, represents one of the most serious defects. The reason is that delamination affects inplane properties, such as bending stiffness and compressive strength [2].

Interlaminar cracks propagate along fiber/resin interfaces through the resin phase between fiber bundles. Fracture toughness, a measure of resistance to crack propagation, is dependent on various material and external factors [3]. For composites with polymeric matrices, these factors include fiber/matrix interfacial strength and constituent properties of the fibers and matrix. If the fiber/matrix interfacial adhesion is appropriate, the ductility of the matrix (resin) appears to be the major factor controlling the toughness of the composite.

1.2 Fracture Mechanics of Composite Materials

Fracture mechanics is an engineering discipline involving the propagation of cracks in a load bearing solid body. The application of fracture mechanics to conventional isotropic materials has been well demonstrated since 1920 when Griffith first established the basic energy equations.

The quantity most often used to predict failure by unstable crack growth is the stress intensity factor "K", a measure of the stress state in the vicinity of a crack tip [4]. For an isotropic material the general expression for K is,

$$K = \alpha P \sqrt{a} \qquad (1)$$

where P is the applied load, a, the flaw size and α is a function determined by the loading conditions and the geometry of the structure. The exact form of α can be determined from stress analysis of the structure for three different modes of loading [5], see Fig. 1.1. Normal stresses give rise to the "opening mode" or mode I loading. The displacements of the crack surfaces are perpendicular to the plane of the crack. Shear in the x-y plane results in mode II or "sliding mode"; the displacement of the crack surfaces is in the plane of the crack and perpendicular to the leading edge of the crack. The "tearing mode" or mode III is caused by shear in the x-z plane. Crack surface displacements are in the plane of the crack and parallel to the leading edge of the crack.

For fiber reinforced materials, fracture mechanics applications are more complicated [6]. In general, adaptation of fracture criteria established for isotropic materials to composites have been of limited success because of the heterogeneous structure of composite materials. For interlaminar fracture characterization, however, fracture mechanics is fairly well established. Fig. 1.2 shows a schematic representation of the micromechanisms responsible for energy absorption during interlaminar fracture of unidirectional composites [7]. Formation of the fracture surfaces of the main crack, plastic deformation and/or microcracking of the matrix in the damage zone around the

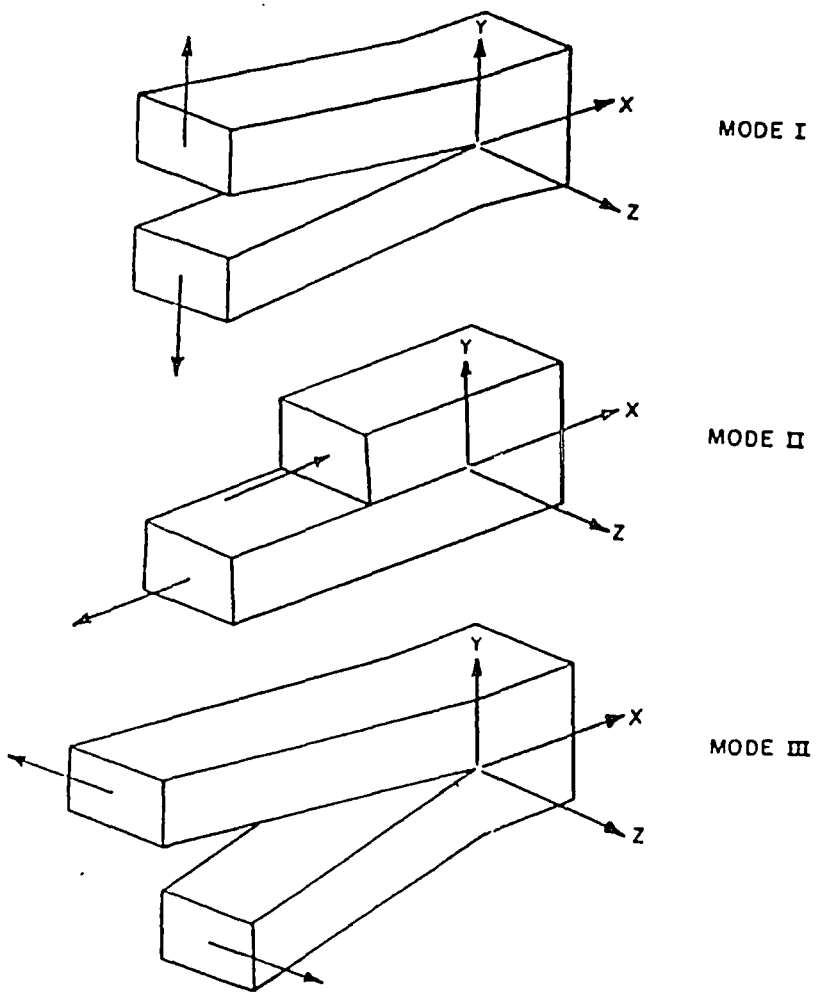

Fig. 1.1 The three basic modes of crack surface displacements [15].

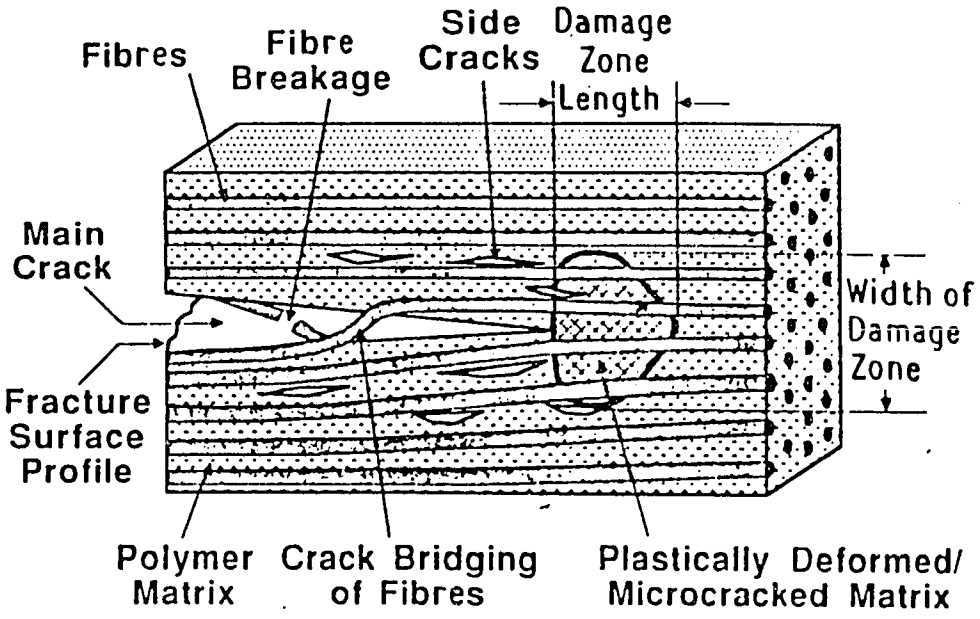

Fig. 1.2 Fracture model [7].

crack, and crack bridging by fibers or bundles are considered to be the major energy absorbing mechanisms.

It is a common practice in interlaminar fracture analysis of composites to use strain energy release rate, G, instead of the stress intensity factor, K. Since G can be evaluated from global load versus displacement response, difficulties encountered in analyzing the crack tip stresses are avoided. The general expression for G is given by;

$$G = \frac{P^2}{2b}\frac{dC}{da} \qquad (2)$$

where b is the material thickness in the vicinity of the crack and dC/da is the change in the compliance "C" (obtained from load deflection curve) of the structure with crack length a. Since dC/da is a global property of a particular specimen, G evaluation is independent of the detailed crack tip stress distribution. Furthermore, dC/da, hence G can be determined experimentally by measuring compliance versus crack length for a structure [4]. The critical value of $G=G_C$ is commonly denoted as the "interlaminar fracture toughness".

1.3 Development of Tough Composites

In response to the demands of the aircraft industry for materials with increased resistance to impact damage and delamination, many methods to improve the interlaminar

fracture toughness have been devised [8]. Most methods focus on the ductility of the matrix. Epoxy, which is a thermoset resin, is the most common family of polymers used in high performance composites. The original aims of epoxy formulators were to obtain epoxies with high strength, modulus and glass transition temperature. As a consequence, the chemical structure of these epoxies contains a large proportion of stiff aromatic groups and polymer chains that are densely cross linked [9]. However, as a consequence of such a structure, a serious disadvantage is their brittleness, leading to low interlaminar fracture resistance. The new generation epoxies, the so called "toughened epoxies", are modified for increased fracture toughness, most commonly with a rubbery or thermoplastic secondary phase present in the epoxy. The secondary particles act as stress concentrators ahead of the crack tip so that the polymer toughness is increased through an increase in the volume of plastically deformed material [10]. One of the merits of elastomer-epoxy dispersion is that the large gain in fracture toughness is accomplished with relatively little loss in tensile strength, modulus and thermal resistance [4].

Polymers generally deform inelastically by two mechanisms, shear yielding and/or crazing. A polymer with a large mode I fracture toughness has the ability to dilatate (increase volume) under plane strain tensile loading [11].

Mechanisms such as chain extension, crazing, void formation followed by shear band formation, and plasticity can contribute to the volume expansion. Crystalline thermoplastics and highly crosslinked thermosets exhibit little tendency to dilatate. They deform by shear yielding (constant volume) although the amount of plastic deformation after yield in thermosets is much less than in thermoplastics. Consequently, in general, thermosets have larger fracture toughness in mode II than in mode I. Amorphous brittle thermoplastics, on the other hand, commonly yield by crazing.

Screening of improved resins is commonly performed by a compression after impact (CAI) test. In this test method a quasi-isotropic laminate is subjected to lateral impact and then loaded in compression to measure residual properties [8]. The increase in post-impact compressive strength of composites made with tough resins has, however, been less than expected. Similarly the delamination toughness does not increase as anticipated. Fig. 1.3 shows the composite mode I interlaminar fracture toughness as a function of resin fracture toughness [12]. Initial increase in resin fracture toughness from the first generation values of 70 J/m^2 results in a significant improvement in the mode I delamination fracture toughness. However, at composite G_{IC} values greater than about 200 J/m^2 further increase in neat resin toughness is met with small incremental increase in the composite delamination fracture

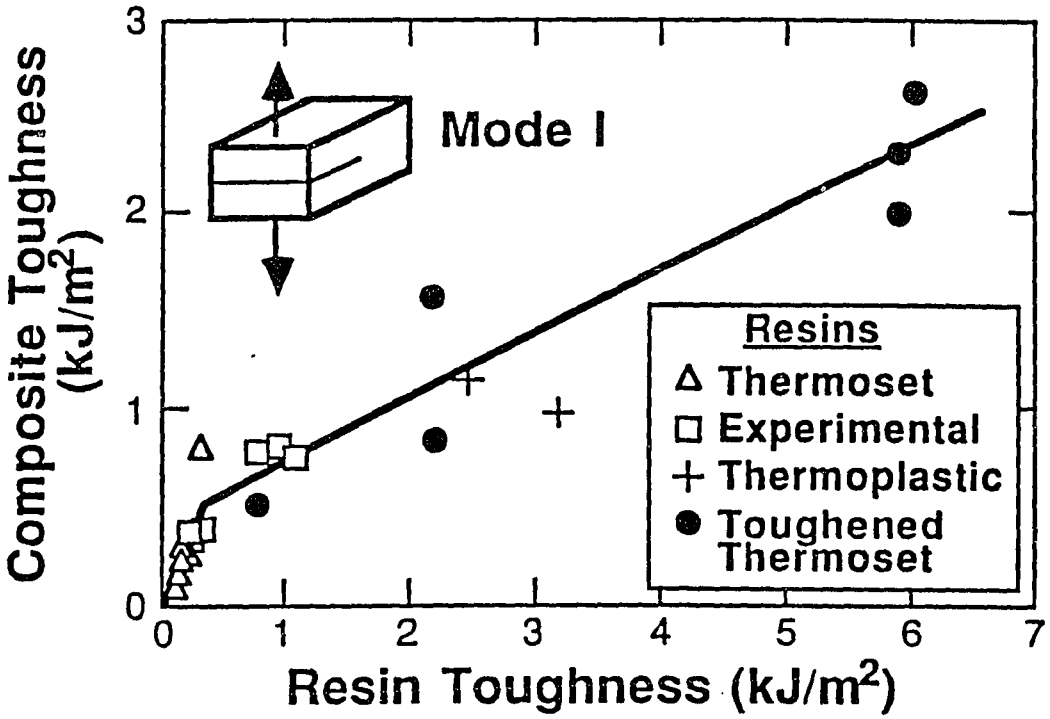

Fig. 1.3 Mode I fracture toughness of composite vs. resin mode I fracture toughness [12].

toughness. Although this problem is still being investigated it is believed that, above a certain level of matrix toughness a saturation in the composite toughness takes place because of the limited ability for expansion of the plastic zone at the crack tip due to the presence of rigid fibers [12, 13], see Fig. 1.2.

A more promising technique to improve interlaminar fracture toughness of composite materials is called "interleaving", which consists of placing a thin, discrete layer of a ductile resin at the ply interfaces, see Fig. 1.4 [8]. This technique is based on the hypothesis that a composite material could be made tougher and more impact resistant by allowing for more expansion of the plastic zone between the plies.

In any fiber reinforced systems the matrix resin provides both stiffness and toughness. In the case of interleaved systems two distinct resins are optimized for a particular role. The matrix resin supports the fibers and provides hot/wet stiffness. On the other hand, the interleaf resin has a high strain-to-failure and enhances the interlaminar fracture toughness. The interleaf resin must also retain its modulus at least up to the composite system's upper use temperature and remain as a discrete layer after the laminate has been cured [8].

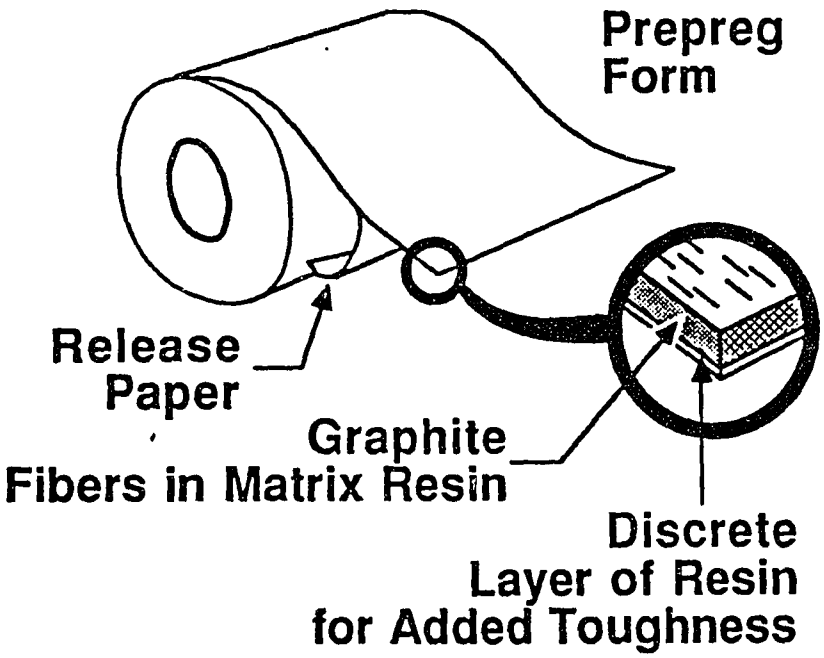

Fig. 1.4 Interleaved laminate construction [8].

Masters [8], showed that interleaving increases laminate compression strength after impact (CSAI) by 50 to 80 %. The size and number of the internal delaminations were greatly reduced in the impacted interleaved laminates compared with those without interleaving (baseline). It was found that a 0.0127 mm (0.5 mil) thick thermoplastic (film E) interleaf increases the mode II fracture toughness, G_{IIC}, of epoxy and bismaleimide composites two to three times. The increase in mode I fracture toughness, G_{IC}, was, however, only about 50 % compared to the baseline laminates with no interleaves. Thermoset interleaves, on the other hand, were more effective in increasing the mode I toughness.

Ishai et al. [14, 15] observed more than a six fold increase in G_{IC} of (0.1 to 1.1 mm thick) thermoset FM 300 interleaved graphite/epoxy compared to those without interleaving. However, in contrast to Masters', they reported a 4 fold increase in G_{IIC} as well. Ishai et al. used mode I precracking while Masters' specimens were not precracked, which may be one reason for the discrepancy in their results.

The concept of interleaving is similar to that of adhesively bonded joints, see Fig. 1.5. Hence, fracture studies of bonded joints may simulate the elastic restraints imposed on plastic zone development due to the presence of stiff fibers in a composite, and enhance understanding of the

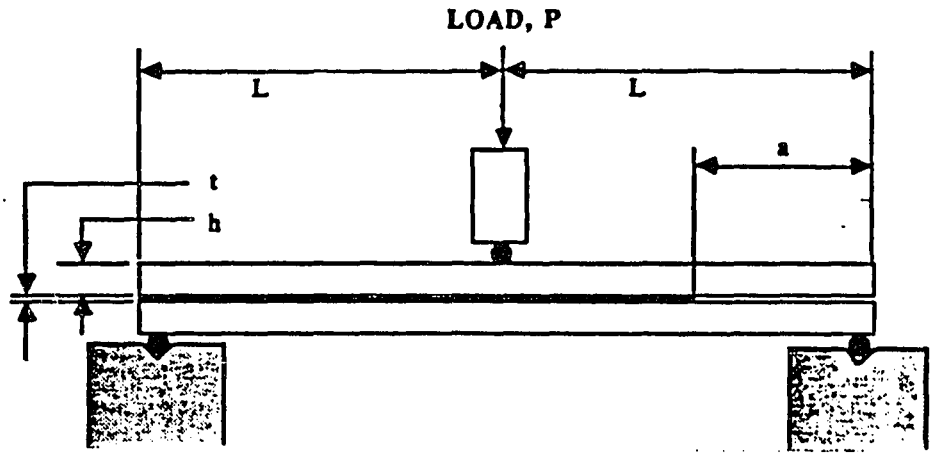

Fig. 1.5 Adhesive joint for mode II fracture toughness testing.

interlaminar fracture of laminated composites [16]. Chai [16] showed that G_{IIC} of adhesively bonded joints exhibits an initial increasing phase followed by a plateau as adhesive thickness is increased, see Fig. 1.6.

Bascom [4], studied mode I fracture of adhesive joints using a tapered double cantilever beam specimen, see Fig. 1.7. Fig 1.8 shows the effect of bond thickness on adhesive G_{IC}. G_{IC} increases sharply with bond thickness.

This study focuses on the interlaminar shear fracture, mode II, of interleaved and baseline (no interleaving) composite materials. Recent studies [8, 14, 15] show that film material, film thickness, constraint of the adjacent plies and adhesion between the interleaf and adjacent plies are the most important factors determining the fracture toughness and impact damage resistance. These results were obtained from separate studies either on only thermoset interleaf systems or with a single interleaf thickness. To obtain more knowledge of the influence of polymer structure, it is important to investigate both thermoplastic and thermoset interleaved composite systems for a reasonable range of interleaf thickness. It is also important to clarify the conflicting results of Masters [8] and Ishai et al. [14, 15] on mode II fracture toughness of thermoset interleaved systems.

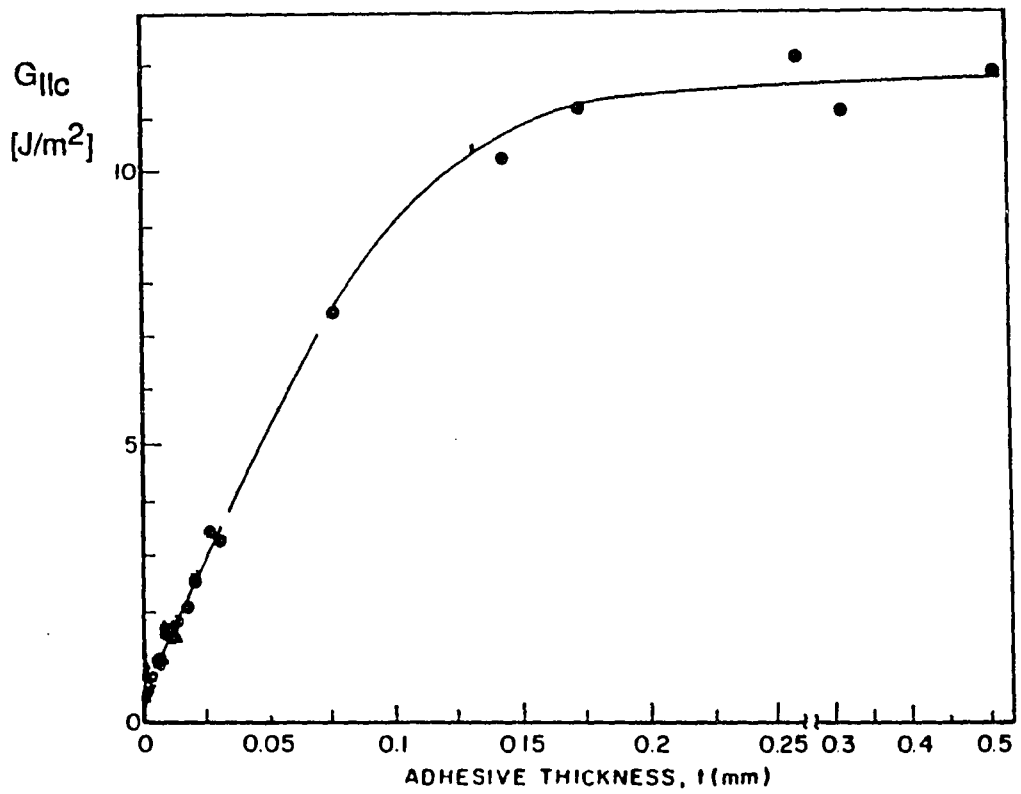

Fig. 1.6 G_{IIc} vs. bond thickness, t, for adhesively bonded specimens. Resin adhesive is BP907 [16].

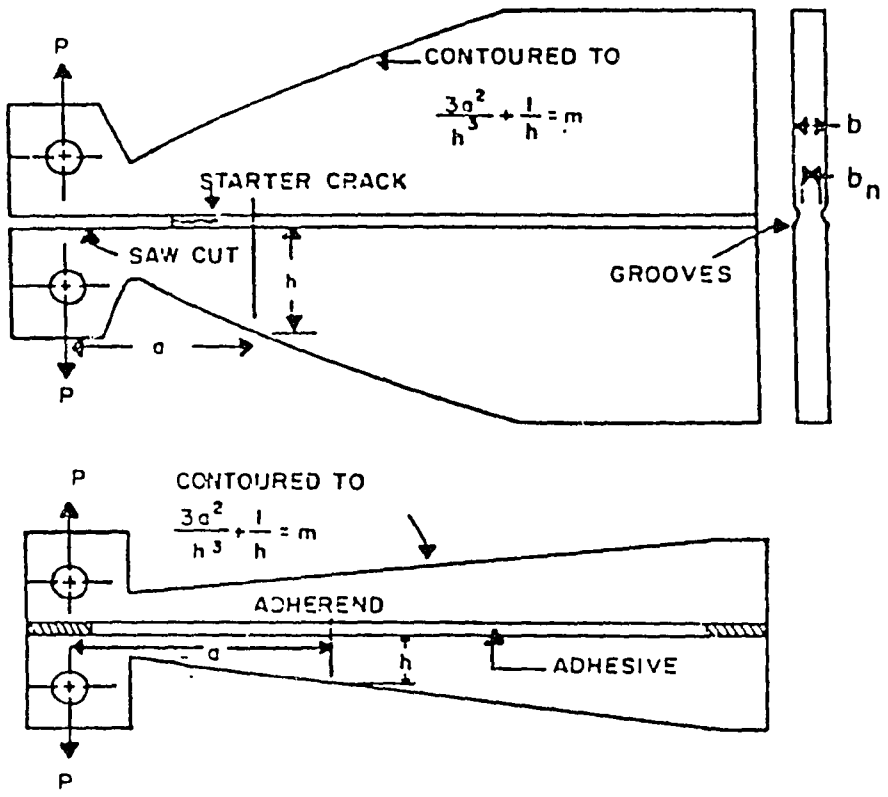

Fig. 1.7 Tapered double cantilever beam specimen [4].

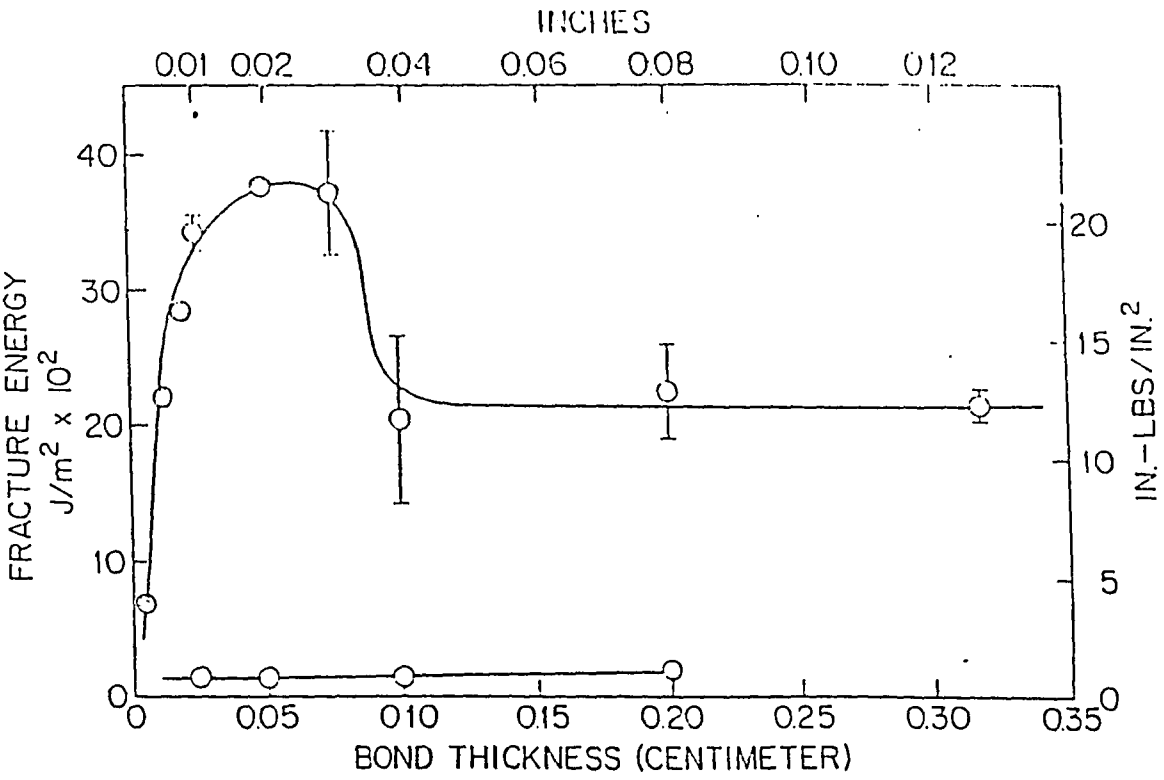

Fig. 1.8 Effect of bond thickness on adhesive G_{Ic} for an unmodified and CTNB (upper points) epoxy resin [4].

The end notched flexure (ENF) test specimen, Fig. 1.9 was used to investigate the effect of interleaving material and interleaf thickness on G_{IIC}. American Cyanamid's IM7/CYCOM 1827 graphite/epoxy prepreg was interleaved with 0.0127, 0.0254, 0.0762, and 0.127 mm (0.5 to 5 mils) thick thermoplastic film E and 0.043, 0.086, 0.172, 0.256, and 0.429 mm (1.7 to 17 mil) thermoset FM 300 I. The overall specimen thickness was kept reasonably constant by varying the number of prepreg plies.

Adhesion in thermoplastic interleaved systems is probably the least investigated factor. In order to describe the type of failure (adhesive/cohesive), and the extent of deformation, fracture surfaces were examined under optical and scanning electron microscopes.

In order to analyze interleaved ENF specimens, the ANSYS finite element program was used to obtain compliance, mode II strain energy release rate, G_{II} and effective stresses for various configurations. The effective stresses were compared with normalized yield strengths of the interleaving materials to estimate the size of the plastic zone. The idea here was to investigate the restraining effect of the stiffer composite layers.

Furthermore, cracked sandwich beam (CSB) theory which

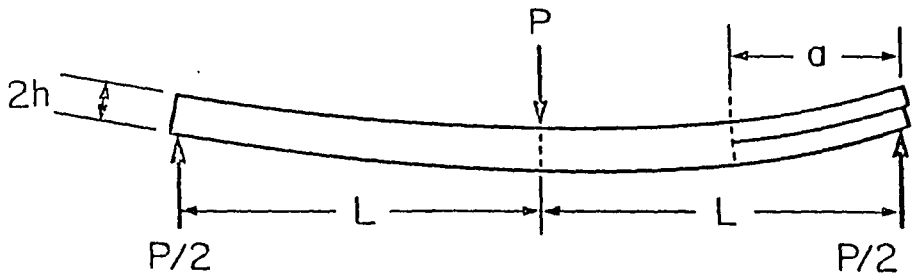

Fig. 1.9 End notched flexure (ENF) specimen.

was originally developed for sandwich constructions [17], was modified to analyze interleaved systems. Finally, CSB theory and finite element results were compared.

Chapter 2 Experimental Procedure

2.1 Materials

All specimens were made from American Cyanamid's IM7/CYCOM 1827 graphite/epoxy prepreg at American Cyanamid according to the appropriate processing specifications. The prepreg had a fiber areal weight of 190 g/m^2 and an average ply thickness of approximately 0.18 mm (7 mil). Three types of ENF specimens were manufactured, namely, baseline, thermoplastic (film E) and thermoset (FM 300 I) interleaved. The thermoplastic (film E) and thermoset (FM 300 I) interleaved specimens will be denoted by "TPI" and "TSI", respectively. The FM 300 I is a nitride rubber modified epoxy while film E is an amorphous thermoplastic. The thermoplastic interleaf thicknesses were 0.0127, 0.0254, 0.0762, and 0.127 mm (0.5 to 5 mil). The desired thermoset interleaf thickness (0.043, 0.086, 0.172, 0.256 and 0.429 mm (1.7 to 17 mil)) was obtained by stacking film adhesive layers (1-10). The interleaf and prepreg were then cocured to form the composite.

Delaminations at the specimen midsurface were obtained by embedding a 0.0254 mm (1 mil) thick inert teflon film between the interleaf and prepreg to define a site for the crack to propagate at the interface, see Fig. 2.1.

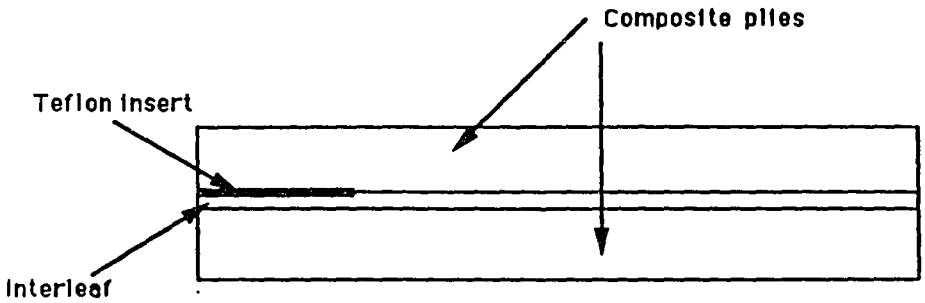

Fig. 2.1 Embedded teflon insert in an interleaved ENF specimen.

2.2 Basic Material Characterization

Mechanical property characterization of IM7/CYCOM 1827 graphite/epoxy was performed by tensile testing of 0^0, 90^0, and $\pm 45^0$ coupons according to standard testing procedures [18]. Only the elastic properties of the composite were determined for subsequent analysis. The test matrix is summarized in Table 2.1. Fig. 2.2 shows the typical stress strain curves. The elastic properties are as follows:

E_1= 149±4 GPa (21.6 Msi)

E_2= 9.4±.2 GPa (1.36 Msi)

G_{12}= 7.5±.4 GPa (1.09 Msi)

ν_{12}= 0.29±.01

Note that the shear modulus G_{12} for IM7/CYCOM 1827 unidirectional composite is larger than typical graphite/epoxy values of 4.5 - 5.5 GPa (0.68 - 0.8 Msi).

2.3 Film E and FM 300 I Stress Strain Behavior

Subsequent analysis requires the stress-strain response of the interleaf materials. Because of the unavailability of materials, data reported in the literature were used. FM 300 I tensile and shear stress strain data shown in Fig. 2.3 were obtained from Ref. [14]. Fig. 2.4 shows the tensile stress-strain curve for film E constructed using the ultimate strength, strain and Young's modulus data provided by American Cyanamid. 0.2 % offset yield strength was used to obtain

Layup	Dimensions [mm]	Gages	No. of replicas	Obtain
0°	1.2 X 13.1	Axial & transverse	3	E_1, ν_{12}
90°	3.1 X 25.4	Axial	2	E_2
±45	1.6 X 25.4	Axial & transverse	2	G_{12}

Table 2.1 Test matrix for IM7/CYCOM 1827 tensile coupons.

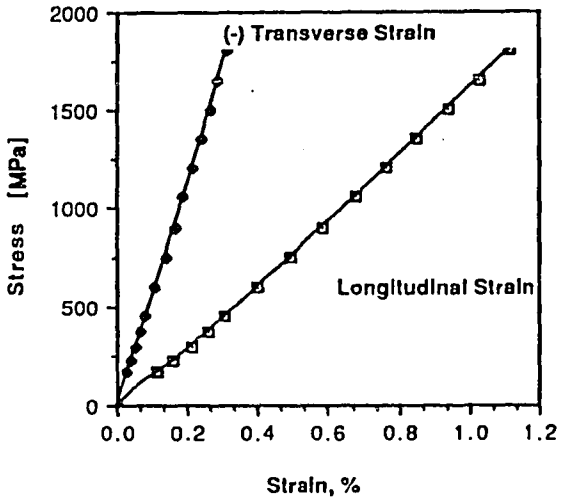

Tensile Stress-Strain Response of [0°]
Graphite/Epoxy Specimen

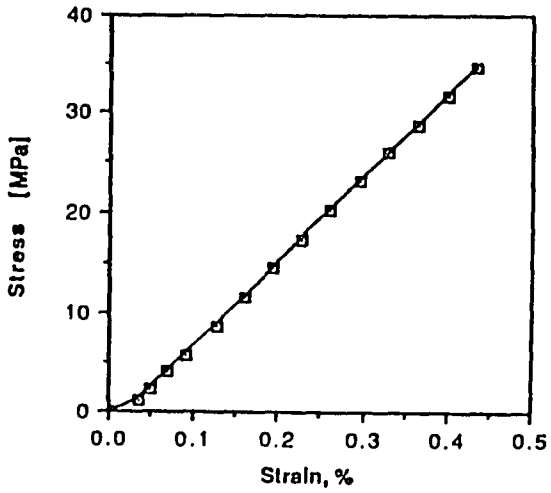

Tensile Stress-Strain Response of [90°]
Graphite/Epoxy Specimen

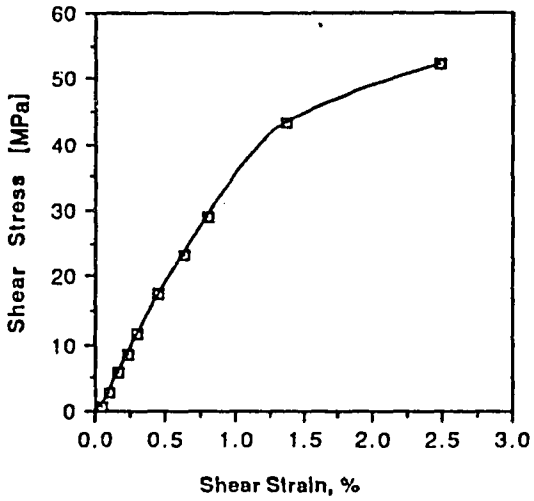

Shear Stress-Strain Relation for IM7/CYCOM 1827

Fig. 2.2 Stress-strain response of IM7/CYCOM 1827.

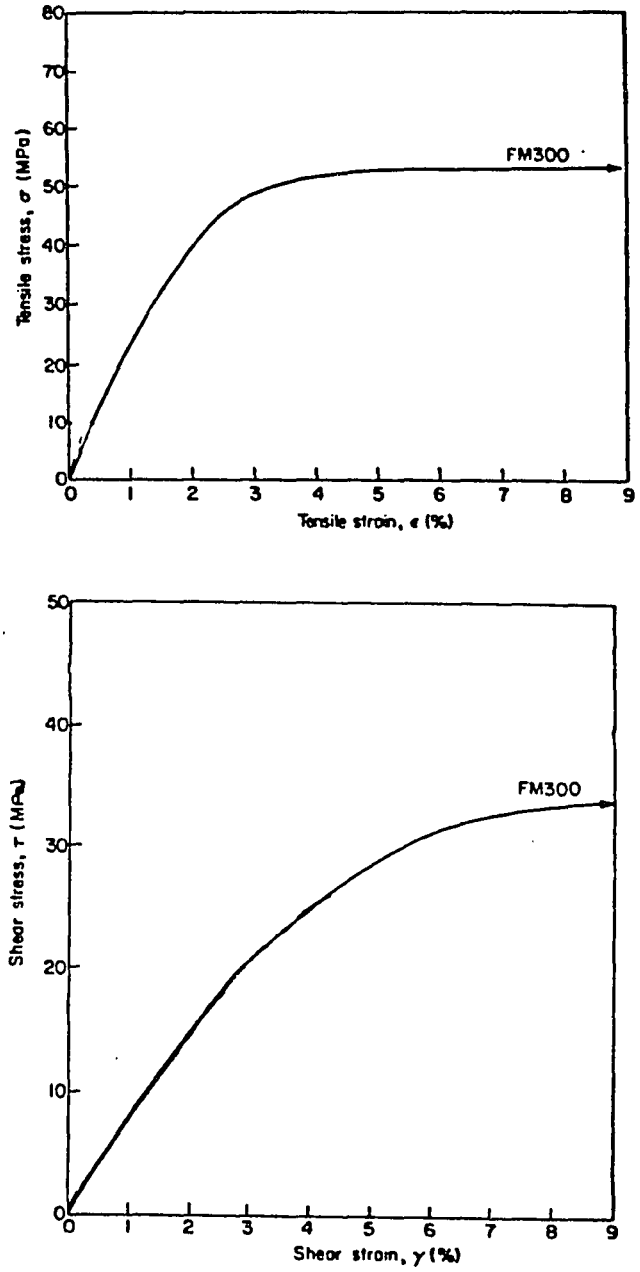

Fig. 2.3 Tensile and shear stress-strain curves of thermoset FM 300 I [14].

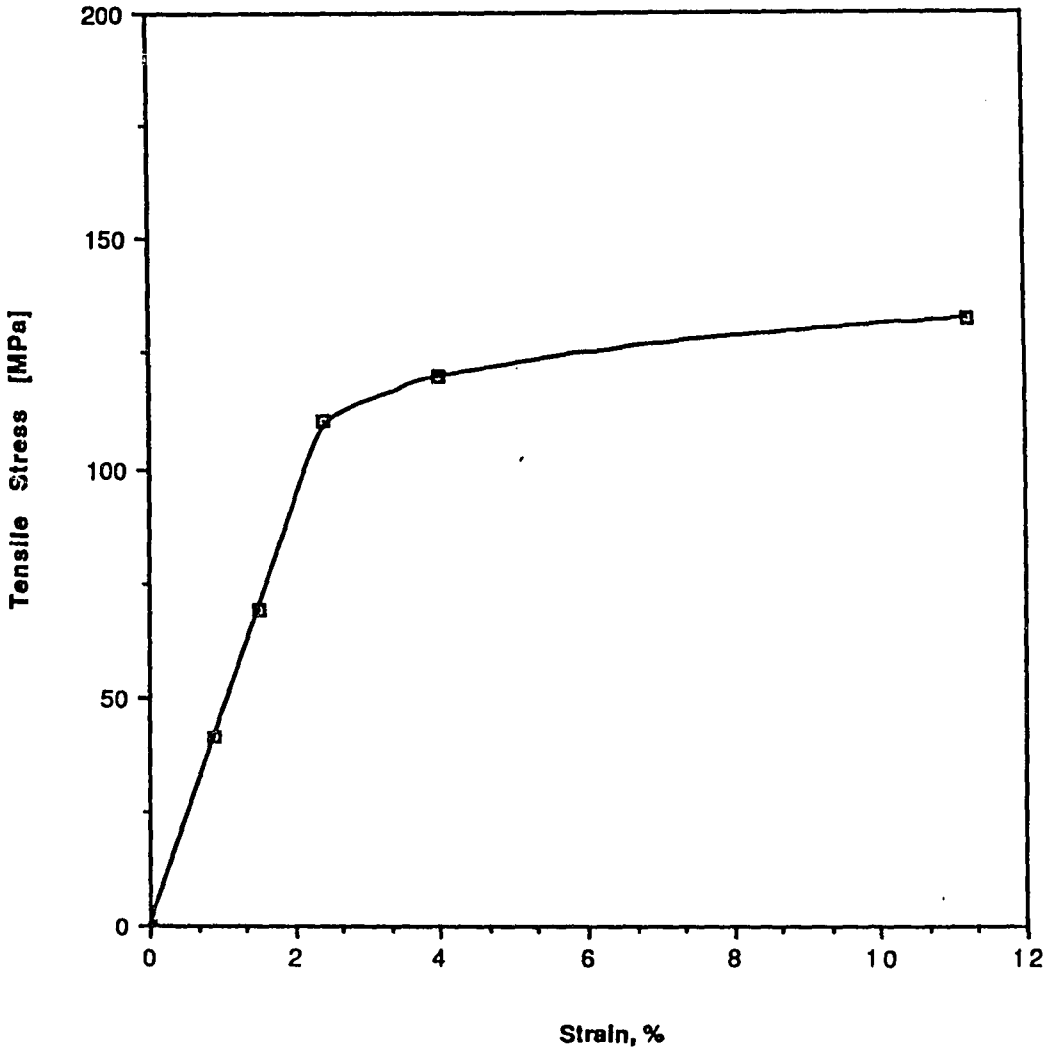

Fig. 2.4 Tensile stress-strain curve of thermoplastic film E .

tensile yield strengths. Elastic properties and yield strength values are shown in Table 2.2. Notice that film E has a yield strength that is more than twice the FM 300 I value.

2.4 Fracture Testing

2.4.1 Specimen Preparation for Microscopy

Prior to fracture testing, the edges of the specimens were polished. One edge was observed under the optical microscope to measure the interleaf thickness and to investigate the details of the mode II crack tip and crack path after growth. Hence, this edge was polished with great care. The opposite edge was polished and subsequently painted with liquid paper to facilitate visual observations of crack initiation and crack length measurements. The polishing procedure was as follows:

- 3 minutes on Buehler Carbimet paper disk 400 grit,
- 3 minutes on Buehler Carbimet paper disk 600 grit,
- 4 minutes on Buehler microcloth with 5.0 micron aluminum oxide powder,
- Final dry polishing on microcloth.

2.3.2 . Precracking

It has been shown that the fracture toughness evaluated from a specimen without precracking is artificially higher than a specimen with a natural crack tip [19]. During

Property	Units	FM 300 I	Film E
E	GPa (Msi)	2.45 (.355)	4.57 (.663)
G	GPa (Msi)	.88 (.128)	1.63 (.237)
ν	---	.38	.4
0.2 % offset, σ_y	MPa (ksi)	53 (7.69)	138 (20.0)

Table 2.2 Material properties of thermoset FM 300 I and thermoplastic film E.

processing a resin rich zone at the end of the teflon insert film is created that blunts the crack tip and increases the resistance to crack growth. Consequently, precracking prior to fracture tests is necessary.

Mode I (tension) precracking is the most common way of introducing a sharp crack [18]. In this technique, the specimen is clamped across the width slightly ahead of the insert, and crack surfaces are wedged open to propagate the crack about 5 mm (0.2 in.). The mode I precracking has, compared to the mode II precracking, the advantage that the crack front can be easily detected on the fracture surfaces after the completion of the fracture test. On the other hand, mode II precracking results in a more linear load versus deflection diagram [19]. Furthermore, it is quite reasonable to assume that the stress state in the material during impact loading is dominated by shear rather than tension [20]. Hence, in this study mode II (shear) precracking was used.

Mode II precracking was performed by placing the specimen in the three point bend fixture such that the crack length was nearly equal to the half-span length ($a/L \approx 1$), i.e. the end of the insert was placed near the center load nose. The specimen was then loaded to propagate the crack from the end of the insert to a position under the center load point. After mode II precracking, specimens were inspected in an optical

microscope to ensure that there was not any resin rich zone in front of the crack.

Specimens with 0.127 mm (5 mil) thick thermoplastic interleaves and 0.086 to 0.43 mm thick thermoset interleaves failed in flexure during mode II precracking attempts. This is evidently a result of the large ductility of these specimens. To avoid flexural failure these specimens were first precracked in mode I by tapping a razor blade. To achieve a mode II crack front, they were precracked in mode II as explained above.

2.4.3 Determination of Interlaminar Fracture Toughness

After precracking, the crack tip was marked on the specimen edge which had been previously painted white to facilitate the visual readings. A traveling microscope (10X) was used to obtain the crack length "a". The crack length is defined as the distance between the crack tip and the imprint of the outer support.

The ENF specimens were loaded in a three-point bend test fixture mounted in a 134 kN (30,000 lb.) universal testing frame (Tinius-Olsen DS 50), see Fig. 2.5. Table 2.3 lists average ENF specimen dimensions. In general, the specimens had a total crack length of approximately 25.4 mm (1 in.), and a total span length, 2L, of 101.6 mm (4 in.) to yield an a/L

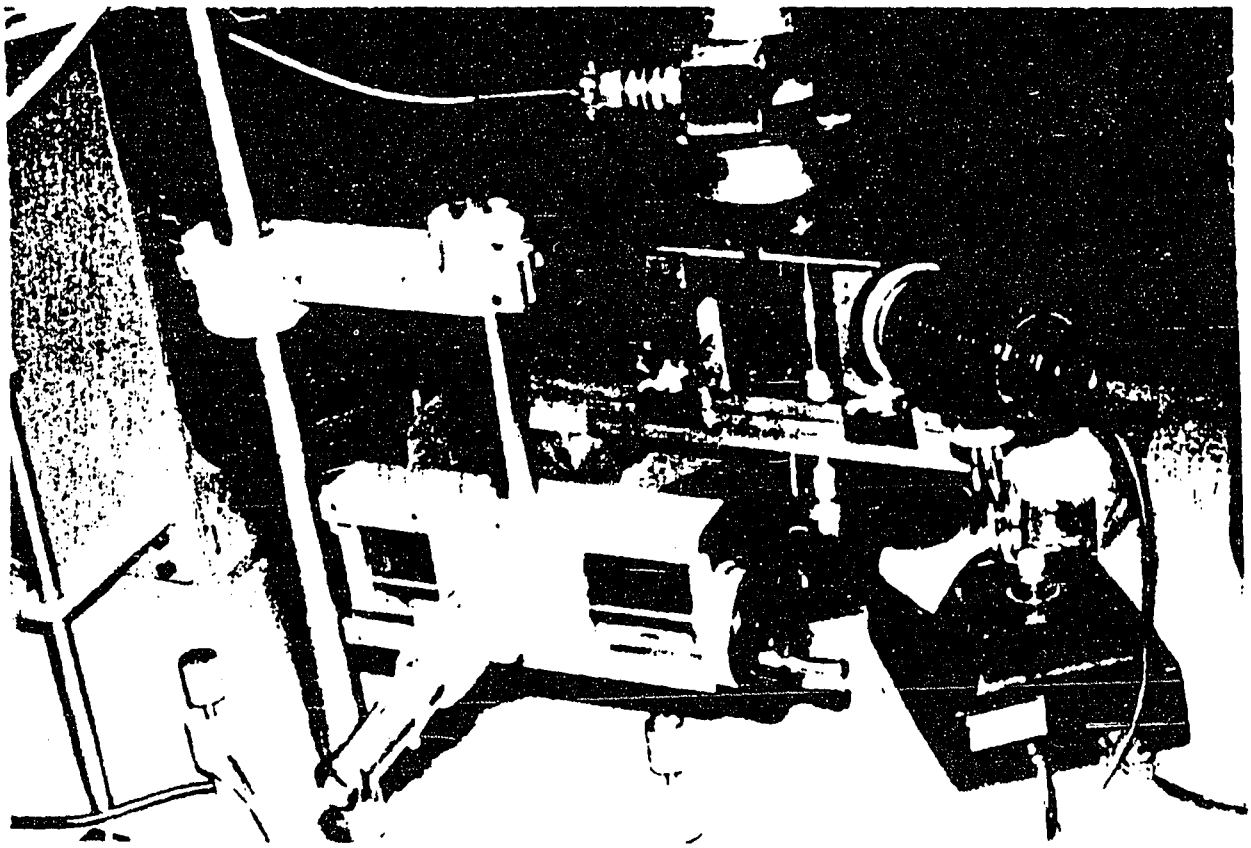

Fig. 2.5 Tinius-Olsen test frame and the ENF fixture.

Interleaf thickness* mm (mil)	Interleaf material	2h mm (in.)	a mm	W mm
0	none	3.43±.01 (.135)	25.4±.12	25.4±.21
.0127 (.5)	Film E	3.43±.05 (.135)	25.4±1.3	25.4±.09
.0254 (1.0)	"	3.45±.03 (.136)	25.4±.55	25.4±.01
.0762 (3.0)	"	3.48±.04 (.137)	25.4±.54	25.4±.1
.127 (5.0)	"	3.53±.08 (.139)	25.4±1.3	25.4±.09
.043 (1.7)	FM 300 I	3.43±.04 (.135)	25.4±.83	25.4±.20
.086 (3.4)	"	3.45±.03 (.136)	25.4±1.7	25.4±.11
.172 (6.8)	"	3.53±.03 (.139)	25.4±1.4	25.4±.11
.256 (10.2)	"	3.60±.06 (.142)	25.4±1.3	25.4±.03
.429 (17)	"	3.71±.08 (.146)	25.4±1.3	25.4±.02

* Buehler Versamet-2 optical microscope was used to measure the interleaf thicknesses with high accuracy.

Note: The above average values were obtained from 5 to 8 specimens and ± refers to one standard deviation.

Table 2.3 End notch flexure beam geometry.

ratio very close to 0.5. Cross-head speed was 2.54 mm/min. (0.1 in./min.) [21]. Five 5 to eight specimens of each geometry were tested.

Specimens were placed in the fixture such that the initial crack was above the interleaf. The deflection was measured by a linear voltage displacement transducer (LVDT), see Fig. 2.5. This approach eliminates the need for machine compliance correction. A real time load-deflection curve was obtained as schematically illustrated in Fig. 2.6.

As the specimen is loaded an initial linear response is observed. Although the ENF geometry is inherently unstable [26], stable crack growth, P_{SC}, as observed by locating the crosshair of a traveling microscope at the tip of the crack [19], is commonly seen. The stable growth causes the compliance of the specimen to increase as observed by a nonlinearity in the load displacement record, see Fig. 2.6. A schematic of stable (subcritical) crack growth is shown in Fig. 2.7. At $P_{C,}$ onset of unstable crack propagation occurs. The crack usually propagates to the center load nose.

2.4.4 Experimental Data Reduction

The critical, nonlinear and/or subcritical strain energy release rates were calculated from the beam theory including shear deformation [21, 22] by substituting the relevant loads,

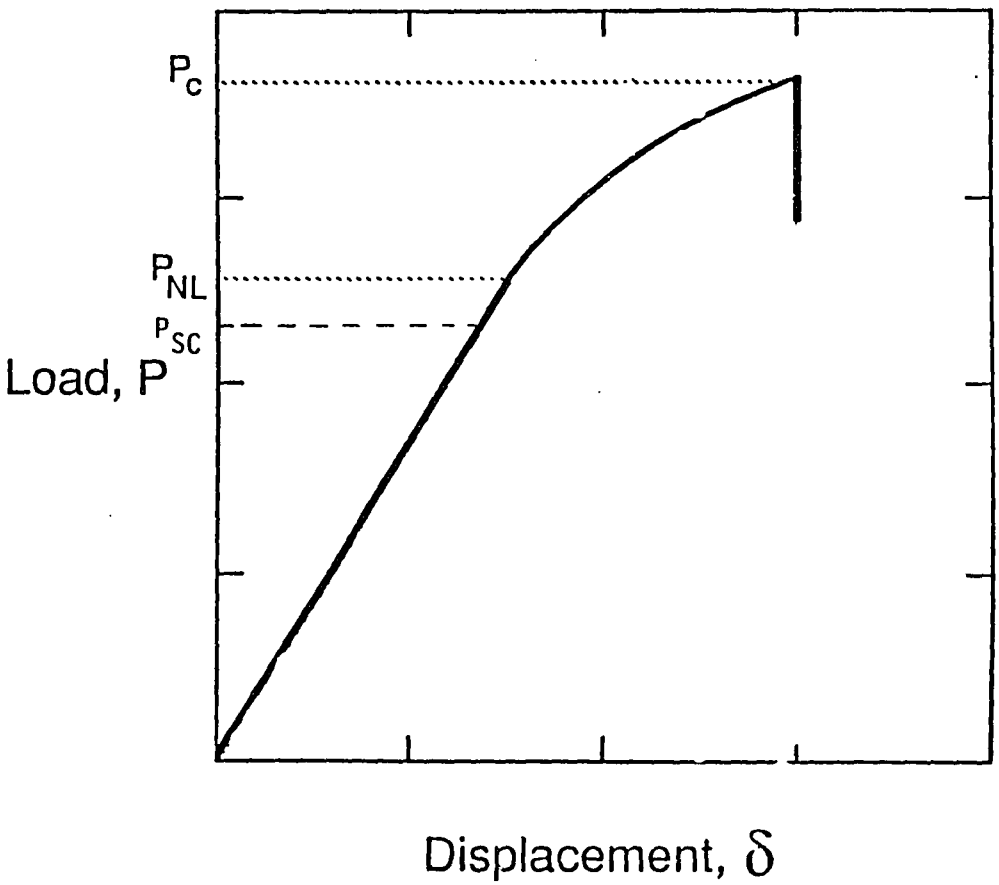

Fig. 2.6 Schematic load-deflection curve for the ENF test. P_{SC}, P_{NL} and P_C are the loads for onset of stable crack growth, nonlinear response and unstable crack growth, respectively.

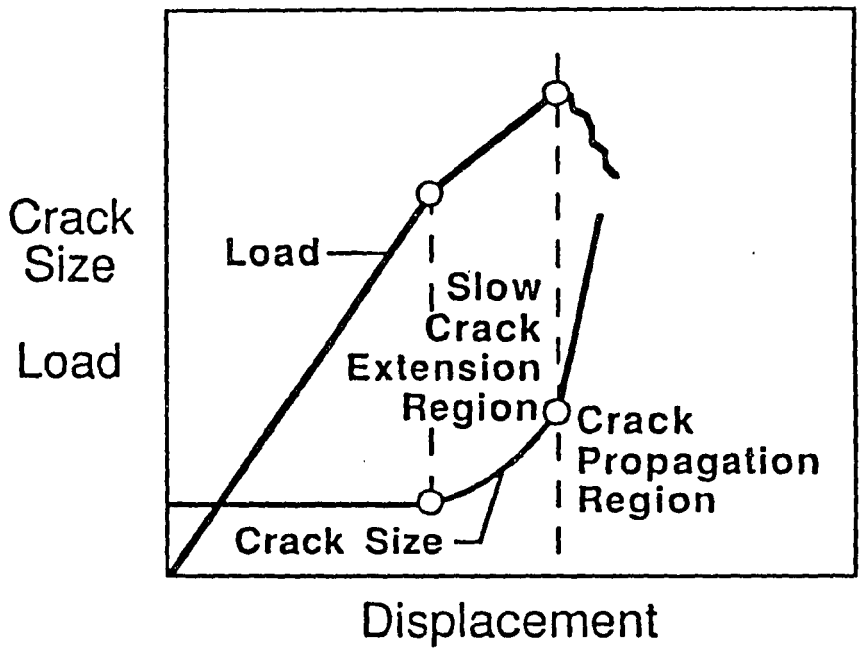

Fig. 2.7 Illustration of subcritical crack extension [22].

namely, P_C, P_{NL} and P_{SC} in,

$$G_{II}^{SH} = \frac{9a^2p^2}{4WL^3} \frac{(C - C^*_{SH})}{\left[1 + 1.5 \left[\frac{a}{L}\right]^3\right]} \qquad (3)$$

where a is the crack length, L is the half span length, W is the width, C is the compliance obtained from the initial linear portion of P-δ curve and C^*_{SH} is the modified shear compliance given by ;

$$C^*_{SH} = \frac{6L + 3a - L^3/a^2}{20\ Wh\ G_{13}} \qquad (4)$$

Chapter 3 Analysis

3.1 Finite Element Analysis

A two dimensional finite element model of the ENF specimen was constructed to calculate the compliance and strain energy release rate. Furthermore, to obtain an insight into the plastic yield process around the crack tip, stress analysis was performed. The beam dimensions were selected to represent those typical of currently used specimens.

The ENF specimen was modeled using four node, isoparametric elements "STIF 42" in the ANSYS finite element code [23]. This element assumes a unit depth and was configured to model plain strain. To prevent crack surface overlapping the frictionless contact problem was incorporated in the analysis by connecting duplicate nodes across the crack interface with truss elements (STIF 12) of zero tensile stiffness and infinite compressive stiffness. As illustrated in Fig. 3.1, STIF 12 is a two node crack interface element which allows the user to specify the compressive stiffness, the angle which the crack face makes with respect to the two defining nodes, and a coefficient of friction for the sliding surfaces.

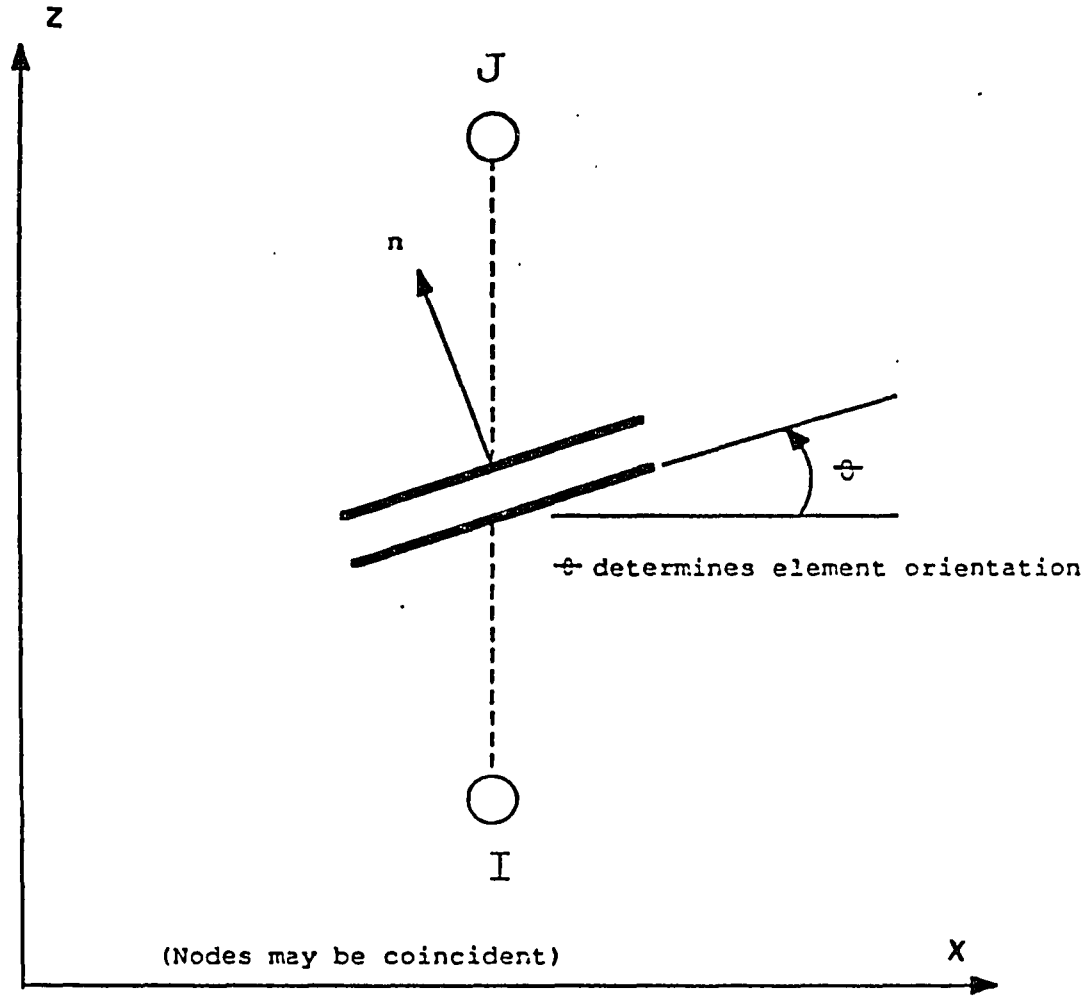

Fig. 3.1 STIF 12 interface element definition [23].

In Fig. 3.2, the finite element model is presented with displacement boundary conditions and loads specified. The horizontal constraint was required to prevent rigid body translation. The basic model was developed starting with a coarse mesh and refining after a few trial and error procedures. The model was constructed such that thermoplastic film E and thermoset FM 300 I interleaves could be defined simply by changing the material properties of the related elements to accommodate 0.0127 to 0.635 mm (0.5-25 mil) thick interleaves at the midplane of the beam. For all cases, a 25.4 mm (1 in.) crack length "a", and 101.6 mm (4 in.) span length, "2L", were used to obtain an a/L ratio of 0.5.

The element size at the crack tip was 0.0127 mm (0.0005 in.) which is consistent with finite element models reported in the literature [24,25]. The detail of the model in the vicinity of the crack tip is shown in Fig. 3.3. Crack tip elements had an aspect ratio of unity.

The following material properties ,some of which are listed in Table 2.1, were used in the analysis:

E_1= 149 GPa (21.6 Msi)

E_2= E_3= 9.4 GPa (1.36 Msi)

G_{12}= G_{13}= 7.5 GPa (1.09 Msi)

G_{23}= 3.1 GPa (0.44 Msi)

ν_{12}= ν_{13}= 0.29 and ν_{23}= 0.54

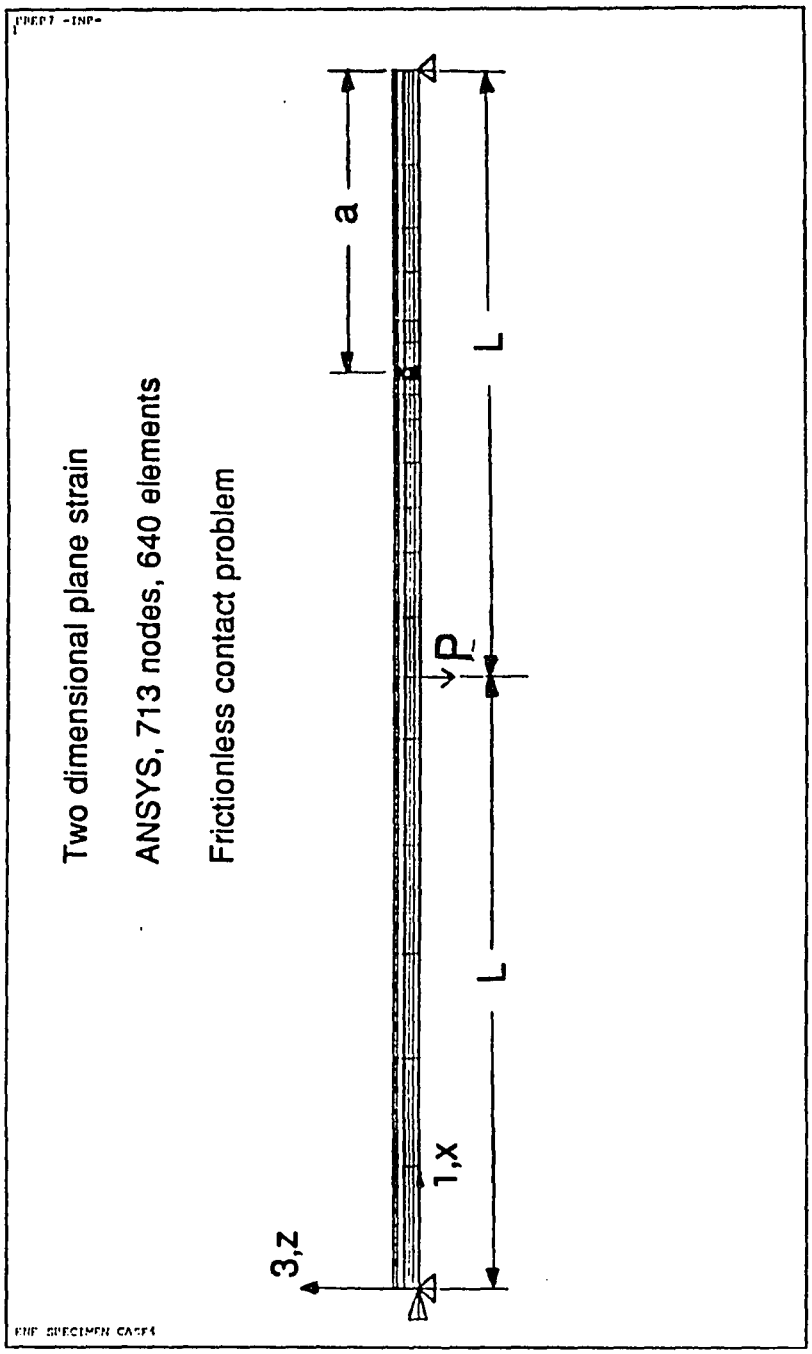

Fig. 3.2 Finite element model of the ENF specimen with the boundary conditions and loads.

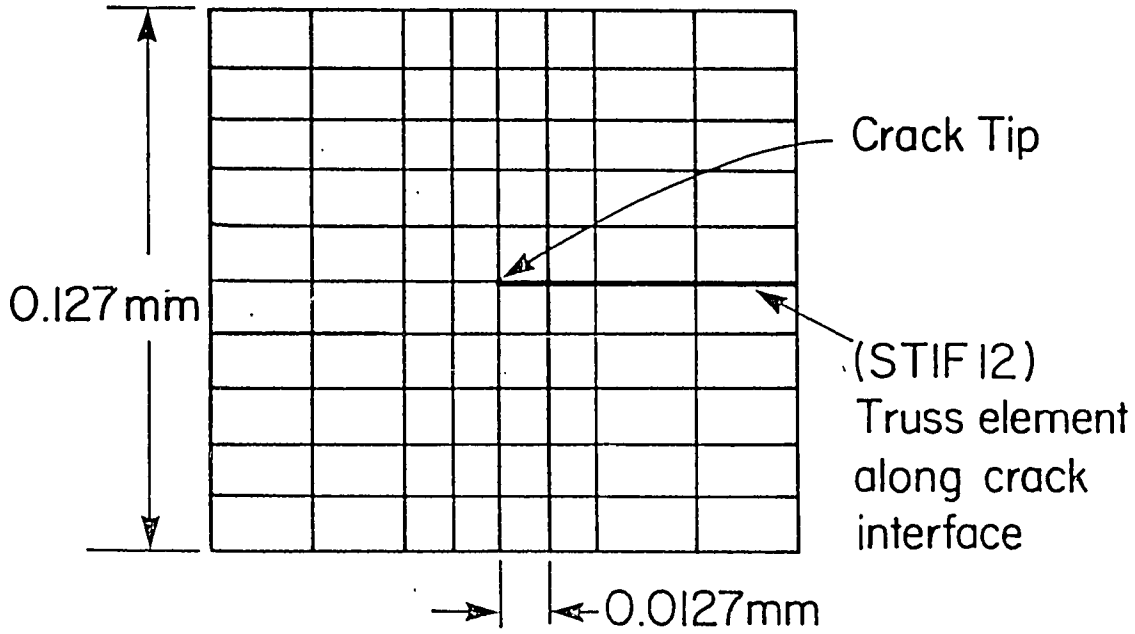

Fig. 3.3 Enlarged view of the crack tip.

For unidirectional composites, interlaminar shear modulus, G_{13}, can be approximated by the inplane shear modulus, G_{12}, without introducing a significant error. Similarly, the flexural modulus can be approximated by the axial modulus of the lamina in the fiber direction E_1.

3.1.1 Compliance of the ENF Specimen

Based on the small deflection assumptions, the compliance $C_{SH}=\delta/P$ of the ENF specimen with shear deformation included is [26]:

$$C_{SH} = \frac{\delta}{P} = \frac{2L^3 + 3a^3}{8E_1 wh^3} \left(1 + \frac{2(1.2L + 0.9a)h^2 E_1}{(2L^3+3a^3)G_{13}}\right) \quad (5)$$

where E_1 and G_{13} are the flexural and interlaminar shear moduli, respectively. Other geometric terms were described in Fig. 1.9.

To assess the accuracy of the finite element model the compliance of the cracked beam without an interleaf (baseline) was calculated using eq. (5) and compared with the finite element value. The ratio of compliance obtained from the present finite element analysis and eq. (5) is 0.989 (1.1 % difference) which is considered acceptable.

3.1.2 Strain Energy Release Rate of the ENF Specimen

Finite element analysis of the ENF specimen was also used

to evaluate the strain energy release rates. The virtual crack closure technique illustrated in Fig. 3.4 was employed [27]. With this technique, the components G_I and G_{II} of the strain energy release rate can be determined,

$$G_I = \lim_{\Delta a \to 0} \frac{1}{2\Delta a} F_c(w_c - w_d) \qquad (6)$$

$$G_{II} = \lim_{\Delta a \to 0} \frac{1}{2\Delta a} T_c(u_c - u_d) \qquad (7)$$

where F_c and T_c are the normal and tangential forces required to hold nodes c and d together. Similarly, the quantities (w_c-w_d) and (u_c-u_d) are the normal and tangential deformations corresponding to mode I and mode II crack propagation. Two finite element computations are required for each strain energy release rate calculation. In the analysis a crack length of 25.4 mm (1 in.) and a crack increment " a" of 0.0381 mm (0.0015 in.) were considered.

Near field solutions for a delamination at an interface between two dissimilar materials show that the singularity is of the form $r^{-1/2 \pm i\Gamma}$ [28-32]. The imaginary part of the singularity, the so called "oscillatory" component Γ causes nonconvergence of the individual strain energy release rate components G_I and G_{II} in a finite element computation. In this analysis this problem was avoided by putting the crack in the middle of the interleaf layer (isotropic). Hence, the

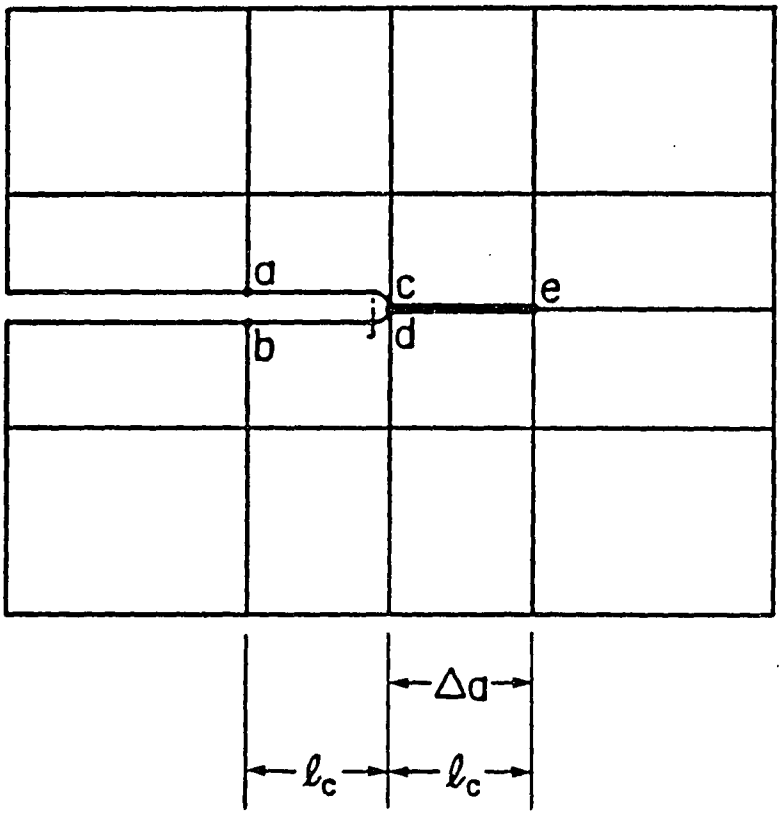

Fig. 3.4 A typical mesh near crack tip to explain virtual crack closure method.

singularity has the classical square root power without the oscillatory component. For 0.0127 and 0.0254 mm (0.5-1 mil) cases the crack was also placed at the interface to check the existence of any oscillation problem. The mode II strain energy release rate values, G_{II}, were only 0.01 % different than the ones with the crack at the center, indicating that there is no oscillation for these cases.

In all cases investigated, the quantity (w_c-w_d) in eq. (6) was identically zero for the finite element mesh presented in Fig. 3.2, meaning that the specimen is in pure shear. To further verify the accuracy of the model, the stress distribution ahead of the crack tip in the crack plane was obtained. Fig. 3.5 shows the stress state at the crack tip. The flexure (σ_x) and interlaminar normal (σ_z) stresses are identically zero along the beam centerline ahead of the crack tip and the interlaminar shear stress, τ_{xz}, is the dominant stress possessing the expected singularity at the crack tip.

For a beam with a rectangular cross section, shear stress is given by the strength of materials formula [33],

$$\tau = 3/2 \ (V/A) \qquad (8)$$

where V is the shear force and A is the area of the beam cross section. Shear stresses far away from the crack tip should

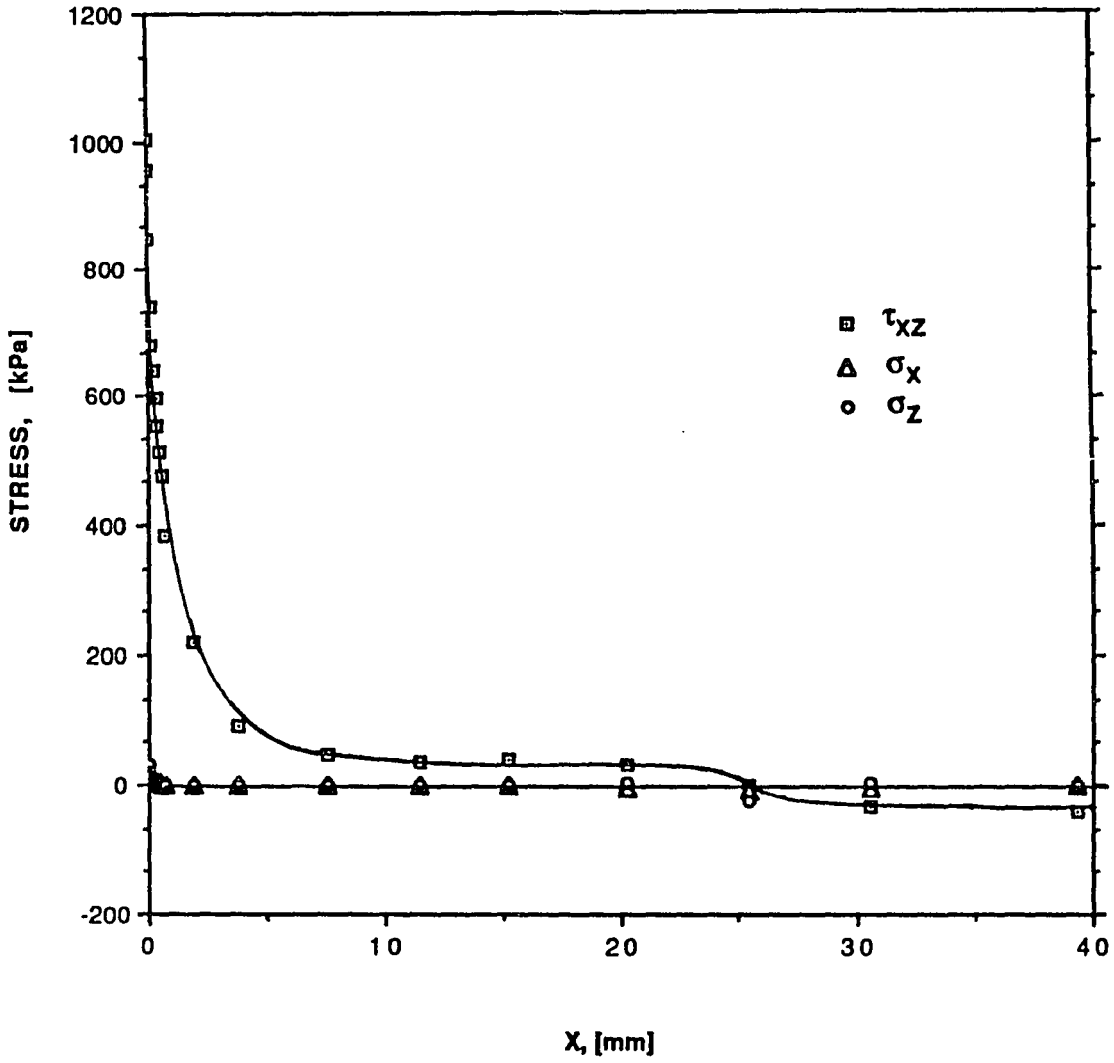

Fig. 3.5 Normal and shear stress distribution ahead of the crack tip (z=0) for the 0.0762 mm (3 mil) thick thermoplastic (film E) interleaved specimen.

approach the stress value of 38 kPA for the beam modeled here with V=2.225 N (0.5 lb.) and A=87.1 mm^2 (0.135 $in.^2$). Indeed, for x>30 mm the shear stress reaches a constant value of 38 kPa which increases confidence in the present model.

3.1.3 Estimation of Yield Zones

A quasi-elastic approach was used to calculate the plastic zone size by assuming linear elastic material response. 0.0762, 0.127, 0.381 and 0.635 mm (3-25 mil) TPI and TSI specimens were investigated. Nodal effective stresses were obtained for those elements that define the interleaf material. In order to avoid errors due to the averaging of stresses obtained from dissimilar materials interleaf-ply interface elements were ignored. A 4.45 N (1 lb.) center force was applied to the model for all cases considered. To investigate the amount of yielding around the crack tip prior to fracture, the average critical load P_c of 819 N (184 lb.) for unstable crack growth in the baseline ENF specimen was used. Rather than multiplying each effective stress value by this load, the yield strengths of the thermoplastic (film E) and thermoset (FM 300 I) interleaf materials were divided by 184 and compared with the finite element effective (von Mises) stresses computed at P=4.45 N.

It has been shown that the hydrostatic (dilatational) stress component of the applied stress tensor affects yielding

of amorphous thermoplastic resins [34]. However, as shown in Fig. 3.5, forward shear is the dominant stress in mode II. Hence, the hydrostatic component was neglected in the analysis.

3.2 Cracked Sandwich Beam (CSB) Theory for Interleaved Composites

Equations used in the experimental data reduction scheme, sect. 2.3.4, are quite accurate for the analysis of ENF specimens without an interleaf material. However, in the case of interleaved ENF specimens, results of the beam theory with shear included may be in error. Hence, it is necessary to investigate the accuracy of the beam theory and improve it to take into account the interleaf material.

Recently, there have been attempts made to include the effect of interleaving in the beam theory equations by incorporating correction factors [15]. In this study, the cracked sandwich beam (CSB) theory for interleaved composites developed by Carlsson et al. [35] was used to compare the finite element and CSB theory results for various interleaf thicknesses. The details of the derivation of the CSB theory are presented in Ref. [35]. In this section only the results of this analysis are given.

With the geometry symbols for the ENF specimen with an

interleaf shown in Fig. 3.6, the expression for the compliance is:

$$C = \frac{L^3(D'_{11})_{BC}}{6b} + \frac{L(A^*_{55})_{BC}}{2bk} + \frac{a^3[(D'_{11})_{AB}-(D'_{11})_{BC}]}{12b} + \frac{a[(A^*_{55})_{AB}-(A^*_{55})_{BC}]}{4bk} \qquad (9)$$

where L, b, and k are the half span length, width and shear correction factor, respectively. (A^*_{55}) and (D'_{11}) are elements of the inverse extensional and bending stiffness matrices, as defined in shear deformation theory. Subscripts BC and AB denote beam sections shown in Fig. 3.6.

The strain energy release rate is given by;

$$G_{II} = \frac{P^2}{8b^2}\left[a^2\left((D'_{11})_{AB} - (D'_{11})_{BC}\right) + \frac{(A^*_{55})_{AB}-(A^*_{55})_{BC}}{k}\right] \qquad (10)$$

where P is the load applied at the beam center.

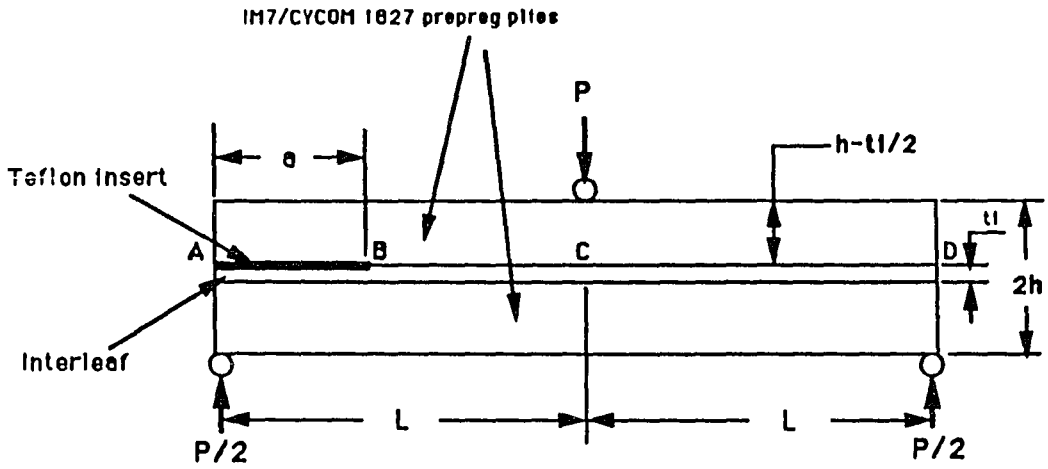

Fig. 3.6 ENF specimen geometry for the cracked sandwich beam (CSB) theory.

Chapter 4 Experimental Results and Discussion

All specimens were observed under an optical microscope prior to and after precracking and after the fracture tests. In order to interpret the fracture toughness test data better, careful microscopic observations were performed. Figs. 4.1 (a)-(c) show typical teflon insert tips for baseline, thermoplastic and thermoset interleaved (TPI & TSI) specimens. It is important to note that although TSI specimens do not possess a resin rich zone in front of the teflon insert, see Fig. 4.1 (c), baseline and TPI specimens do. It was also observed that the resin rich zone can be very long and thick for thermoplastic interleaves. A 0.0127 mm thermoplastic interleaved specimen had a resin pocket typically 5.1 mm (0.2 in.) long and 0.36 mm (0.014 in.) thick. As shown in Fig. 4.1.b, the thermoplastic film E is not perfectly flat near the teflon insert. Hence, during processing some resin gets trapped between interface and film resulting in a thick resin zone.

Fig. 4.2 is a micrograph of a specimen with thermoplastic interleaf (0.0127 mm) before and after mode II precracking. It was observed that precracking initiates an interfacial

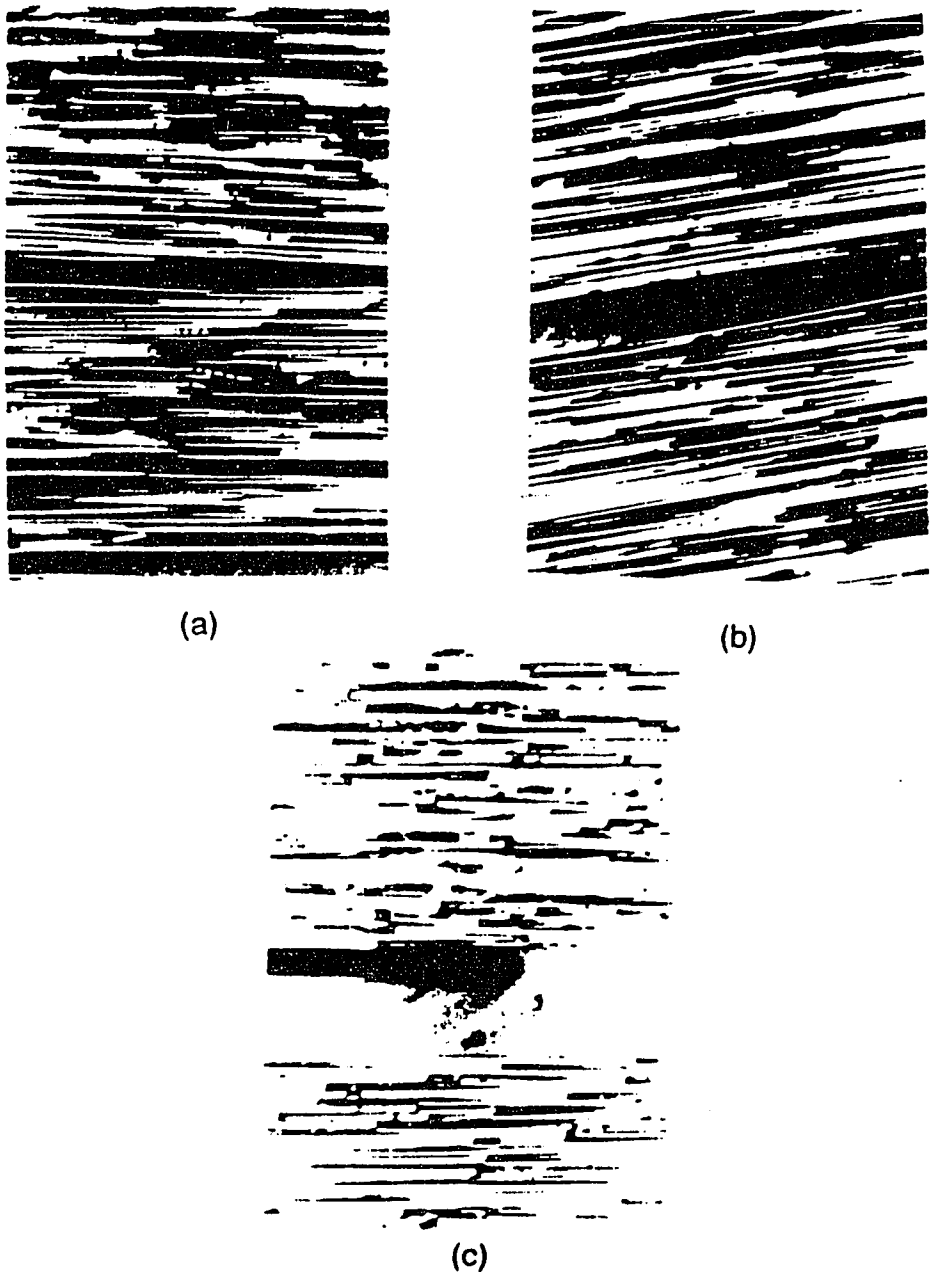

Fig. 4.1 Edge view of the crack tip zone before precracking. (a) Baseline (no interleaving) specimen, 0.0254 mm thick teflon insert (black) and resin rich zone, (b) 0.0127 mm film E interleaf (curved) and teflon insert in a resin rich zone, 165X, (c) 0.086 mm FM 300 I interleaf and teflon insert but no resin rich zone, 165X.

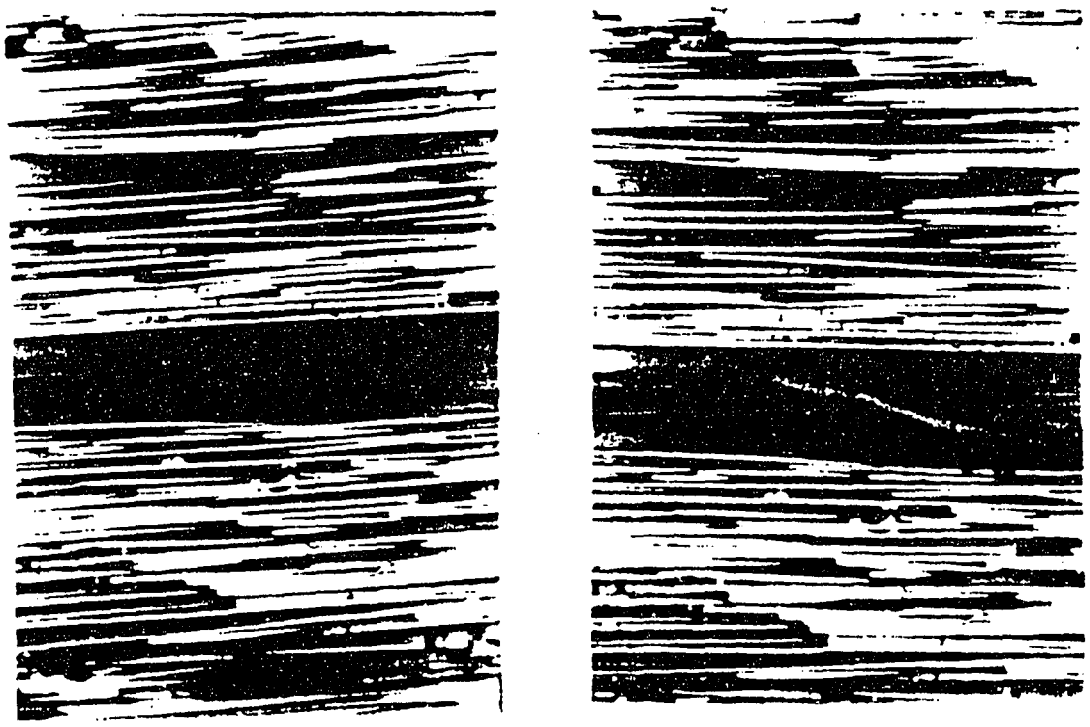

Fig. 4.2 Edge view of 0.0127 mm film E interleaved specimen, 165X. (a) teflon insert and interleaf before precracking, (b) crack tip after precracking.

crack between the film and composite rather than a cohesive failure in TPI specimens. In contrast, as shown in Fig 4.3 (a), the crack grows through the interleaf in TSI specimens. One possible reason for this is that, TSI specimens were manufactured by film stacking. Hence, there may be less resistance to crack growth between interleaf layers than at composite/interleaf interface. Thermoplastic interleaves were available in each thickness used here, and they were adhesively bonded on the prepreg layers as single films.

As it was mentioned in sect. 2.4.2, some of the specimens failed in flexure during mode II precracking. Consequently, for those specimens it was necessary to initiate the crack first in mode I (tension) then in mode II (forward shear). Fig.4.3 (b) shows a typical mode I crack tip. Notice that both mode I and mode II crack tips have unique appearances which reflect the loading conditions under which they are initiated. The mode I crack tip is sharp and straight while the mode II crack tip has a series of sigmoidal shaped microcracks with an orientation of 45^0 to the fiber direction which is the principal normal stress plane, see Fig. 4.3 (a).

Figs. 4.4 & 4.5 show typical load versus deflection diagrams for the thinnest and thickest TPI and TSI ENF specimens, respectively. The onset of crack growth observed with the travelling microscope is marked with an "x" on the

(a)

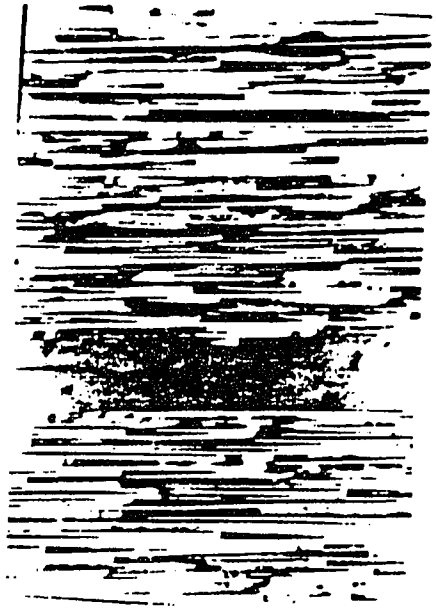

(b)

Fig. 4.3 Mode II and mode I crack tips. (a) mode II crack tip of 0.256 mm FM 300 I interleaved specimen, 83X, (b) mode I precrack of 0.084 mm FM 300 I interleaved specimen, 165X.

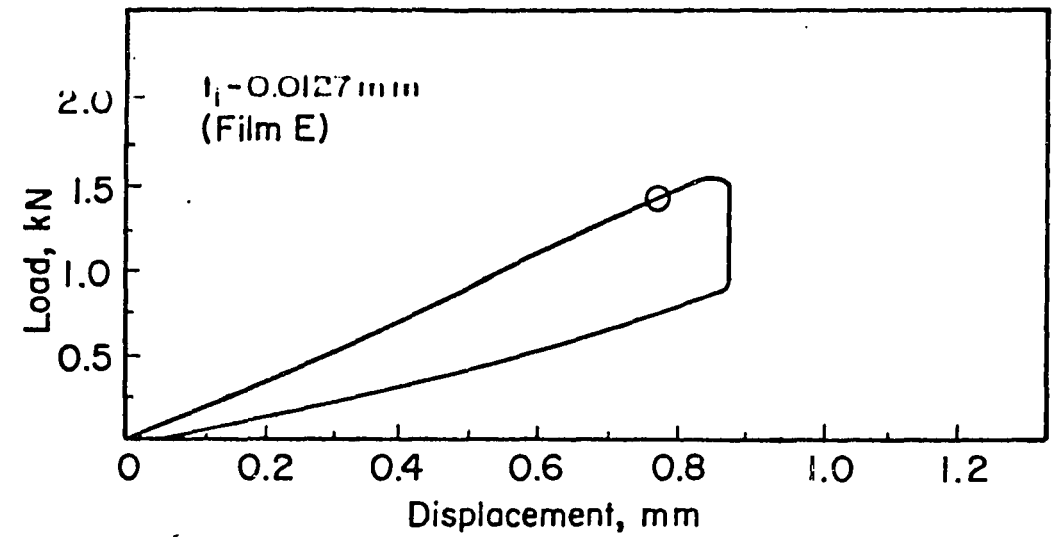

(a)

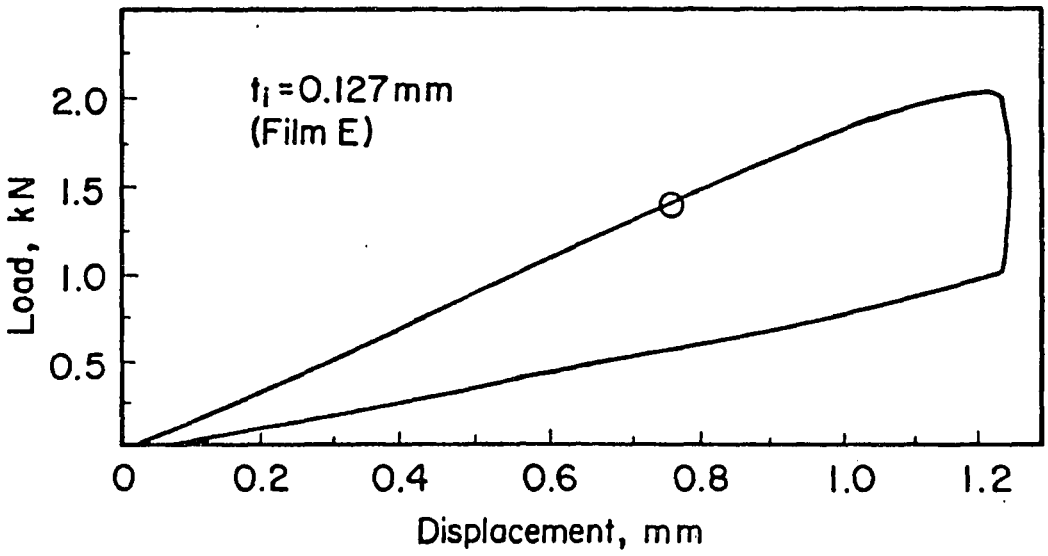

(b)

Fig. 4.4 (a) & (b) load deflection diagrams of 0.0127 and 0.127 mm film E interleaved specimens, respectively.

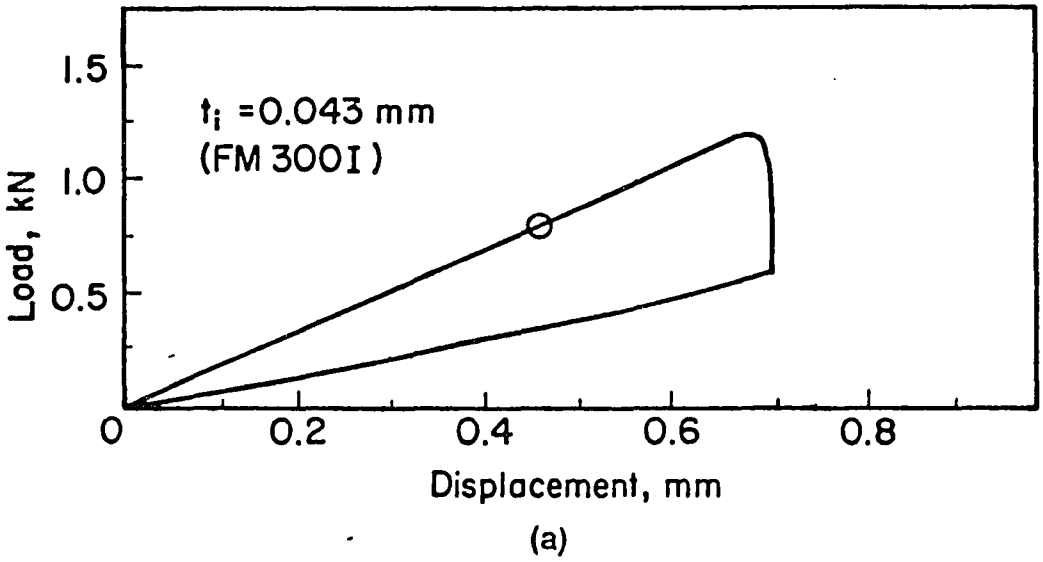

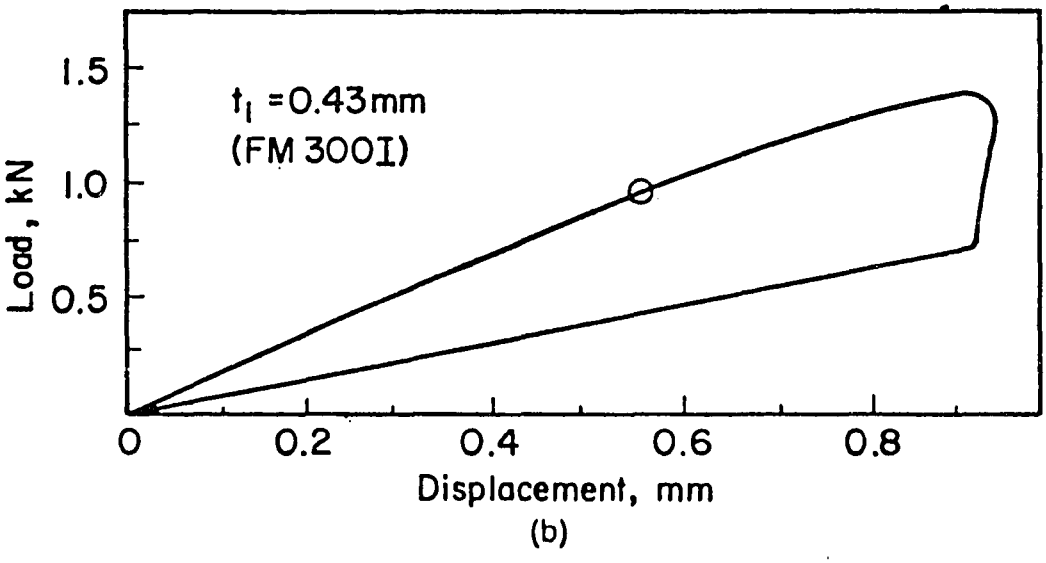

Fig. 4.5 (a) & (b) load deflection diagrams of 0.043 and 0.43 mm FM 300 I interleaved specimens, respectively.

P-δ curve. The degree of nonlinearity is significant for the thick interleaves of both systems. This is consistent with the increased degree of nonlinearity observed with increased bond thickness in adhesively bonded joints [16].

The fracture toughnesses, G_{IISC}, G_{IINL}, G_{IIC} defined according to Fig. 2.6, were determined using the beam theory formulas (with shear deformation included) given in sect. 2.4.4. Table 4.1 is a list of the average fracture toughnesses and compliances obtained from 5 to 8 specimens of each kind.

It is important to restate that, the total thickness of the specimens was kept approximately constant by reducing the number of prepreg plies for the thicker interleaves. However, compliance values in Table 4.1 show that even a slight increase in thickness of the specimen, see Table 2.3, results in a lower compliance value.

4.1 Thermoplastic Interleaves

Fig. 4.6 shows a plot of critical strain energy release rate, G_{IIC}, versus interleaf thickness for thermoplastic interleaved specimens. There is an initial sharp increase in G_{IIC} from the baseline value of 650 J/m^2 to 2720 J/m^2 ($\approx$ 4 times) for the 0.0127 mm TPI specimens. It is interesting to note that the relative increase in G_{IIC} for 0.0127 mm (0.5 mil)

Interleaf thickness mm(mil)		Compliance (m/N) x 10^{-5}	G_{IIsc} J/m^2 (in.lb/in^2)	G_{IINL} J/m^2 (in.lb/in^2)	G_{IIc} J/m^2 (in.lb/in^2)
0	Baseline	5.164±.20	461±58 (2.6)	542±35 (3.1)	652±48 (3.73)
.127 (.5)	Film E	4.986±.28	1643±138 (9.4)	2066±55 (11.8)	2715±40 (15.5)
.0254 (1)	"	5.416±.37	191±58 (1.1)*	207±50 (1.2)*	322±33 (1.8)*
.0762 (3)	"	5.139±.26	1145±58 (6.54)	1642±270 (9.4)	1769±123 (10.1)
.127 (5)	"	5.315±.26	1275±390 (7.3)	1959±46 (11.2)	4266±117 (24.4)
.043 (1.7)	FM 300 I	5.063±.16	1004±140 (5.7)	1751±130 (10)	1909±94 (10.9)
.086 (3.4)	"	5.238±.30	1649±168 (9.4)	1649±171 (9.4)	2527±66 (14.4)
.172 (6.8)	"	5.439±.15	1467±108 (8.4)	1467±90 (8.4)	2219±84 (12.7)
.256 (10.2)	"	5.167±.19	1916±108 (10.9)	1916±100 (10.9)	2725±108 (15.6)
.429 (17)	"	5.097±.38	1435±30 (8.2)	1435±25 (8.2)	2075±100 (11.9)

* Poor adhesion between interleaf and composite.

Table 4.1 Compliance and fracture toughness data.

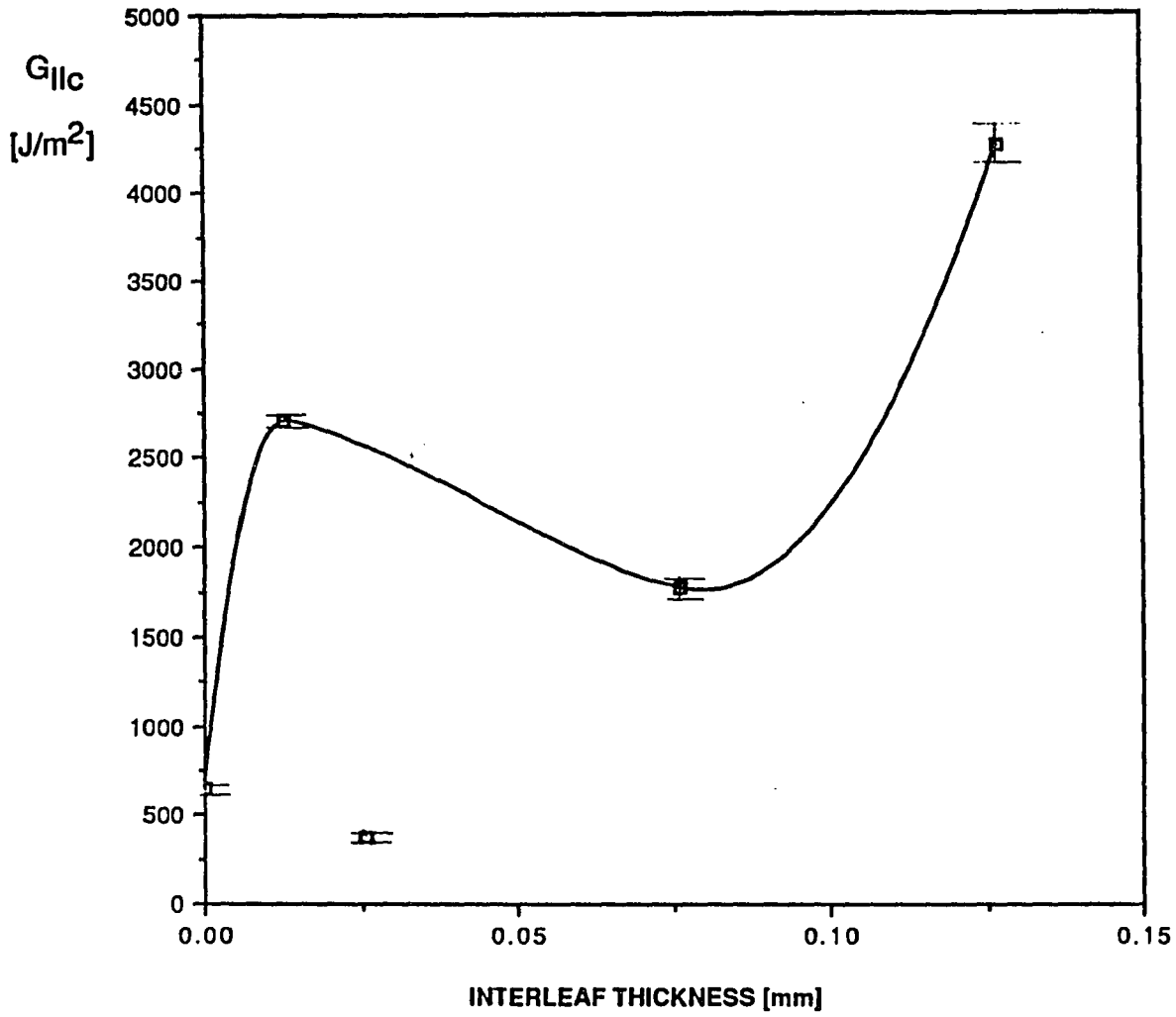

Fig. 4.6 Mode II fracture toughness vs. thermoplastic (film E) interleaf thickness.

TPI specimens is consistent with Masters' results for AS4/1808 graphite/epoxy interleaved with film E of the same thickness. He found that interleaving increased G_{IIC} from 1310 J/m^2 to 3850 J/m^2 ($\approx$ 3 times) for the same type of specimen. The G_{IIC}, for 0.0254 mm (1 mil) TPI specimen is surprisingly low, 320 J/m^2. This point was neglected in curve fitting, see Fig. 4.6. It is noteworthy that seven specimens tested for this case gave consistent G_{IIC} values with a standard deviation of only 33 J/m^2, indicating an adhesion problem which is likely due to contamination on that particular interleaf during composite manufacture. The fracture toughness for 0.0762 mm (3 mil) TPI specimen is slightly lower than that of the 0.0127 mm thick interleaf, (1770 J/m^2 with a standard deviation of 123 J/m^2). The largest fracture toughness, 4270 J/m^2, was obtained for the thickest (0.127 mm) interleaf.

Figs. 4.7 (a) and (b) are micrographs of the 0.0254 and 0.0762 mm (1 and 3 mil) TPI specimens before precracking. A thick dark line along the interface is observed which might be an indication of poor adhesion between the interleaf and adjacent plies. For comparison, the micrograph of a 0.127 mm TPI specimen is shown in Fig. 4.7 (c) which reveals no distinct dark line along the film/composite interface. Indeed, the interface shown in Fig. 4.7 (c) is very similar to the one for a TSI, see Fig. 4.1 (c).

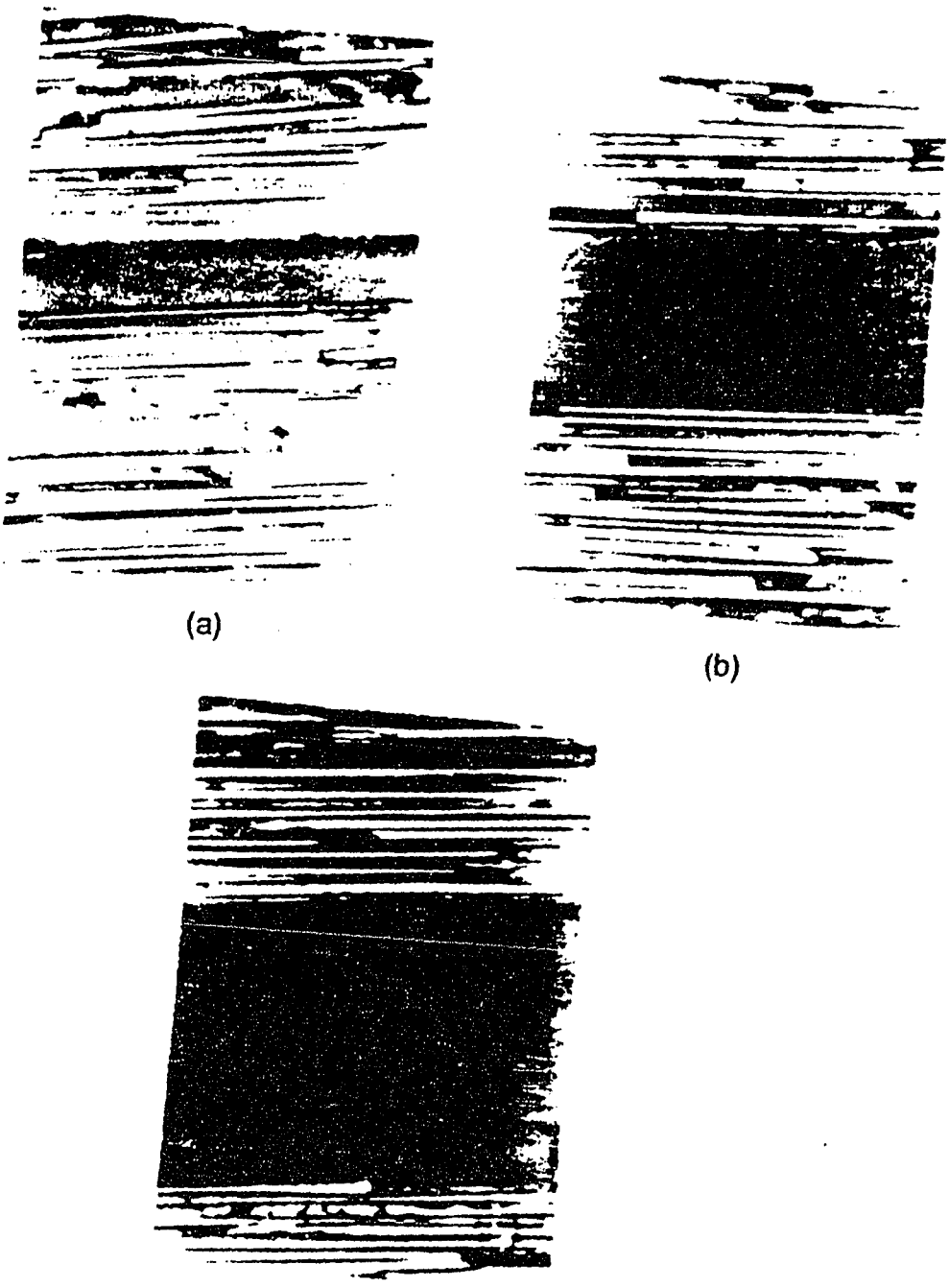

Fig. 4.7 Edge views of film E interleaved specimens before precracking, 330X. (a) 0.0254 mm film E, (b) 0.0762 mm film E, (c) 0.127 mm film E.

Figs. 4.8 (a) and (b) are post fracture micrographs of the crack in 0.0127 and 0.0254 mm (0.5 and 1 mil) TPI specimens. The crack surfaces were slightly separated to enhance observation of the crack path. In the 0.0127 mm (0.5 mil) TPI specimen the crack grows in the composite as well as at the film/composite interface. On the other hand, in 0.0254 mm (1 mil) interleaved one, the crack grows at the interface only. Furthermore, the crack path for the 0.0254 mm thick interleaf is smoother (smooth line) than that of the 0.0127 mm, which is further evidence of little resin deformation and poor adhesion.

In order to gain more insight, the specimens were split apart for further inspection. Fig. 4.9 shows the fracture surfaces of TPI specimens. Both the 0.0762 and 0.0254 mm (3 and 1 mil) TPI specimens were easy to break apart. The interleaf film E peeled off as a single ply and the fracture surfaces were very clean and shiny. On the other hand, the 0.0127 mm thick interleaf showed signs of considerable amount of deformation. Another interesting observation was the existence of bundles of fibers stuck on the 0.127 mm (5 mil) thick film, see Fig. 4.10. These specimens were extremely difficult to break apart. Therefore, it is clear that adhesion was not a problem with 0.127 mm (5 mil) thick TPI specimen. More importantly, Fig. 4.10 suggests the existence of fiber bridging in mode II (forward shear) loading although it is

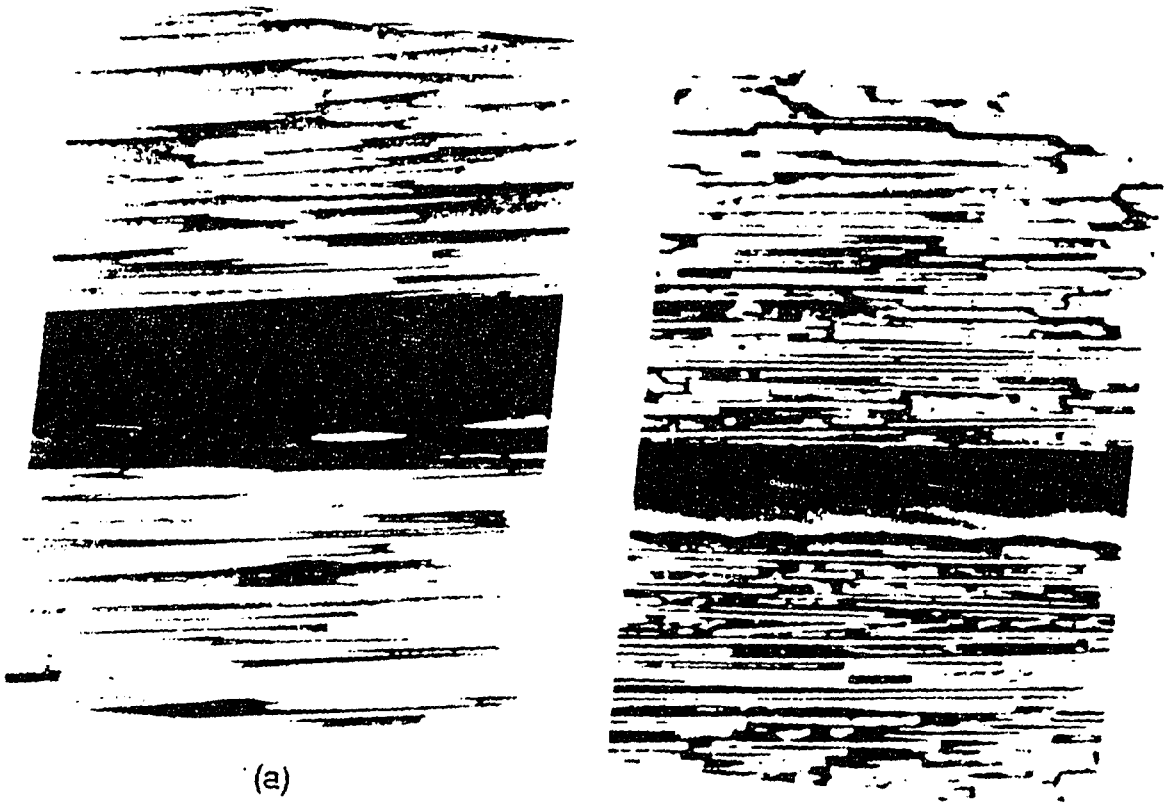

Fig. 4.8 Edge views of film E interleaved specimens after testing, 165X. (a) crack growing through the plies in 0.0127 mm film E interleaved specimen, (b) interfacial crack with very little deformation, 0.0254 mm film E interleaved specimen.

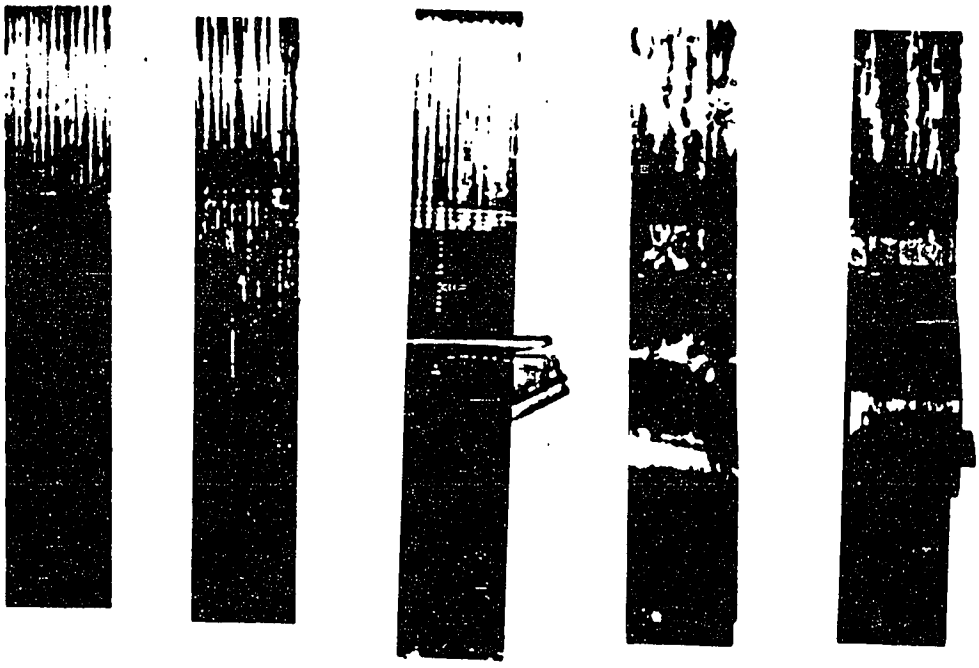

Fig. 4.9 Fracture surfaces of film E interleaved specimens.

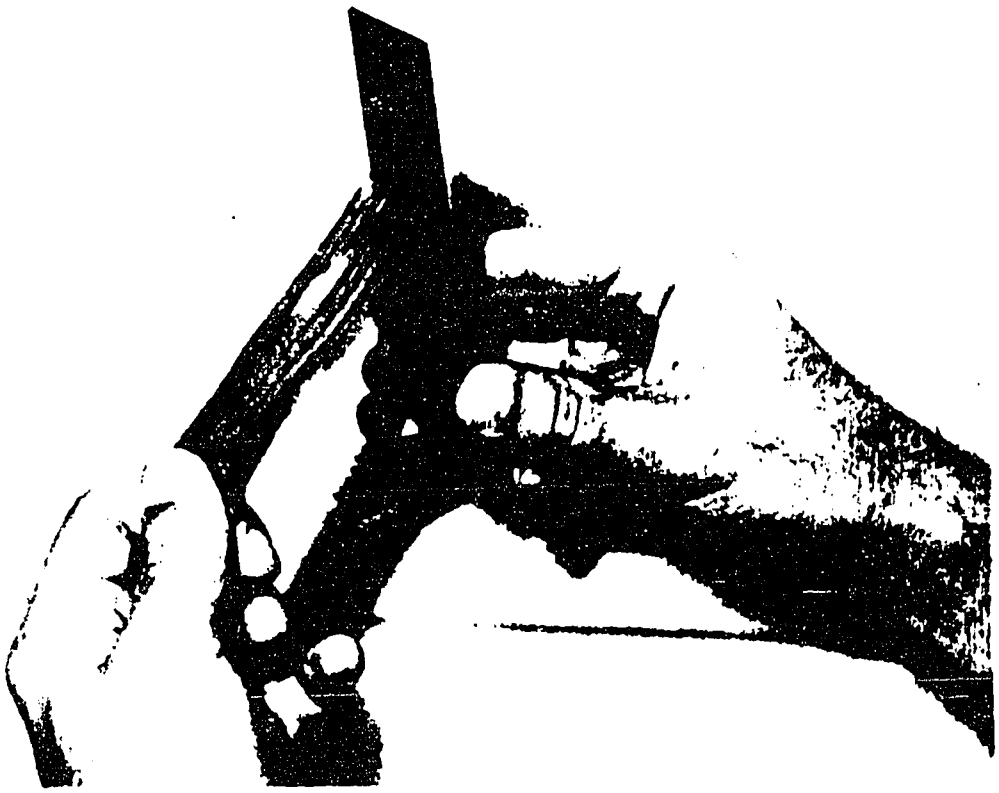

Fig. 4.10 Fiber bundles on 0.127 mm thick film E interleaf.

usually observed in mode I (tension) delamination [36]. Hence, the very large fracture toughness for this case (≈ 6.5 times the baseline value) can be attributed mostly to the fiber bridging, because the apparent deformation on the rest of the film was not very different from the other specimens.

The fracture surfaces were also investigated under an optical microscope. The area of main interest was the deformation zone very close to the initial crack tip. This region corresponds to the crack initiation region where the fracture toughness is measured. Figs. 4.11 (a)-(c) show the fracture surfaces of 0.0127, 0.0254 and 0.0762 mm (0.5, 0.1 and 3 mil) TPI specimens. The 0.0127 mm film, Fig. 4.11 (a), has a rough appearance with traces and strips of fibers on it. The surface is almost fully covered with the film which means a good adhesion. The round entities are film E deformed in the direction of shear loading (crack propagation direction). Masters [8] observed exactly the same features with the same kind of interleaf. This deformation mechanisms is very similar to the shear lip formation mechanism suggested for mode II deformation of ductile polymers [37], see Fig. 4.12. In accordance with the previous observations, the 0.0254 mm thick TPI, Fig. 4.11 (b) has a flat, clean fracture surface showing no indication of deformation even at 200X magnification. Fig. 4.11 (c) has the same magnification as Fig. 4.11 (a). Note that the deformation of the 0.0762 mm film is less than that

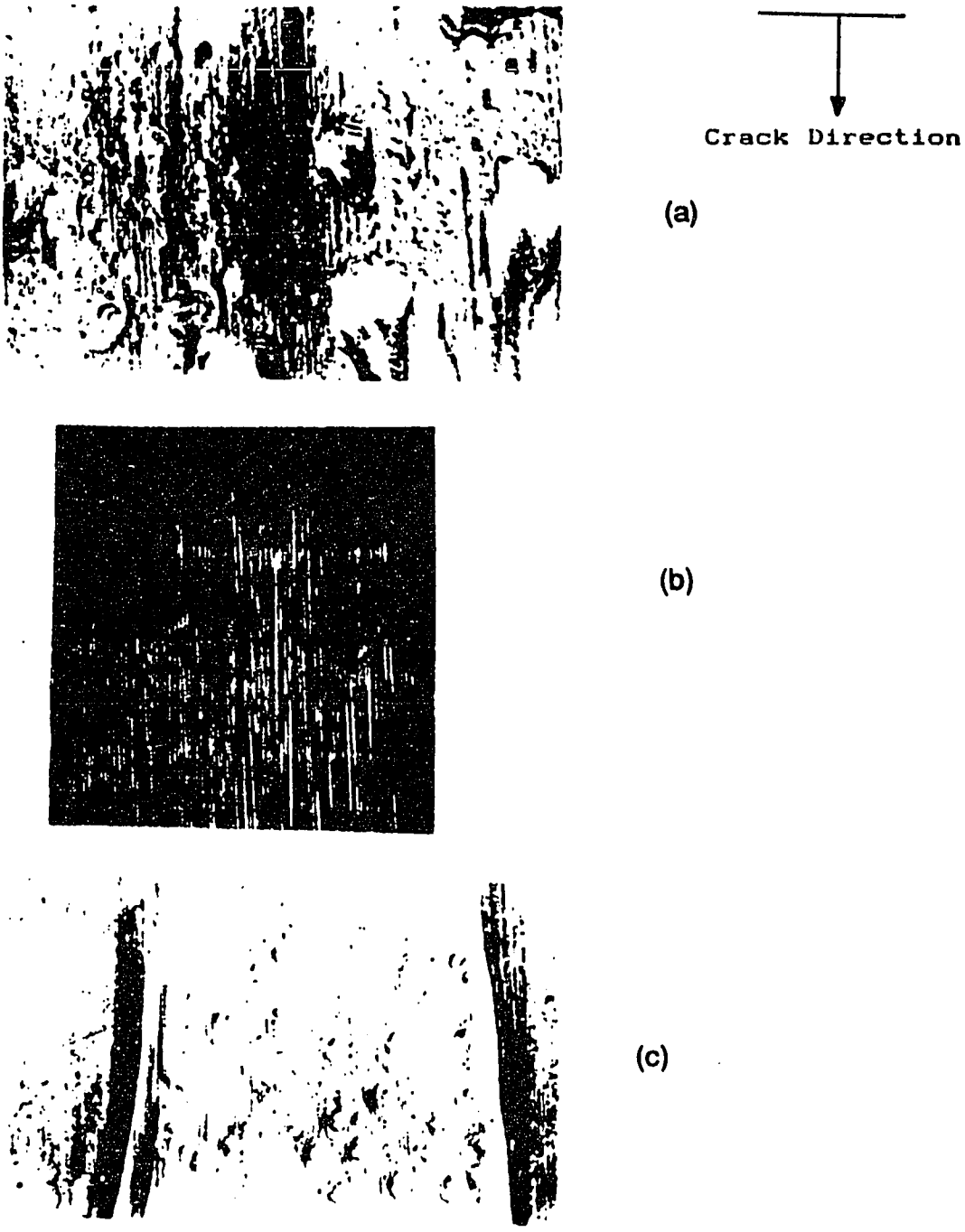

Fig. 4.11 Fracture surfaces of film E interleaved specimens in the vicinity of the original crack tip. (a) 0.0127 mm film E, 41X, (b) 0.0254 mm film E, 200X, (c) 0.0762 mm 41X.

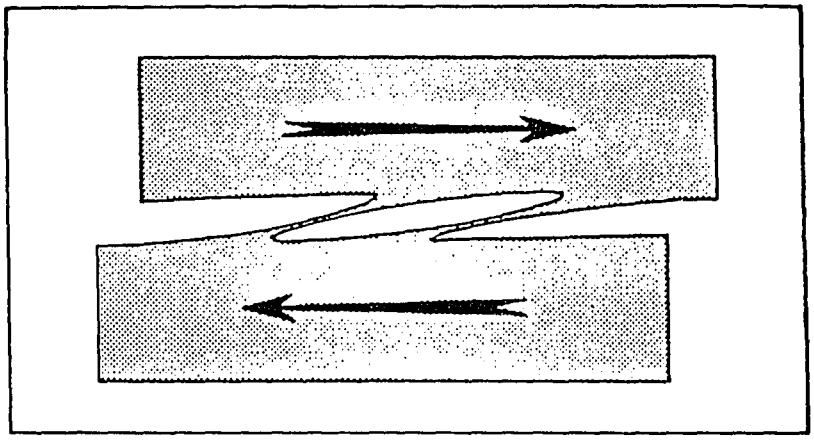

Fig. 4.12 Schematic of suggested mechanism for shear lip formation in the PEEK matrix during mode II fracture [36].

of the 0.0127 mm film indicating local adhesion problem. These observations verify the previous results and help explain the fracture toughnesses obtained for TPI specimens.

Figs. 4.13 (a)-(b) are micrographs of fracture surfaces of a 0.127 mm (5 mil) TPI specimen. As previously shown in Fig. 4.10, the 0.127 mm film has bundles of fibers stuck on it. Therefore, the surfaces seen in Figs. 4.13 (a) and (b) are essentially IM7/CYCOM 1827 prepreg plies. Although there is some matrix deformation as evidenced by the hackles (i.e. regions of epoxy matrix between the fibers that show a "factory roof" appearance), the major toughening mechanism still seems to be the fiber bridging. The white islands of resin material in Fig. 4.13 (b) are epoxy (CYCOM 1827) resin between the prepreg and the interleaf (i.e. not thermoplastic film).

Fig. 4.14 shows the subcritical and nonlinear fracture toughnesses of thermoplastic film E interleaved specimens. These curves have the same trend as the critical strain energy release rate versus interleaf thickness curve shown in Fig. 4.6, except for 0.127 mm (5 mil) thick interleaved specimen. As mentioned before, a significant energy absorbing mechanism during interlaminar fracture of the 0.127 mm TPI specimens is fiber bridging. Subcritical crack growth and onset of nonlinearity which precedes unstable crack growth, however,

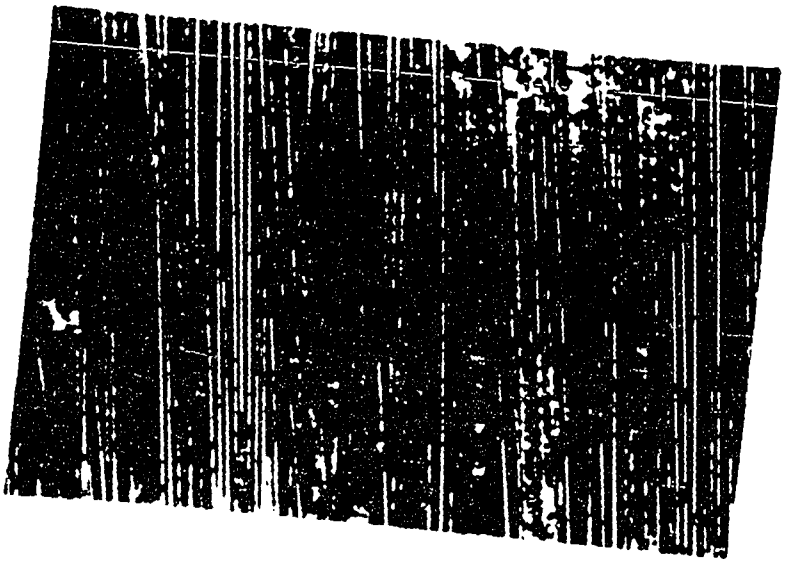

(a)

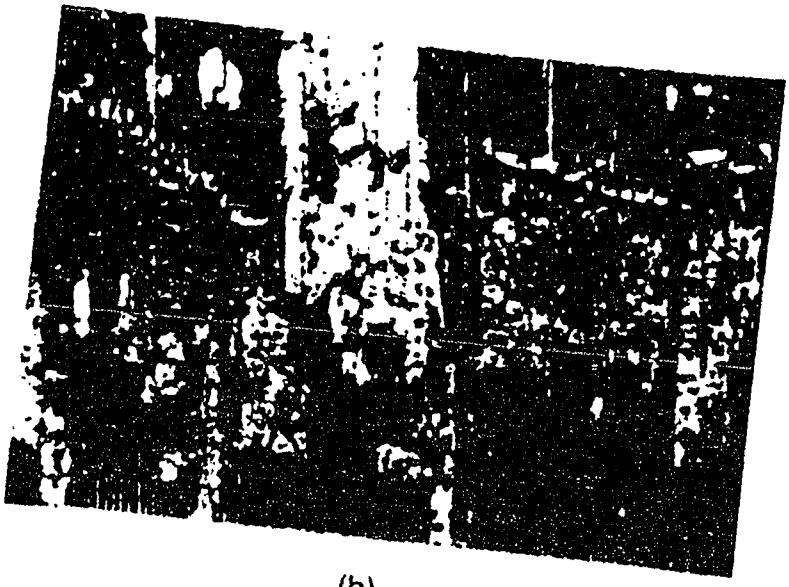

(b)

Fig. 4.13 (a) & (b) fracture surfaces of 0.127 mm film E interleaved specimen, 165X.

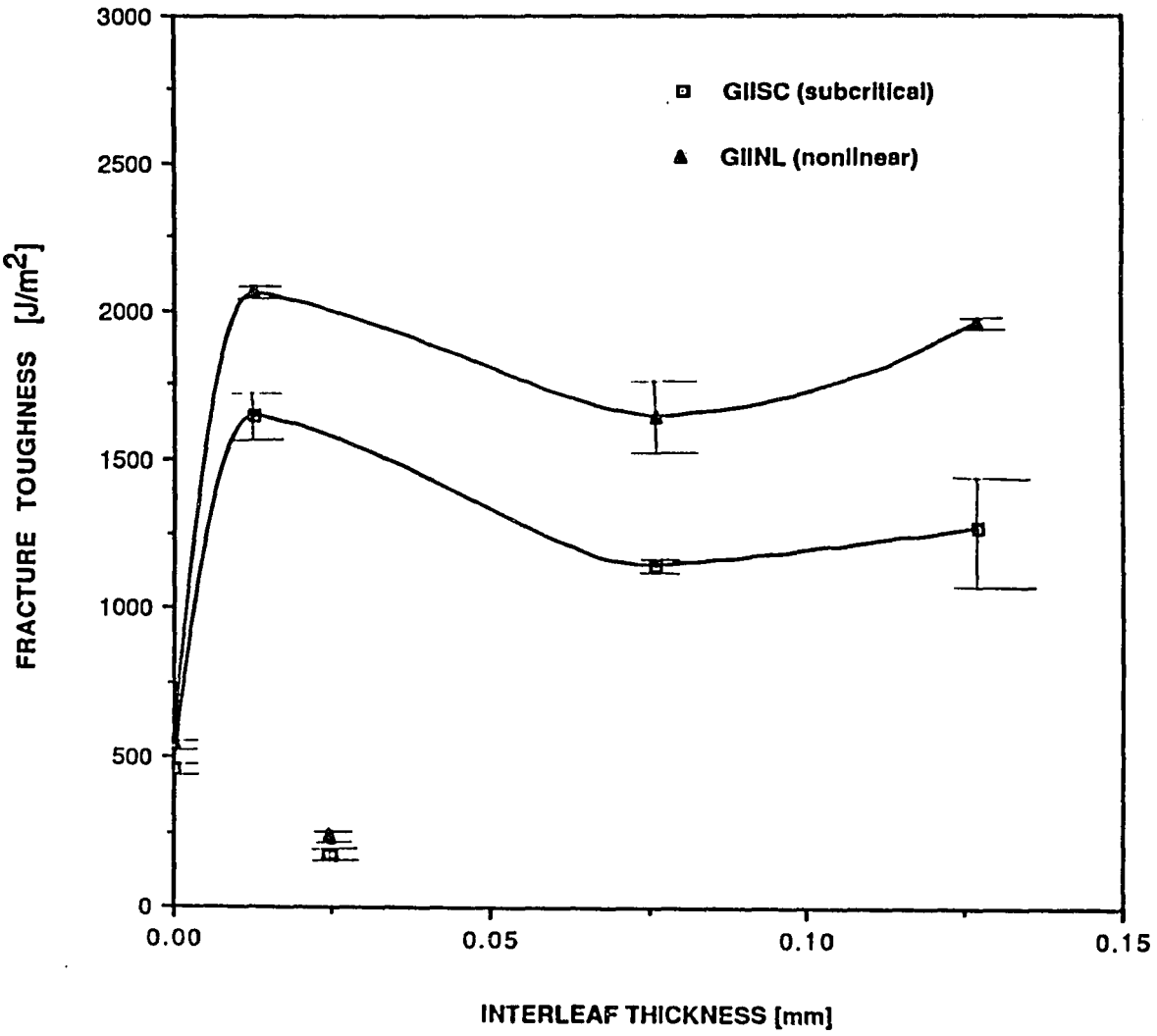

Fig. 4.14 Mode II nonlinear and subcritical fracture toughness vs. thermoplastic (film E) interleaf thickness.

are mostly due to plastic yield and/or viscoelasticity in the vicinity of the crack tip and coalescence of microcracks in the interleaf layer. Therefore, for 0.127 mm interleaved specimen, subcritical and nonlinear crack growths occur at much lower loads than the unstable crack growth.

The large difference between the fracture toughness curves in Fig. 4.14 show that for thermoplastic film E interleaved IM7/CYCOM 1827 graphite/epoxy the onset of subcritical and nonlinear crack growth do not coincide, except for the baseline case (uninterleaved). Furthermore, the difference increases with the interleaf thickness.

4.2 Thermoset Interleaves

Fig. 4.15 shows the G_{IIC} versus interleaf thickness for thermoset (FM 300 I) interleaved (TSI) specimens. Similar to the thermoplastic results, there is an initial sharp increase in fracture toughness from the baseline value of 650 J/m^2 to 2530 J/m^2 for the 0.086 mm (3.4 mil) TSI specimen ($\approx$ 4 times). Also note that the variation in fracture toughness with thermoset interleaf thickness is not as dramatic as for the thermoplastic interleaves. The maximum fracture toughness, 2730 J/m^2, was obtained for 0.256 mm (10.2 mil) interleaf thickness. This value is very close to the fracture toughness of 0.0127 mm (0.5 mil) TPI specimen, 2720 J/m^2. Hence, It is possible to obtain a fracture toughness that is four times the

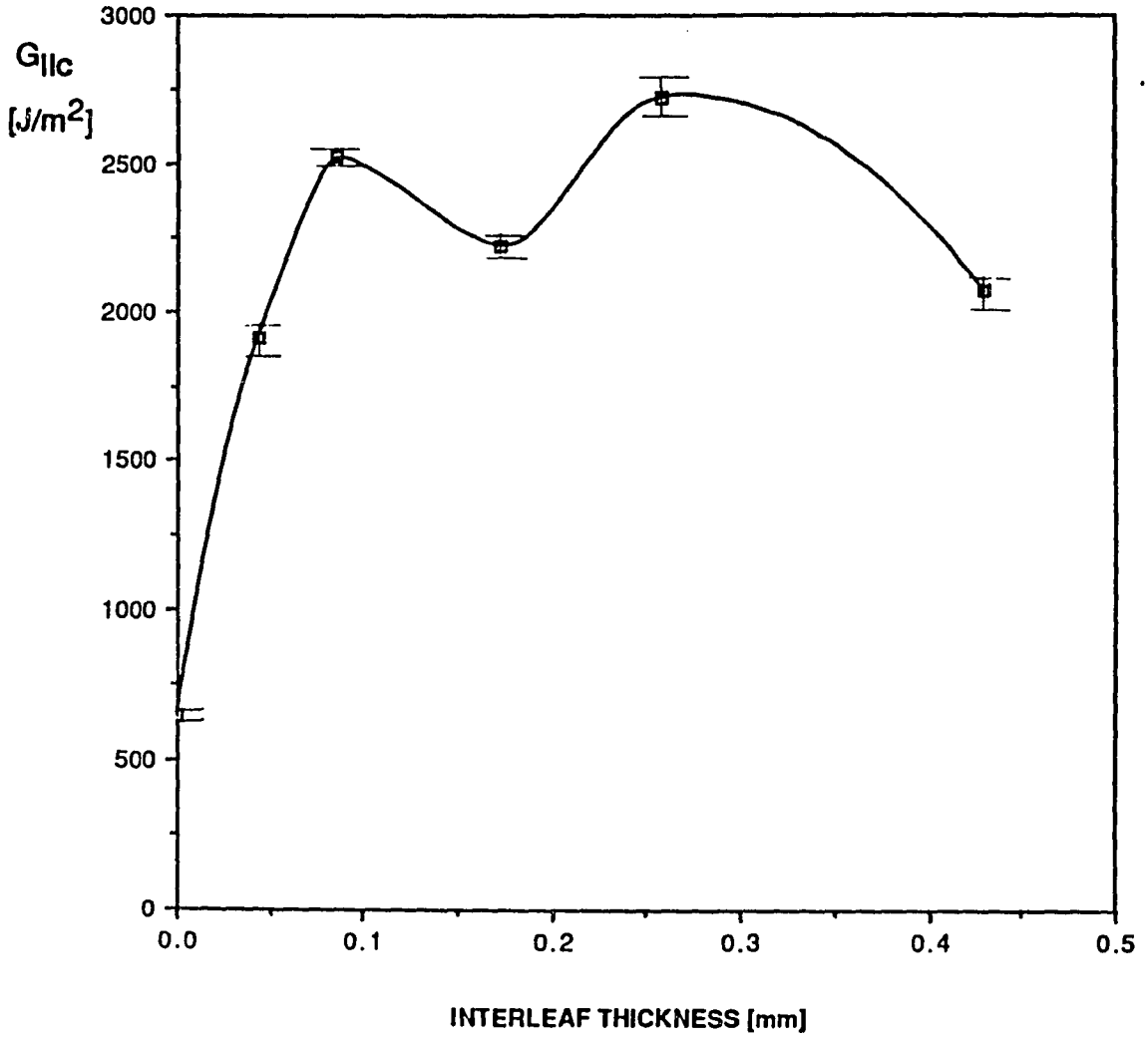

Fig. 4.15 Mode II fracture toughness vs. thermoset (FM 300 I) interleaf thickness.

baseline value with a twenty times thinner thermoplastic film. This is evidently a result of the desirable combination of mechanical properties of the thermoplastic polymer.

The TSI specimens were also examined in an optical microscope. A scanning electron microscope (SEM) was only needed for the investigation of fracture surfaces of thick interleaved specimens. Samples for SEM were cut using a Buehler Isomet low speed saw and cleaned in a Buehler Ultramet III sonic cleaner.

Figs. 4.16 (a)-(c) are the post-fracture micrographs of the edges of the 0.086, 0.256 and 0.429 mm (3.4-17 mil) TSI specimens. Note the difference in magnifications. It is important to note that in TSI specimens the crack does not follow a single, straight path. Instead, as was shown in Fig. 4.3, it grows in the principal stress plane at a 45^0 angle to the maximum shear direction. Also, there are several secondary cracks growing simultaneously as the specimen is loaded. Figs. 4.16 (a)-(b) show a secondary crack which essentially starts horizontally at the specimen midplane and grows at both ends in a 45^0 angle towards the interfaces. Fig. 4.16 (c) shows the end of a secondary crack joining the main (original) one at the bottom interface. The summary of crack initiation and growth observed in TSI specimens is shown schematically in Fig. 4.17.

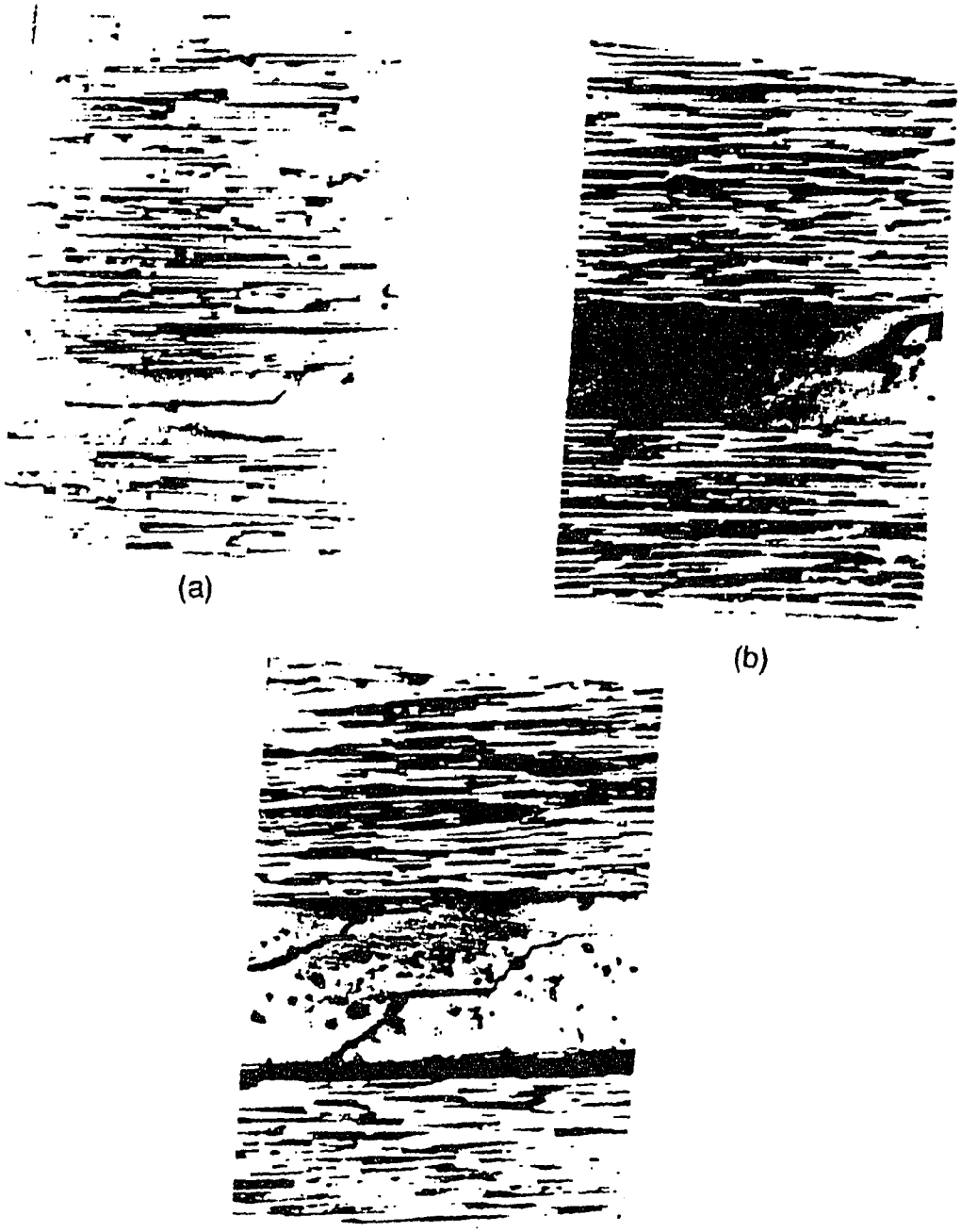

Fig. 4.16 Edge views of FM 300 I interleaved specimens. (a) formation of a secondary crack in a 0.086 mm interleaf, 165X, (b) a developed secondary crack in a 0.256 mm thick interleaf, 83X, (c) secondary cracks joining the main one in a 0.43 mm thick interleaf, 83X.

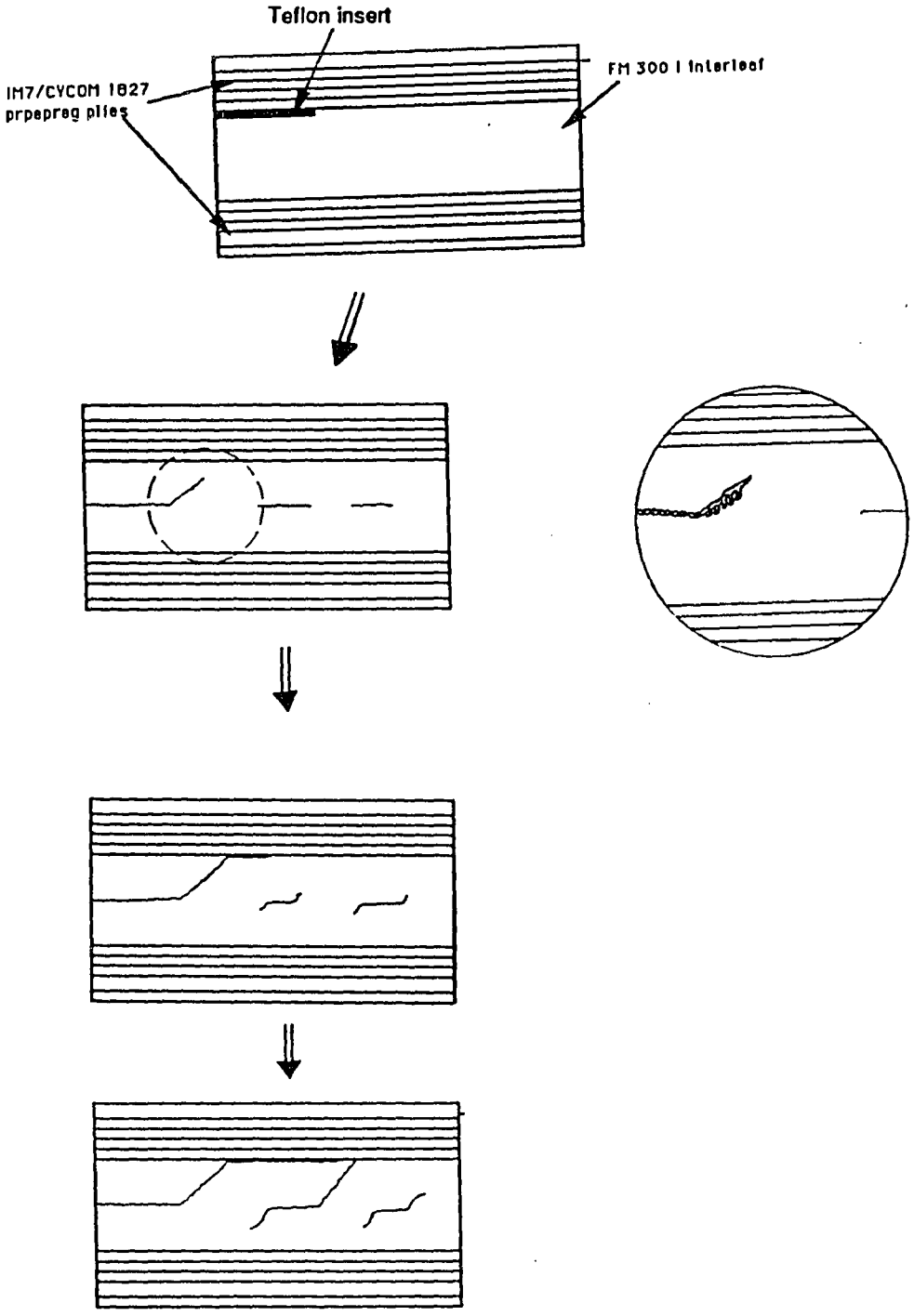

Fig. 4.17 Schematic of crack initiation and propagation in thermoset (FM 300 I) interleaved IM7/CYCOM 1827 under mode II loading.

Figs. 4.18 (a)-(d) are the post- fracture micrographs of 0.043 and 0.086 mm (1.7 and 3.4 mil) TSI specimens. Fig. 4.18 (a) shows a crack changing its path between the two interfaces in accordance with Fig. 4.17. In Fig. 4.18 (b) the crack grows through the plies, which is a further evidence of very strong adhesion between the IM7/CYCOM 1827 prepreg plies and the FM 300 I interleaves. Note the 45^0 angle in Fig. 4.18 (a) and the deformed interleaf in Figs. 4.18 (c) and (d).

Figs. 4.19 (a)-(c) are micrographs of 0.256 mm (10.2 mil) TSI specimen which has the largest fracture toughness, 2730 J/m^2 recorded for thermoset interleaves. Note that the magnification is 83X which is half the one in Fig. 4.18. Even at this low magnification there is a considerable amount of deformation observed, as evidenced by the sigmoidal shaped microcracks.

Figs. 4.20 (a) and (b) are micrographs of the fracture surfaces of 0.043 and 0.086 mm (1.7 and 3.4 mil) TSI specimens. Again hackles appear to be formed by the coalescence of a series of sigmoidal shaped microcracks. Note that these occur in the interleaf and not in the epoxy matrix. Although both micrographs look similar, Fig. 4.20 (b) has slightly larger amount of deformation which might account for the larger fracture toughness obtained with the 0.086 mm (3.4 mil) TSI specimens.

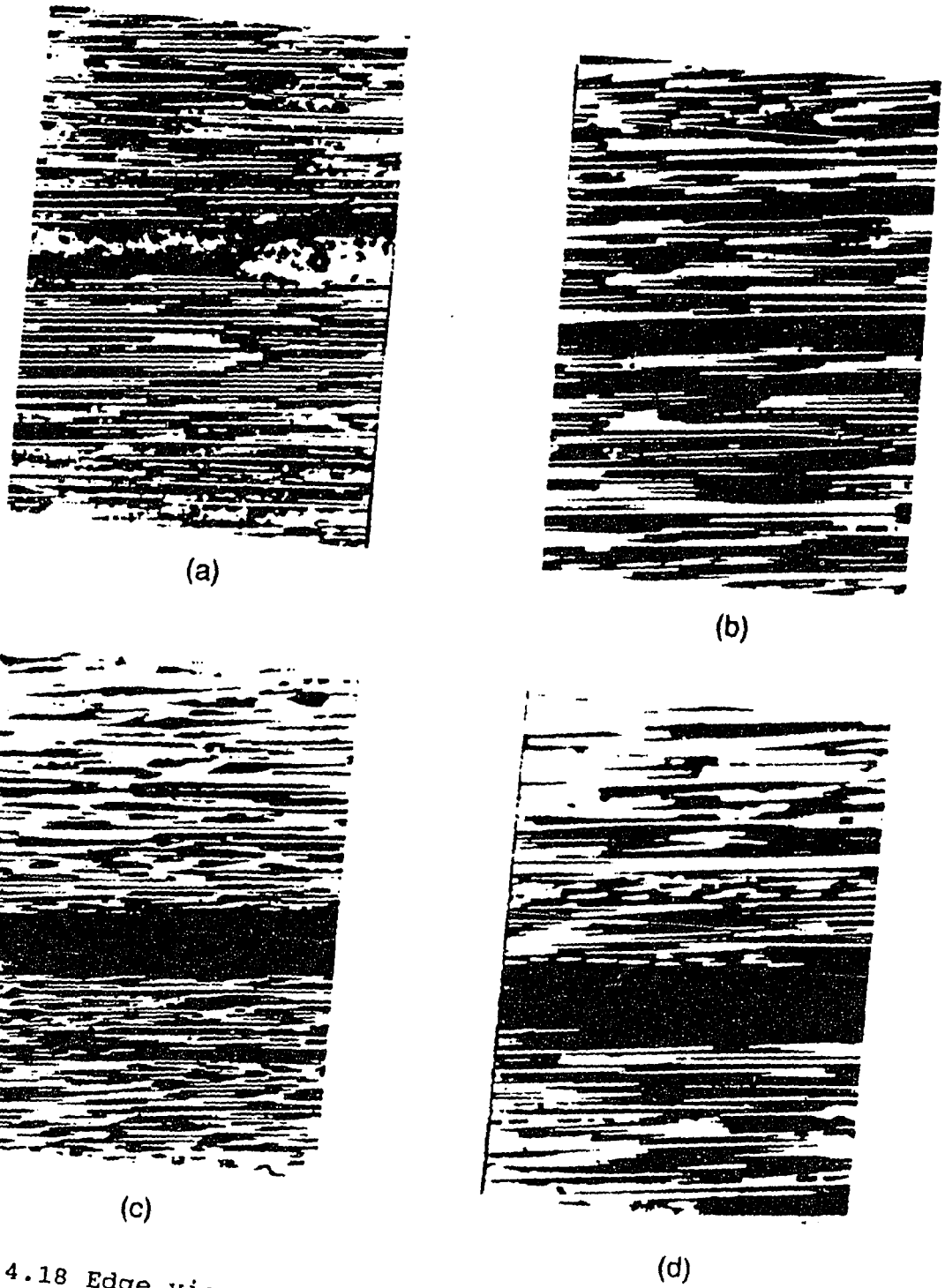

Fig. 4.18 Edge views of FM 300 I interleaved specimens. (a) crack changing its path in a 0.043 mm thick interleaf, 330X, (b) crack growing through the plies in a 0.043 mm interleaf, 165X, (c) & (d) larger deformations than (a) & (b) for 0.086 mm interleaf, 165X.

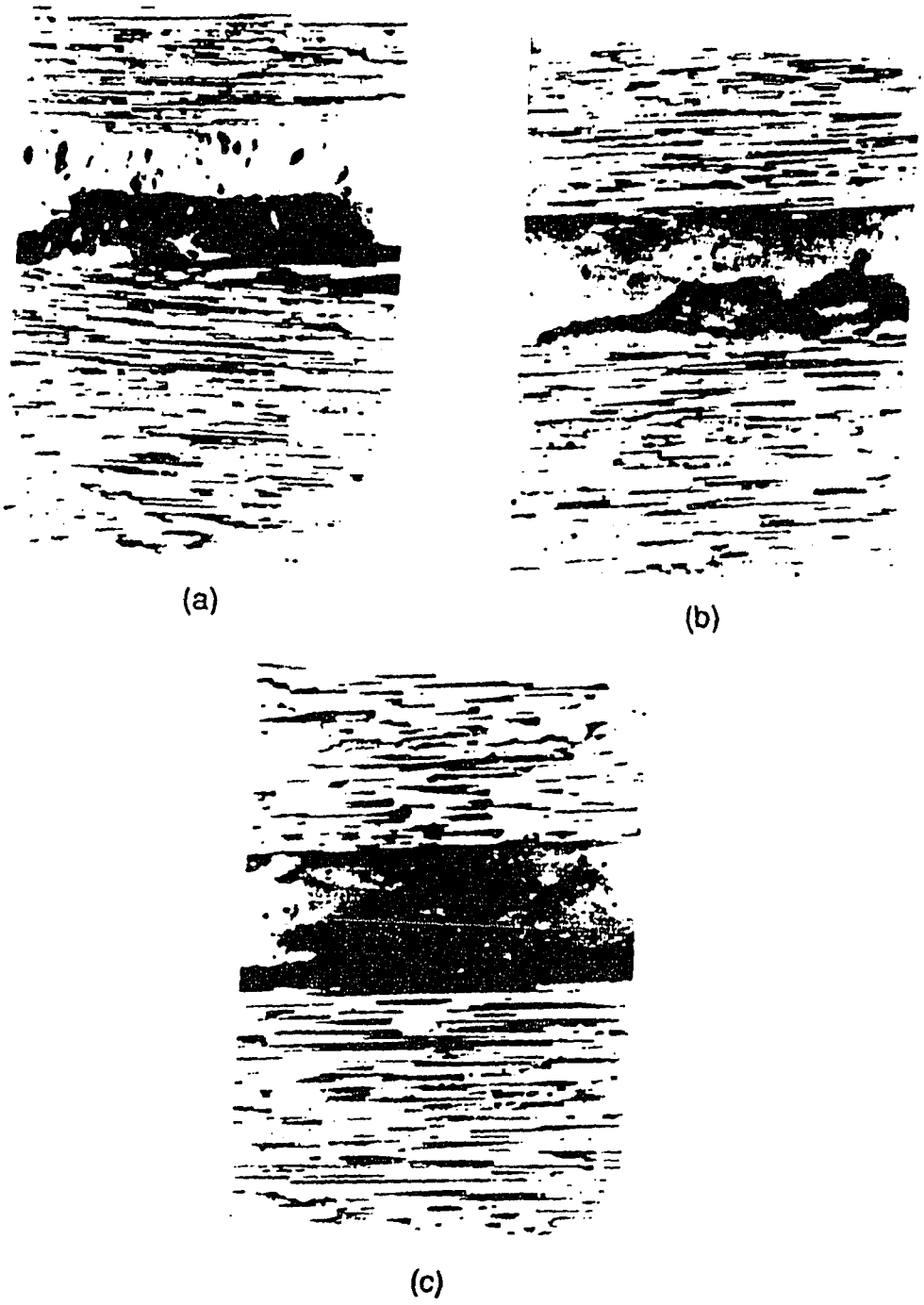

Fig. 4.19 Edge views of 0.256 mm FM 300 I interleaved specimens, 83X, (a) mode II crack tip, (b) coalescence of microcracks, (c) microcracks joining the main crack along the interface.

(a)

(b)

Fig. 4.20 (a) & (b) hackles on the fracture surfaces of 0.043 and 0.086 mm thermoset FM 300 I interleaved specimens, 41X, respectively.

Figs. 4.21 (a)-(c) are SEM micrographs of the fracture surfaces of 0.172, 0.256 and 0.429 mm TSI specimens. Note the leaf like artifacts in Figs. 4.21 (a) and (c) at very high magnifications. Bradley et al. [38] observed similar features on mode II dominated fracture surfaces of tough Hexcel T6T145/F155 graphite/epoxy system. Fig. 4.21 (b) is the fracture surface of 0.256 mm (10.2 mil) TSI specimen with a considerable amount of hackles and stress whitening which agrees with the large fracture toughness of this specimen.

Fig. 4.22 shows the subcritical and nonlinear fracture toughness versus thermoset FM 300 I interleaf thickness. The trends of these curves are very similar to that of the critical strain energy release rate versus interleaf thickness shown in Fig. 4.15. Note that no fiber bridging was observed for FM 300 I interleaved specimens.

In contrast to thermoplastic film E interleaved ones, for thermoset FM 300 I interleaved specimens the subcritical and nonlinear fracture toughnesses coincide for almost the full thickness range. This suggests that for thermoset FM 300 I interleaved IM7/CYCOM 1827 yielding of the interleaf and coalescence of microcracks occur simultaneously.

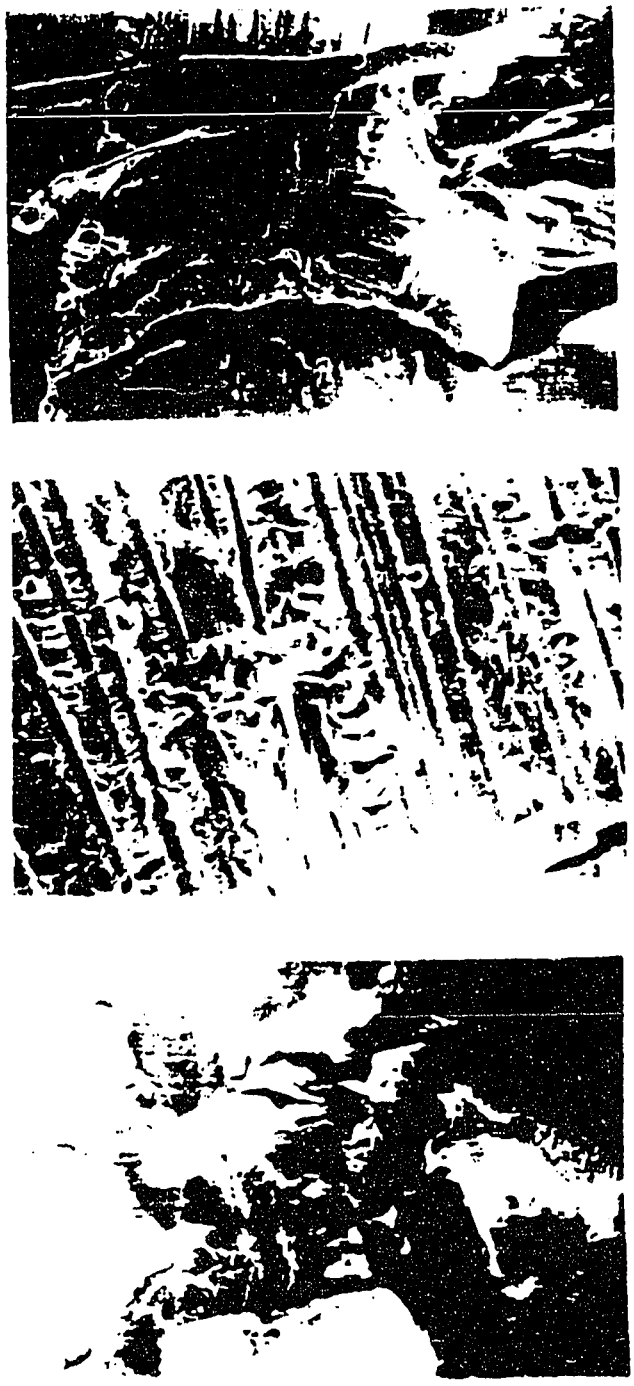

Fig. 4.21 Fracture surfaces of FM 300 I interleaved specimens under SEM, (a) 0.172 mm interleaf, 250X, (b) 0.256 mm interleaf, 50X, (c) 0.43 mm interleaf, 280X.

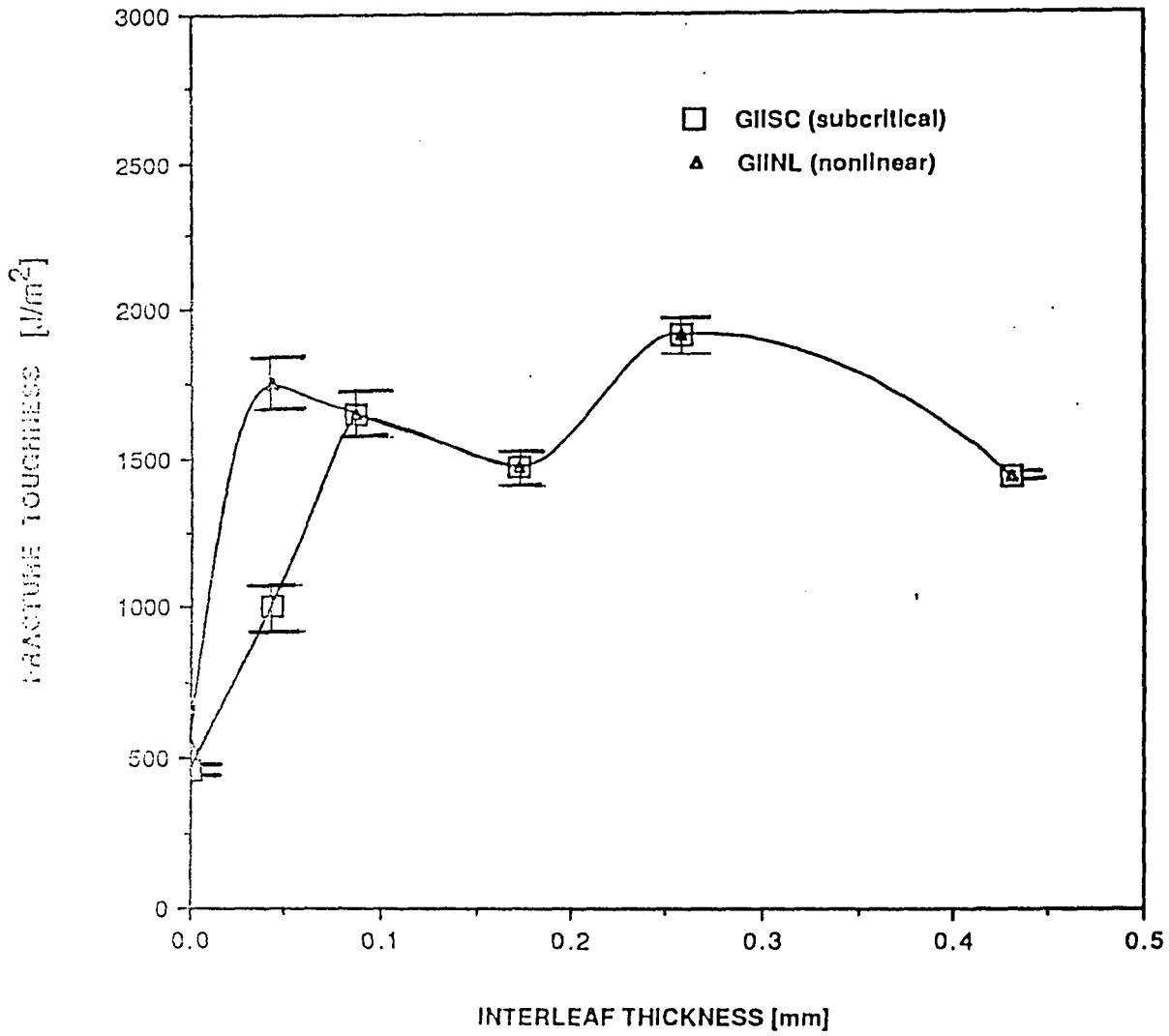

Fig. 4.22 Mode II nonlinear and subcritical fracture toughnesses vs. thermoset (FM 300 I) interleaf thickness.

Chapter 5 Analytical Results

5.1 Compliance and Strain Energy Release Rate of Interleaved ENF Specimens

In chapter 4 fracture toughness data were reduced by the beam theory with shear deformation included. However, as noted in sect. 3.2, for interleaved specimens, depending on the interleaf material and thickness these results may be in error. In order to investigate the accuracy of the beam theory, compliance and strain energy release rates were obtained from finite element analysis (FEA) for thermoplastic and thermoset interleaved (TPI and TSI) specimens for various interleaf thicknesses, see sect. 3.1.

A compliance ratio is defined as the ratio of compliance values obtained from FEA to the compliance for homogeneous ENF beams calculated using eq. (5) in sect. 3.1.1. The total specimen thickness was kept constant, 3.43 mm (0.135 in.), while increasing the interleaf thickness. For geometry and material properties see sect. 3.1.

Fig. 5.1 shows the compliance ratio versus interleaf thickness for TPI and TSI specimens (film E and FM 300 I). As expected, the finite element beam theory including shear

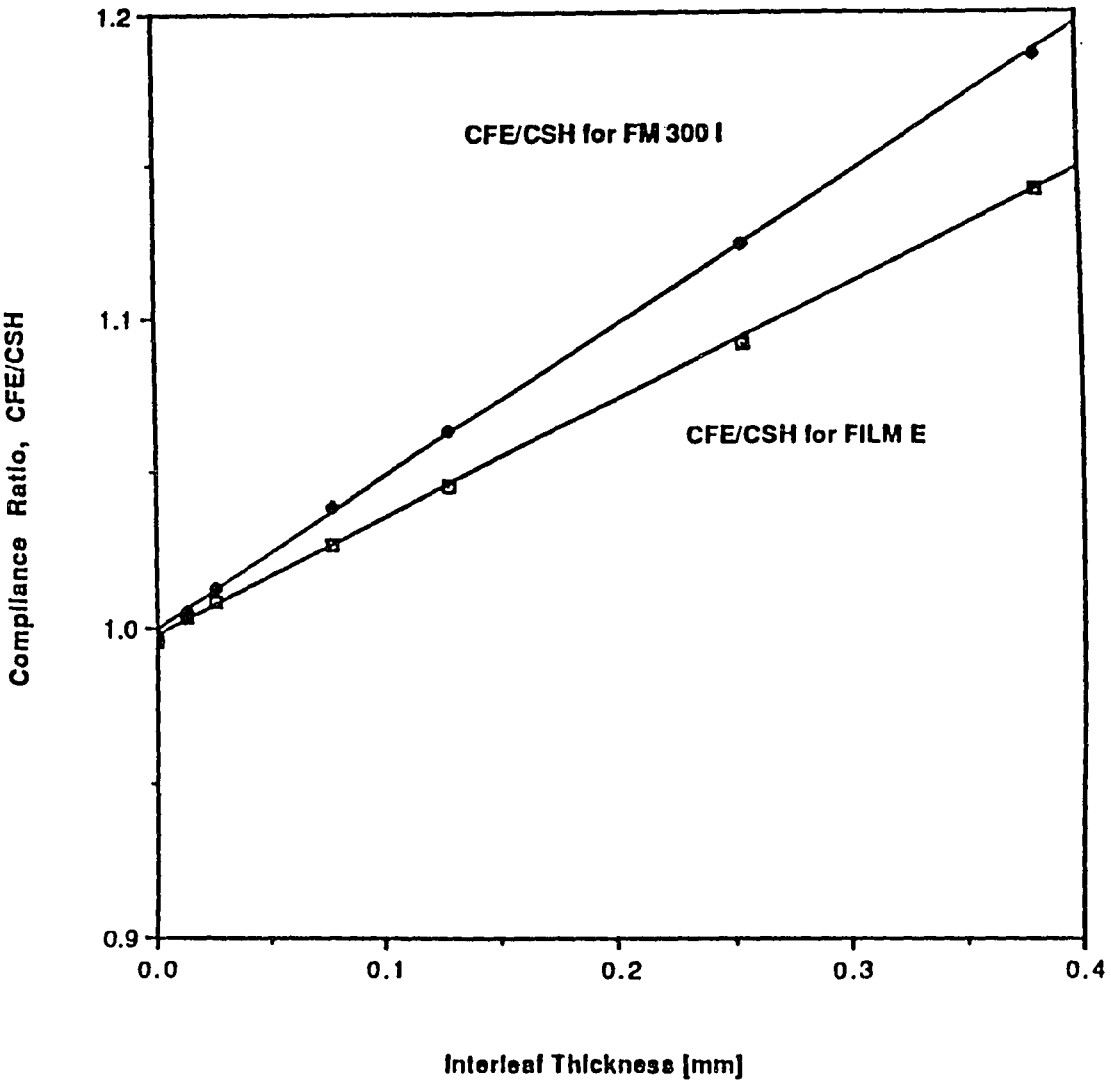

Fig. 5.1 Ratio of the compliances obtained from the finite element analysis and the beam theory with shear for the baseline case.

deformation agree very well for the baseline case. However, as the interleaf thickness increases, FEA gives larger compliance values than the homogeneous beam theory. The difference is slightly more pronounced for FM 300 I which has a Young's modulus almost half of that of film E. For 0.4 mm (16 mil) thick interleaf the difference between the FEA and beam theory becomes 15 % and 20 % for TPI and TSI specimens, respectively.

The strain energy release rate, G_{II}, for the homogeneous ENF specimen can be derived by differentiating the compliance expression, eq. (5) with respect to crack length [26],

$$G_{II}^{SH} = \frac{P^2}{2w} \frac{dC_{SH}}{da} \tag{12}$$

$$G_{II}^{SH} = \frac{9a^2P^2}{16E_1w^2h^3} \left(1 + 0.2\left(\frac{E_1}{G_{13}}\right)\left(\frac{h}{a}\right)^2\right) \tag{13}$$

where G_{II}^{SH} is the strain energy release rate including shear deformation.

Table 5.1 is a list of normalized strain energy release rates for the TSI specimens. Again there is a remarkable agreement for the baseline case, 0.9 % difference. However, as the interleaf thickness is increased, the difference

Interleaf material	G_{II}^{FE}/G_{II}^{SH}
Baseline	1.009
0.0254 mm (1 mil)	1.011
0.0762 mm (3 mil)	1.015
0.127 mm (5 mil)	1.148
0.381 mm (15 mil)	1.65

G_{IIsh}=0.015 J/m^2

Table 5.1 Comparison of the strain energy release rates obtained from the FEA for TSI specimens and the beam theory with shear included for the baseline case, a/L=0.5, P=4.45 N (1 lb.).

increases up to 65 % for the 0.38 mm (15 mil) thick interleaves.

Finally, the compliances and strain energy release rates obtained from the cracked sandwich beam (CSB) theory for interleaved composites, see sect. 3.2, were compared with the FEA results. Fig 5.2 is a comparison of the compliances for the more compliant TSI specimens. FEA gives slightly larger compliance values for all cases and the difference increases for increasing interleaf thickness. For the baseline case the difference is 0.5 % and it reaches to 5.5 % for 0.4 mm (16 mil) thick interleaf.

Strain energy release rate ratio between the CSB theory and FEA are listed in Table 5.2. In general, CSB theory and FEA results are close for the thickness range considered. It is important to note that, although individually both methods give increasing strain energy release rates for increasing interleaf thickness, the ratio is almost constant.

From the above results it can be concluded that, data reduction scheme based on homogeneous beam theory including shear deformation is fairly accurate for the thermoplastic interleaf thicknesses (0.0127 to 0.127 mm) considered in this study. However, for the thickest thermoset interleaves the

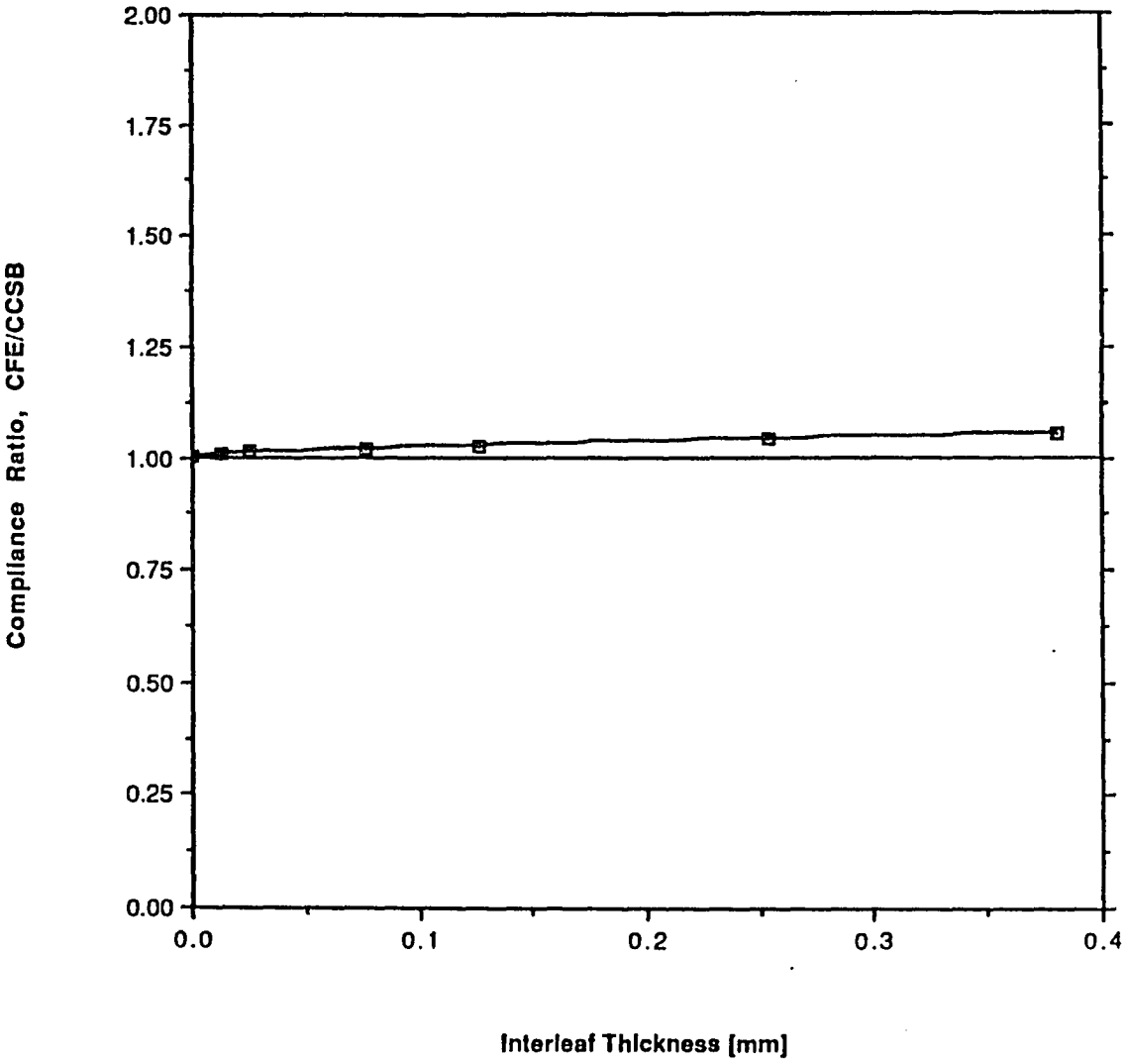

Fig. 5.2 Comparison of the finite element analysis and cracked sandwich beam theory (CSB) compliances.

Interleaf material	G_{II}^{CSB}/G_{II}^{FE}
Baseline	0.974
0.0254 mm (1 mil)	1.006
0.0762 mm (3 mil)	1.057
0.127 mm (5 mil)	0.992
0.381 mm (15 mil)	0.931

Table 5.2 Comparison of the strain energy release rates obtained from the cracked sandwich beam (CSB) theory and FEA for TSI specimens, a/L=0.5, P=4.45 N (1 lb.).

interleaf needs to be taken in to account in the data reduction scheme for G_{IIC}.

5.2 Yield Zone Estimates

The volume of the plastically deformed polymer at the crack tip between plies in a composite is considered to be very important for toughness transfer from matrix to composite [7, 12-13]. It has been argued that, above a certain level of matrix toughness, a saturation in the composite toughness takes place and this occurs when the plastic zone around the crack tip becomes restricted due to the presence of rigid fibers.

Interleaving, as discussed in sect. 1.3, is based on the hypothesis that a composite material could be made tougher and more impact resistant by allowing for more expansion of the plastic zone between the plies. Indeed, fracture toughness test results presented in chapter 4 show that interleaving increases the mode II fracture toughness tremendously, i.e. four to six times the baseline value.

Because the fracture energy of toughened composites is largely derived from the plastic deformation process at the crack tip under constraint of the rigid elastic plies, it would be of great interest if yield zone dimensions could be predicted.

In this study, a quasi-elastic approach was used to calculate yield zone dimensions (height and length) for 0.0762, 0.127, 0.381 and 0.635 mm (3, 5, 10 and 25 mil) TPI and TSI specimens by comparing the FEA effective (von Mises) stresses with normalized yield strengths of the interleaves, see sect. 3.1.3. The total specimen thickness was kept constant while the interleaf thickness was varied and a crack was assumed to be symmetrically located at the center of the interleaf.

Figs. 5.3 (a)-(d) show upper parts of the estimated yield zones in TPI specimens. For 0.0762 and 0.127 mm (3 and 5 mil) thick interleaves, Fig. 5.3 (a) and (b), the yield zone height extends to the interface, and is quite elongated having a length of 7.7 and 4.6 times (0.587 and 0.584 mm) the interleaf thicknesses, respectively. For 0.381 mm (15 mil) thick interleaf, Fig. 5.3 (c), the interleaf is not fully yielded. The height of the yield zone is 0.127 mm (1/3 of the total interleaf thickness) and has a length of only 0.73 t_i (0.278 mm). For 0.635 mm (25 mil) interleaf thickness, the height and the length of the yield zone are the same as those of the 0.351 mm thick one, 0.127 and 0.279 mm, respectively.

Fig. 5.4 shows the height of the yield zone versus thermoplastic interleaf thickness. It is clear that after a thickness of about 0.13 mm, the plastic zone height remains

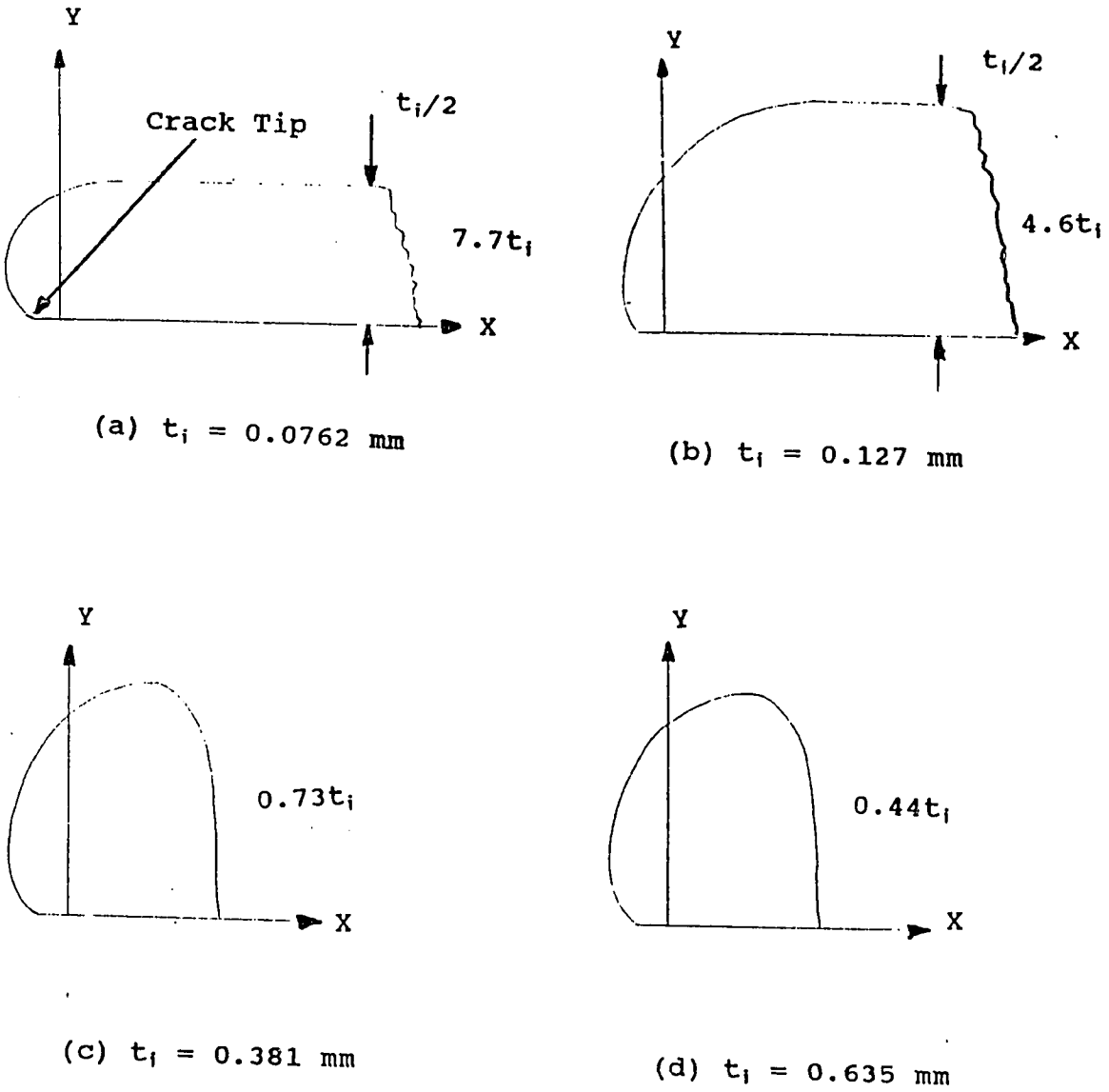

Fig. 5.3 Yield zones for a range of thermoplastic (film E) interleaf thicknesses.

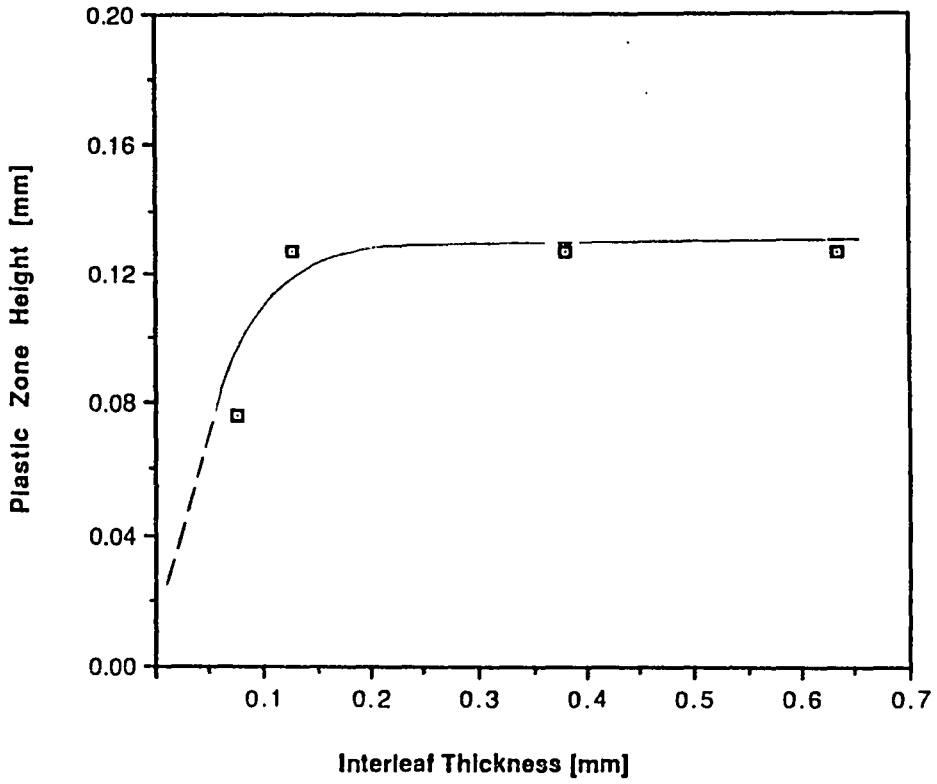

Fig. 5.4 Yield zone height versus thermoplastic interleaf thickness.

the same indicating that no further transfer of toughness occurs. This value can also be considered as the optimum interleaf thickness provided that other deformation mechanisms such as fiber bridging are negligible. In qualitative agreement with Fig. 5.4, fracture toughness of TPI specimen shown in Fig. 4.6, increases considerably for the thin interleaves and remains almost constant for thicker ones, i.e. 0.0762 mm (3 mil) interleaf thickness. Also note that, microscopic observation indicated an adhesion problem with 0.0254 and 0.0763 mm (1 and 3 mil) thick TPI specimens and further increase for thicker interleaves, 0.127 mm (5 mil), was mostly due to fiber bridging.

Figs. 5.5 (a)-(d) are estimated yield zones for TSI specimens for the same range of interleaf thicknesses as TPI specimens. It is seen that, for all cases the yield zone heights extend beyond the interleaf/composite interface (i.e. fully yielded interleaves). Similar to the TPI specimens, the yield zone length decreases with increasing interleaf thickness.

To further investigate the restrictions on plastic zone imposed by the rigid composite plies, the yield zone height (plastic zone size) was calculated using Irwin's model [5];

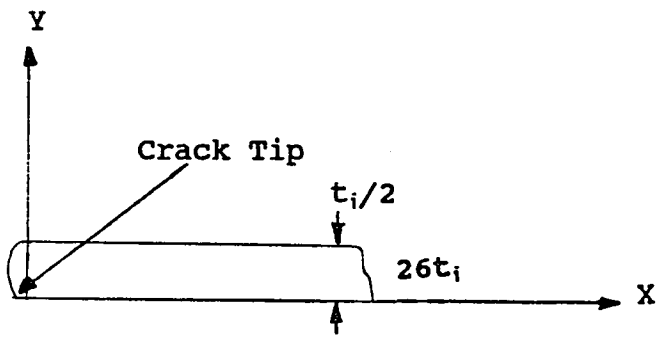

(a) t_i = 0.0762 mm

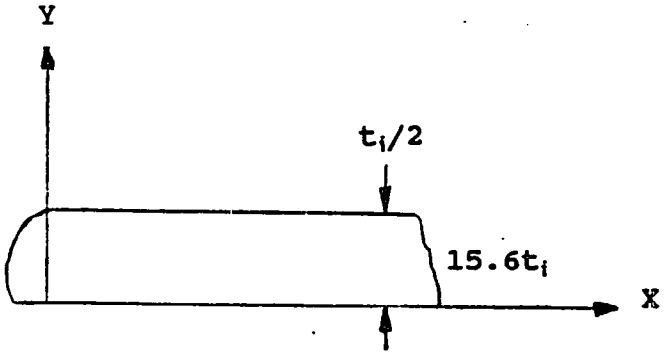

(b) t_i = 0.127 mm

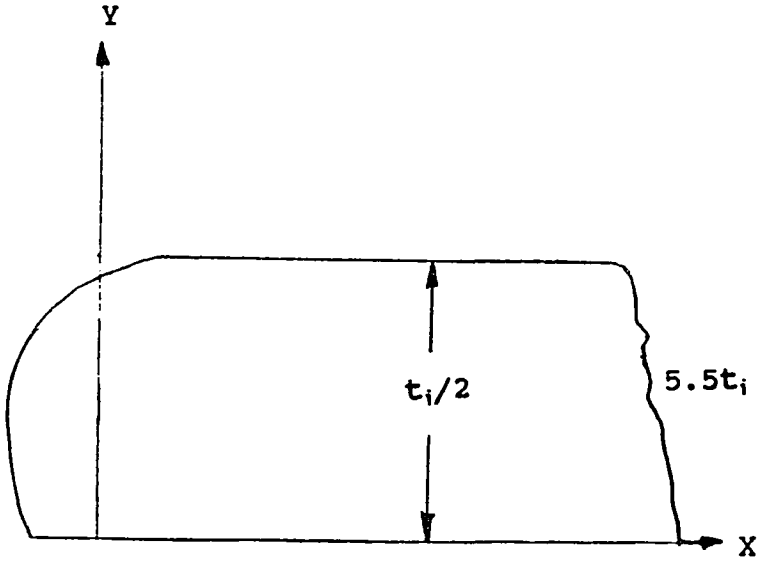

(c) t_i = 0.381 mm

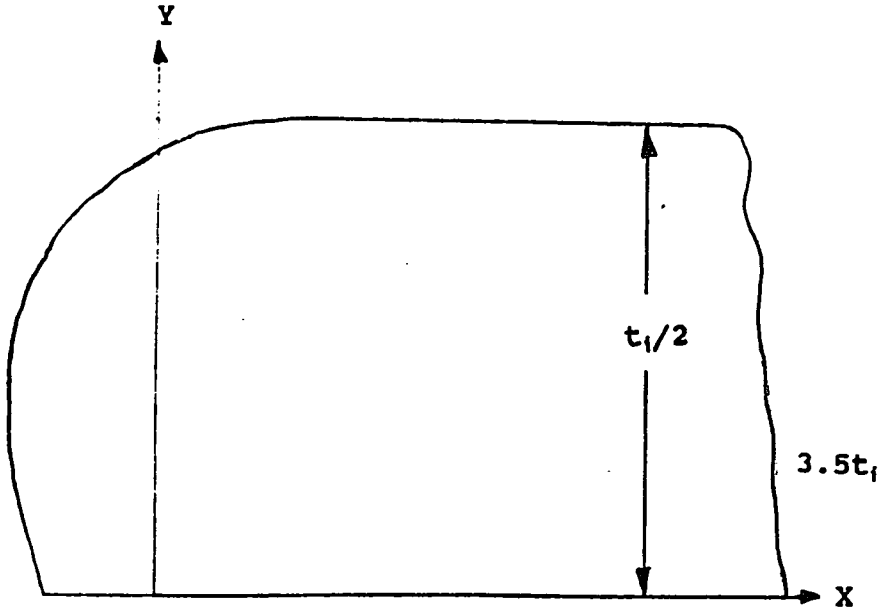

(d) t_i = 0.635 mm

Fig. 5.5 Yield zones for a range of thermoset (FM 300 I) interleaf thicknesses.

$$r_p = \frac{K^2_{IIc}}{2(\pi\tau^2_y)} \approx \frac{E\,G_{IIc}}{2(\pi\tau^2_y)} \qquad (11)$$

where r_p is radius of the yield zone, K_{IIC} is mode II critical stress intensity factor, G_{IIC} is mode II critical strain energy release rate, τ_y (=0.5 σ_y) is yield strength in shear and E is the Young's modulus.

The strain energy release rates obtained from FEA for 0.225 N (1 lb.) load were multiplied by the square of 41 N ($G_{IIC} \alpha P_c^2$, see sect. 1.2) to compare the results obtained from eq. (11) with the yield zone estimates shown in Figs. 5.3 and 5.5.

Table 5.3 is a comparison of the yield zone heights for TPI and TSI specimens. Irwin's model agrees quite well with the yield zone estimates obtained from the analysis of the stress distributions ahead of the crack tip.

Fig. 5.6 shows ratio of plastic zone heights to interleaf thickness versus the thickness of the interleaves for TPI specimens. Again, it is clearly seen that, Irwin's model and FEA stress analysis give very close results. It is important to note that for the thinnest interleaf, 0.0762 mm (3 mil), the ratio is greater than one, which indicates that the free

Interleaf thickness mm (mil)	G_{IIC} J/m^2 (in.lb/in^2)		r_p (Irwin's model) mm (mil)		r_p (FEA stress results) ** mm (mil)	
	TPI*	TSI*	TPI*	TSI*	TPI*	TSI*
.0762 (3)	508 (2.90)	518 (2.96)	.079 (3.1)	.287 (11.3)	.0762 (3)	.0762 (3)
.127 (5)	562 (3.21)	587 (3.35)	.086 (3.4)	.330 (13.0)	.127 (5)	.127 (5)
.381 (15)	796 (4.55)	840 (4.80)	.122 (4.8)	.467 (18.4)	.127 (5)	.381 (15)
.635 (25)	1069 (6.11)	1142 (6.52)	.163 (6.4)	.635 (25)	.127 (5)	.635 (25)

* Thermoplastic and thermoset interleaved specimens.

** see sect. 3.1.3

Table 5.3 Strain energy release rates and yield zone heights for TPI and TSI specimens.

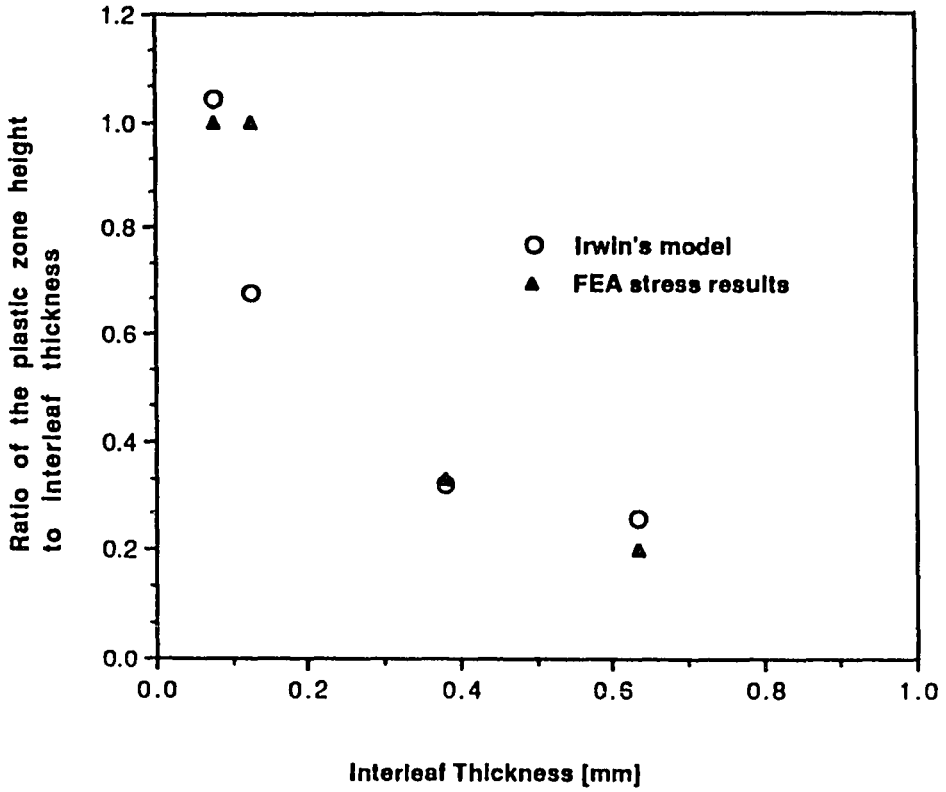

Fig. 5.6 Ratio of yield zone height to interleaf thickness versus thickness of the interleaf for TPI specimens.

expansion of the plastic zone is constrained by rigid plies and yield zone spreads into the fiber layers. Furthermore, initial decrease in the ratio is very steep showing that for interleaves thicker than about 0.0762 mm (3 mil) the toughness translation becomes less and less efficient.

Fig. 5.7 shows ratio of plastic zone height to interleaf thickness versus thickness of the interleaf for TSI specimens. For 0.0762, 0.127 and 0.381 mm (3, 5 and 15 mil) interleaves Irwin's model predicts that the yield zone is severely restricted by the composite plies (i.e. ratios are $\approx$ 3.75 and $\approx$ 2.6, respectively). Only for the thickest, 0.635 mm (25 mil) TSI the yield zone height is almost the same as the interleaf thickness as determined by both methods. Similar to TPI specimens, fracture toughness of TSI specimen, as previously shown in Fig. 4.15, is in fairly good agreement with Fig. 5.7. There is a steep increase up to 0.256 mm (10.2 mil) interleaf thickness which is followed by a gradual decrease. It can be predicted that the optimum thermoset interleaf thickness is in the range of 0.256-0.381 mm (10 to 15 mil).

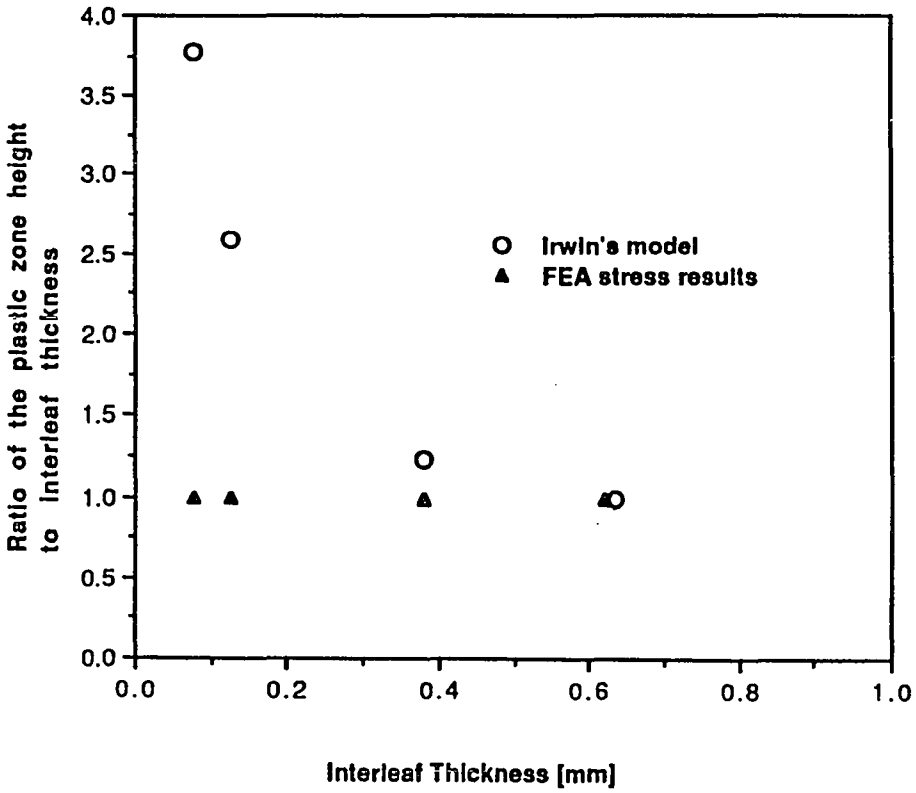

Fig. 5.7 Ratio of yield zone height to interleaf thickness versus thickness of the interleaf for TSI specimens.

Chapter 6 Conclusions and Recommendations

6.1 Conclusions

This study focused on the interlaminar shear fracture, mode II, of baseline (no interleaving), thermoplastic (film E) and thermoset (FM 300 I) interleaved composite materials. The results of this investigation led to the following conclusions:

- Mode II precracking initiates a crack at the composite/interleaf interface in thermoplastic interleaved (TPI) specimens. In contrast, the crack is within the interleaf in thermoset interleaved (TSI) specimens.

- Mode I and mode II crack tips have unique appearances reflecting the loading conditions under which they are initiated. The mode I crack tip is sharp and straight while mode II crack tip has a series of sigmoidal shaped microcracks with an orientation of 45^0 to the fiber directions.

- The degree of nonlinearity in P-δ curve increases with interleaf thickness and is significant for thick interleaves of both thermoset and thermoplastic systems.

- The mode II fracture toughness, G_{IIC}, of 0.0127 mm thick TPI specimens is about four times the baseline value. Adhesion seems to be a problem with 0.0254 and 0.0762 mm TPI specimens. This is very likely to be due to some kind of a contamination on the surface of those particular films. The 0.127 mm TPI has extremely good adhesion showing indications of fiber bridging and has very large G_{IIC}, about 6.5 times the baseline value.

- For TPI specimens onset of subcritical crack growth and nonlinearity do not coincide (nonlinearity occurs after subcritical crack growth) except for the baseline case, and the difference between them increases with the interleaf thickness.

- Although, interleaving is more effective in improving the fracture toughness, G_{IIC}, of TPI specimens, it is possible to obtain comparable G_{IIC} values with thick TSI specimens.

- In contrast to TPI, for TSI specimens the subcritical and nonlinear fracture toughnesses coincide which may be due to the adhesion problem observed in TPI specimens.

- The beam theory with shear included is accurate for specimens which have no interleaving. However, for thick interleaves data reduction procedure need modification

because of increased compliance and strain energy release rate.

- Compliance and strain energy release rate predicted with the cracked sandwich beam (CSB) theory are close to the finite element results.

- Quasi-elastic stress analysis of both TPI and TSI specimens showed that the yield zone height reaches an optimum value (0.127 and 0.635 mm for TPI and TSI specimens, respectively) and remains constant for increasing interleaf thickness. Furthermore, yield zone heights predicted from Irwin's model and analysis of finite element stress results are in quite good agreement verifying the restraining effect of rigid elastic plies on expansion of yield zone.

- Results of this study should contribute to the general understanding of the thermoplastic and thermoset interleaved composites.

6.2 Recommendations

- Microscopic investigation of yield zones can be a useful tool to explain the mechanism of toughness translation in interleaved composites. It is well known that in metals, plastically deformed material can be detected by polishing and etching techniques. In polymers and composites, however

deformation mechanisms are different and may require more elaborate techniques. It may be wise to use neat resin compact tension test specimens to develop a proper etchant to use with the composite.

- In this study, the yield zone sizes were computed based on elastic stresses. However, because of yielding, there will be stress redistribution. Thus, yield zone size can be predicted more realistically by an elasto-plastic model of the crack tip deformation which takes into account the post-yielding stress-strain behavior of the interleaf.

References

1. P. A. Lagace, "Impact Response of Graphite/Epoxy Fabric Structures", Mechanics of Composites Review, Bal Harbour, Florida, Nov. (1988).
2. K. B. Su, "Mechanisms of Interlaminar Fracture In A Thermoplastic Matrix Composite Laminate", 5th International Conference On Composite Materials, July 30 Aug. 1, 1985, San Diego.
3. T. J. Chapman, "Rate and Temperature Effects On Mode II Interlaminar Fracture Toughness In Composite Materials", Bachelor of Science Thesis, University of Delaware, May 1986.
4. D. L. Hunston, A. J. Kinloch, S. J. Shaw, S. S. Wang, "Characterization of The Fracture Behavior of Adhesive Joints", Adhesive Joints, Edited by K. L. Mittal, Plenum Publishing Corp., 1984.
5. David Broek, Elementary Fracture Mechanics, Martinus Nijhoff Publishers, 4 th. Ed., p. 9, (1986).
6. E. M. Wu, "Application of Fracture Mechanics to Anisotropic Plates", Journal of Applied Mechanics, Vol. 34, Dec. 1967, p. 967.

7. K. Friedrich, R. Walter, L. A. Carlsson, A. J. Smiley, J. W. Gillespie Jr., "Mechanisms for Rate Effects On Interlaminar Fracture Toughness of Carbon/Epoxy and Carbon/PEEK Composites", Journal of Materials Science, Vol. 24, (1989), p. 3387-3398.

8. J. E. Masters, "Development of Composites Having Improved Resistance to Delamination and Impact", Final Report for Period September, 1984-June, 1987, AFWAL/MLBC, WFAFB.

9. L. Berglund, "Fracture Toughness of Carbon Fiber/PEEK Composites", Linkopin Studies in Science and Technology, Dissertation, No. 159, (1987).

10. A. F. Yee, "Modifying Matrix Materials for Tougher Composites", Toughened Composites, ASTM STP 937, Norman J. Johnston, Ed. , ASTM, Philadelphia, (1987), p.383-396.

11. W. S. Johnson, P. D. Mangalgiri, "Influence of The Resin On Interlaminar Mixed-Mode Fracture", Toughened Composites, ASTM STP 937, Norman J. Johnston, Ed., ASTM, Philadelphia, (1987), p. 295-315.

12. D. L. Hunston, "Composite Interlaminar Fracture: Effect of Matrix Fracture Energy", Com. Tech. Rev. , Vol.4, (1984), p.176.

13. W. L. Bradley, R. N. Cohen, "Matrix Deformation and Fracture In Graphite Reinforced Epoxies", Delamination and Debonding of Materials, ASTM STP 876, W. S. Johnson, Ed., ASTM, Philadelphia, (1985), p. 389-410.

14. O. Ishai, H. Rosenthal, N. Sela, E. Drukker, "The Effect of Selective Interleaving On Interlaminar Fracture Toughness of Graphite/Epoxy Composite Laminates", Composites, Vol. 19, No. 1, Jan., 1980, p. 49-54.

15. N. Sela, O. Ishai, L. Banks - Sills, "The Effect of Adhesive Thickness On Interlaminar Fracture Toughness of Interleaved CFRP Specimens", Composites, Vol. 20, No. 3, May, 1989, p. 257-264.

16. H. Chai, "Shear Fracture", Int. J. of Fracture, Vol. 37 (1988), p. 137-159.

17. L. A. Carlsson, L. S. Sendlein, S. L. Merry, "Characterization of Face Sheet/Core Shear Fracture of Composite Sandwich Beams", Submitted to J. Comp. Mat. 1989.

18. L. A. Carlsson, R. B. Pipes, Experimental Characterization of Advanced Composite Materials, Prentice-Hall, Inc., (1987), p. 53-62.

19. L. A. Carlsson, J. W. Gillespie, B. R. Trethewey, "Interlaminar Fracture of Graphite/Epoxy and Graphite/PEEK", Journal of Reinforced Plastics and Composites, Vol. 5, July 1986, p. 170-187.

20. T. K. O'Brien, G. B. Murri, S. A. Salpeker, "Interlaminar Shear Fracture Toughness and Fatigue Thresholds for Composite Materials", NASA TM-89157, Aug. 1987.

21. Test Procedure for The End Notched Flexure (ENF) Specimen ASTM D30.02.02 Round Robin, 1987.

22. L. A. Carlsson, J. W. Gillespie, "Mode II Interlaminar Fracture of Composites", Application of Fracture Mechanics to Composite Materials, (K. Friedrich Ed.), Elsevier, Amsterdam, in press.

23. ANSYS Engineering Analysis System User's Manual, Swanson Analysis Systems Inc., 1987.

24. J. W. Gillespie, L.A. Carlsson, R. B. Pipes, "Finite Element Analysis of The End Notched Flexure Specimen for Measuring Mode II Fracture Toughness", Comp. Sci. Tech., Vol.27, (1986), p. 177-197.

25. T. Kevin O'Brien, Gretchen B. Murri, Satish A. Salpekar, "Interlaminar Shear Fracture Toughness and Fatique Thresholds for Composite Materials", NASA TM-89157, Aug. 1987.

26. L. A. Carlsson, J. W. Gillespie, R. B. Pipes, "On The Analysis and Design of The End Notched Flexure Specimen for Mode II Testing", J. Com. Mat., Vol. 20, (1986), p. 594-605.

27. E. F. Rybicki, M. F. Kanninen, "A Finite Element Calculation of Stress Intensity Factors By A Modified Crack Closure Integral", Eng. Frac. Mech., Vol. 9, (1977), p. 931-938.

28. F. Erdogan and G. D. Gupta, "Layered Composites with An Interface Flaw", Int. J. Solids Struct., Vol. 7, (1971), p. 1089-1107.

29. M. L. Williams, "The Stresses Around A Fault or Crack In Dissimilar Media", Bull. Seismol. Soc. Amer., Vol. 49, (1959), p. 199-204.

30. I. S. Raju, J. H. Crews, Jr., M. A. Aminpour, "Convergence of Strain Energy Release Rate Components for Edge-Delaminated Composite Laminates", Eng. Frac. Mech., Vol. 30, No. 3, (1988), P. 383-396.

31. C. T. Sun, M. G. Manoharan, "Strain Energy Release Rate of An Interfacial Crack Between Two Orthotropic Solids", Proc. Am. Soc. for Composites, 2nd Tech. Conf., 23-25 Sept., 1987 Technomic, p. 49.

32. R. E. Smelser, "Evaluation of Stress Intensity Factors for Bimaterial Bodies Using Numerical Crack Flank Displacement Data", Int. J. Frac., Vol. 15, No. 2, April 1979, p. 135-143.

33. Gere & Timoshenko, Mechanics of Materials, PWS Publishers, (1984), p. 205.

34. S. S. Sternstein, L. Ongchin, "Yield Criteria for Plastic Deformation of Glassy High Polymers In General Stress Fields", Am. Chem. Soc., Div. Polym. Prepr., Vol. 10, (1969), p. 1117-1124.

35. L. A. Carlsson, A. Aksoy, "Analysis of End Notched Flexure (ENF) Specimens with Interleaves", to be published.

36. W. S. Johnson, P. D. Mangalgiri, "Investigation of Fiber Bridging In Double Cantilever Beam Specimens", NASA-TM 87716, April 1986.

37. Engel L. H., Klingele, G. W. Ehrenstein, H. Schaper, An Atlas of Polymer Damage, Carl Hanser Verlag, 1981, p. 139.

38. W. M. Jordan, W. L. Bradley, "Micromechanisms of Fracture In Toughened Graphite/Epoxy Laminates", Toughened Composites, ASTM STP 937, Norman J. Johnston, Ed., ASTM, Philadelphia, (1987), p. 95-114.